國立交通大學

電子物理學系

博士論文

以氫化物氣相磊晶法開發氮化鎵基板研究

Study of GaN Substrates Developed by Hydride Vapor Phase Epitaxy

研 究 生: 黃 信 雄

指導教授: 李 威 儀 博士

中華民國 九十七 年 九 月

以氫化物氣相磊晶法開發氮化鎵基板研究

Study of GaN Substrates Developed by Hydride Vapor Phase Epitaxy

研 究 生: 黃 信 雄　　Student:Hsin-Hsiung Huang

指導教授: 李 威 儀　　Advisor:Dr. Wei-I Lee

國立交通大學
電子物理研究所
博士論文

A Thesis
Submitted to Department of Electrophysics
College of Science
National Chiao Tung University
in partial Fulfillment of the Requirements
for the Degree of
Doctor of Philosophy
in
Electrophysics

September 2008

Hsinchu, Taiwan, Republic of China

中華民國　九十七 年 九 月

以氫化物氣相磊晶法開發氮化鎵基板研究

研 究 生: 黃 信 雄　　　　　　　　　指導教授: 李 威 儀

國立交通大學電子物理研究所

中文摘要

由於缺乏晶格匹配的基板，三族氮化物元件只能採用異質磊晶的方式，利用晶格常數不同的材料來當作基板，因此有缺陷密度過高，以及因為熱膨脹係數不同造成晶體彎曲甚至破裂的問題。對於低電流密度的元件（例如LED)，這些問題的影響不大，但是對於高電流密度元件（例如藍光LD)、高功率元件或UV元件而言，影響就相當可觀，若有單晶三族氮化物基板來進行同質磊晶，不但可以降低晶格常數不匹配所造成的缺陷密度、熱膨脹係數不同所造成的彎曲；更可大幅簡化元件的製程及提昇元件的可靠度。未來在光電元件產業的發展上，單晶三族氮化物基板必然具有舉足輕重的地位。對於國內學術界而言，若有單晶三族氮化物基板（GaN、AlN 等）作為研究基礎，在相關領域的研究上等於直接躍遷至不同的競爭平台上。

本論文的研究方向在於使用氫化物氣相磊晶法成長氮化鎵厚膜，其中最大的問題在於如何克服因熱膨脹係數不同所產生的熱應力所導致的晶片破裂，我們運用了一些 ELOG 所衍生的方法及溫度梯度成長方法來克服應力的問題，並獲得良好的成效。經由氫化物氣相磊晶所成長的厚膜再利用雷射剝離的方法將厚膜從原生基板上分開，而得到獨立氮化鎵基板。我們分別使用了掃描式電子顯微鏡，陰極螢光，光致螢光，拉曼光譜，霍爾量測，高解析 X 光，原子力顯微鏡，微分干涉差光學顯微鏡等工具來量測氮化鎵基板的特性。除此之外，以氫化物氣相磊

晶所成長的氮化鎵化學特性也經由濕式化學蝕刻法加以研究，其不同晶面的活化能也分別經由實驗值計算出來。

總之，厚度超過300微米的透明氮化鎵厚膜已經開發出來，其差排密度大約介於 10^6 到 $10^7 cm^{-2}$ 之間，霍爾電阻大約是 0.09 Ω-cm，未摻雜的載子濃度大約是 $1.6x10^{17}\ cm^{-3}$，X 光搖擺曲線的半高寬大約是 150 秒。在成長厚度增加以及磊晶條件最佳化後，這些特性都可以再改善。

單晶三族氮化物基板將是推動下一代三族氮化物元件發展的關鍵載具，希望經由本論文研究計劃後，未來可以穩定提供高品質的單晶三族氮化物基板給其他學界單位進行研究使用，以對國內的光電發展盡一份心力。

Study of GaN Substrates Developed by Hydride Vapor Phase Epitaxy

Student:Hsin-Hsiung Huang Advisor:Dr. Wei-I Lee

Department of Electrophysics
National Chiao Tung University

Abstract

Due to the lack of lattice-matched substrates, current nitride base devices are mainly hetero-epitaxially grown on lattice mismatched substrates. The large mismatches in lattice constants between substrates and epitaxial films cause high defects densities. Furthermore, differences in thermal expansion coefficients between substrates and epitaxial films induce large warpage or bowing of the epi-layers. While these disadvantages may not limit the performance of low current density devices, such as LEDs, they will certainly severely affect high current density devices, such as blue laser diodes and high power electronic devices. The availability of freestanding GaN substrates will provide the overgrown GaN epi-layers the advantages of reduced defects, less bowing, improved reliability, as well as greatly simplified device process afterwards. It is believed that free-standing nitride substrates will play vital roles in the next stage of GaN and InAlGaN devices development.

In this thesis, we used the HVPE system to study the GaN wafer fabrication.

Several methods for preventing the crack of GaN thick-film during the HVPE epitaxy process were used in this thesis, including the epitaxial lateral overgrowth, air-bridged, dot air-bridged, and temperature ramping technique. These methods can effectively preventing the crack of GaN thick-film in HVPE growth process. After the GaN thick-film prepared, the laser lift-off technique was used to separate the GaN thick-film from original substrate. The freestanding GaN thick-film was obtained after these processes. The characteristics of freestanding GaN were analysised by SEM, CL, Raman spectroscopy, PL, Hall measurement, HRXRD, AFM, and Normaski OM. Furthermore, the chemical properties of HVPE GaN were also studied by wet chemical etching. The activation energy was calculated of different crystal facets of GaN.

Overall, the thickness more than 300 μm freestanding GaN was obtained by these strain reduced methods. The color is transparent and the dislocation density is in the range of 10^6 to 10^7 cm^{-2}. The resistivity is about 0.09 Ω-cm. The undoped carrier concentration is about $1.6x10^{17}$ cm^{-3}. The FWHM of HRXRD rocking curve is about 150 aresec. The performance can be improved after increasing the thickness and optimizing the growth conditions.

The project of this thesis is dedicated to provide free-standing nitride substrates to other researchers in Taiwan in the future. It is hoped that we can hence provide a major new vehicle for our domestic research on nitride devices.

誌 謝

從進入交大唸博士班，很快的已經過了四年又一個月了，在這段時間嘗試了很多人生中的第一次：第一次在國際會議上站上台用英文報告、第一次投稿期刊論文、第一次寫專利、第一次寫大型計劃、第一次修全部用英文授課及討論的課程、第一次實驗室全體出動烤肉，第一次到大山背看螢火蟲……等等，有太多第一次的經驗可以回味，可以感動。

在這段期間首先要感謝李威儀老師全力的支持和指導，老師開放的指導方式可以使學生養成獨立思考的能力，還記得第一次到老師辦公室門口時，看到的博士學位與加拿大雁的故事，印象很深刻。其次要感謝碩士班的指導教授－杜立偉老師，在碩士班期間被訓練成的嚴謹做事態度，至今依然受用，也感謝杜老師在博士班期間量測設備上的支持。再來要感謝的是實驗室的博士班同學－豐格，雖然沒有一起畢業，但我還記得一起修課，一起考試的回憶，相信你的選擇對你的人生是正確的，祝福你。博士班學弟奎銘，你的加入讓我更無後顧之憂，可以放手進行更多的實驗構想，加油！下一個畢業的一定是你。還有在台大光電博士班的學弟虹諭，你的數據讓我的第一篇期刊論文順利誕生。碩班學弟妹，廷立、佩倫、宏瑋，你們對實驗室現有機台的架設幫忙很多。還有振豪，你的加入讓我們在MOCVD 上有強力的後援。還有其他碩士班的學弟妹，怡麟、子強、彥偉、溫壬、柄均、源根、文謙、治華、仲山、凱翔、偉誠、定儒，以及新加入的博士班生力軍－彥顯、尹豪，你們使我的領導規劃能力以及人生的體驗有更長足的進步。

還有工研院的蔡政達經理蔡董，感謝您給我機會可以進入工研院，開拓了更高的視野，劉柏均博士的共同討論，使我的經驗更加茁壯，郭義德郭大哥，主立、志銘、東煒，郁香姐，以及小媽瑞琴姐，還有許多工研院的伙伴，你們也都使我的實驗經驗受益良多。

再來要深深感謝的是我的父親－黃華山先生以及母親－丁麗敏女士，你們無怨無悔的付出，才有今天的我。還有我的兩位妹妹郁文、及郁惠，感謝妳們在我求學期間較沒有經驗能力時對父母親全心全力的照顧，使我可以安心求學，沒有後顧之憂，再來的責任就交給我吧！

還有我的未婚妻－妮婉，沒有妳的溫柔的全力支持，我沒辦法這麼快拿到學位。還有家中的阿貓阿狗－吉米、小藍波、Angel、皮蛋，你們在主人心情苦悶時總是不離不棄的陪在我身邊，讓我搔小肚肚，安慰主人的心。

套用陳之藩先生的一句話，要感謝的人太多了!那就謝天吧!

Contents

Chinese Abstract…………………………………………………………..……………i

English Abstract………………………….……………………………………………...iii

Acknowledge………………………………………………………………………………v

Contents……………………………………………………………………………………vii

Tablet Contents..x

Figure Contents…………………………………………..…….……………………..xi

Chapter 1 Introduction…………………………………………………………..………1

1.1 History of Gallium Nitride Base Optoelectronic Devices and Properties……….……………………………………………………………………1

1.1.1 History of GaN Devices…………………….………………………...1

1.1.2 Structure and Properties of GaN……………….……………………3

1.2 Introduction to Hydride Vapor Phase Epitaxy Technique…………………4

1.3 Effect of Strain in Gallium Nitride……………………………………….…...8

1.3.1 Calculation of strain in GaN Epitaxy Film……..…………...……...8

1.3.2 Effect of Emission in GaN on Strain…………………………..….10

1.3.3 Strain and Raman Spectrum in GaN……………………………..13

1.4 References……………………………………………………………………16

Chapter 2 Air-bridged Epitaxial Lateral Overgrowth......................................47

2.1 High-Void Air-Bridged Technique……………………………………..47

2.1.1 Introduction of Air-Bridged Technique…………………….………47

2.1.2 Experiment……………………………………………………49

2.1.3 Result and Discussion…………………………………………50

2.1.4 Conclusion……………………………………………………..54

2.2 Strain reduced GaN thick film grown by hydride vapor phase epitaxy

utilizing dot air-bridged structure……………………………………...54

2.2.1 Introduction……………………………………………………55

2.2.2 Experiment……………………………………………………56

2.2.3 Result and Discussion…………………………………………57

2.2.4 Conclusion……………………………………………………..60

2.3 References……………………………………………………………..62

Chapter 3 Using Temperature Ramping Technique to Grow Crack-Free

GaN Thick-Film by Hydride Vapor Phase Epitaxy…………..…..77

3.1 Introduction……………………………………………………………77

3.2 Experiment…………………………………………………….………78

3.3 Result and Discussion……………………………………….…………79

3.4 Conclusion……………………………………………………………..83

3.5 References……………………………………………………………..84

Chapter 4 Introduction to Laser Lift-off…………………..…………………94

4.1 Introduction to Laser Lift-Off Technique………………..……………..94

4.2 Laser Lift-Off System…………………………………………….…….97

4.3 Results and Discussion………………………………………..…..99

4.4 References…………………………………………………………103

Chapter 5 Extended Micro-tunnels in GaN Prepared by Wet Chemical Etch…………………………………………………………...118

5.1 Introduction……………………………………………………………..118

5.2 Experiment………………………………………………………….……..120

5.3 Result and Discussion……………………………………….………..121

5.4 Conclusion…………………………………………………………....127

5.5 References…………………………………………………………129

Chapter 6 Conclusion……………………………………………….…...144

Appendix A……………………………………...………………………...148

Publication List…………………………………...…...……………………...164

Tablet Contents

Tab. 1-1 The properties of gallium nitride……………………………………….28

Tab. 1-2 The methods of bulk GaN growth……………………………………...34

Tab. 1-3 Raman selection rule for optical phonon in wurtzite structure…………...44

Tab. 1-4 Familiar Raman phonon frequency values in wurtzite structure of GaN…45

Tab. 1-5 Raman calibration factor…………………………………………….46

Tab. 2-1 Thermal expansion coefficient of wurtzite crystal………….………..……76

Tab. 3-1 The properties of GaN wafer of NOD Lab………………………………93

Tab. 4-1 The Comparsion of Nd:YAG and excimer KrF lasers…………………..115

Tab. 5-1 Dangling bonds and surface energy of GaN facets……………………...142

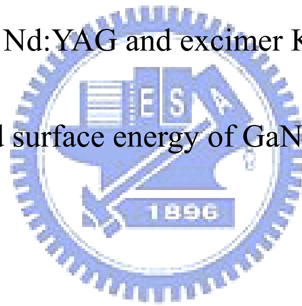

Figure Contents

Fig. 1-1 The applications of nitride base optoelectronic devices………………..23

Fig. 1-2 The optimum transform efficiency of different material in visible Region…………..……………………………………………………………24

Fig. 1-3 The evolution of solid state lighting from 1920………..………………..25

Fig. 1-4 The relationship of lattice constant and energy gap of different compound semiconductors……………..………………………………26

Fig. 1-5 The clinographic projection of the wurtzite structure of GaN. The c and a are the lattice constant……………………….……………………...27

Fig. 1-6 The phase diagram of GaN………………………..……………………..31

Fig. 1-7 The sketch of HVPE system……………………………..………………32

Fig. 1-8 The reactor of HVPE system………………………..………………...33

Fig. 1-9 The growth model in vapor phase epitaxy of GaN…………..………..35

Fig. 1-10 Equilibrium partial pressures of gaseous species inside the reactor……..38

Fig. 1-11 The Stress distribution in thick-film with substrate……………………...39

Fig. 1-12 The Band structures and respective transition in GaN…………………..40

Fig. 1-13 Strain dependence of the free exciton resonance energies in wurtzite GaN…………………………..……………………………………………41

Fig. 1-14 The scheme of Raman and Reyleigh scattering…………………………42

Fig. 1-15 Optical phonon modes in wurtzite structure crystal……………………..43

Fig. 2-1 Schematics and SEM images of the conventional pendeo and the HVAB structures after HVPE regrowth………………..……………65

Fig. 2-2 Plane and cross-sectional CL images of the conventional pendeo and the HVAB structures……………………..……………..……………66

Fig. 2-3 Schematics of growth mechanism and SEM images of initial state of the HVPE regrowth in the conventional pendeo structure and the HVAB structures…………………………………..………………67

Fig. 2-4 Azimuthal dependence of the FWHM of GaN (002) and (102) HRXRD rocking curve of the conventional pendeo and the HVAB structures......68

Fig. 2-5 Reciprocal space maps around the (002) point of c-plane GaN grown by HVPE……………………………………………..……………69

Fig. 2-6 Raman spectra of E_2(high) phonon frequency of the conventional pendeo and the HVAB structure……….……………………………70

Fig. 2-7 Schematic of the GaN thick-film fabrication process with the dot air-bridged structure by HVPE………………………………………71

Fig. 2-8 SEM image of the dot air-bridged structure…………..…………………72

Fig. 2-9 The CL image of GaN thick-film of the dot air-bridged structure……...73

Fig. 2-10 CL image and Raman spectra of the dot air-bridged Sample.......………74

Fig. 2-11 Photography of a 300 μm GaN thick-film in 1.5-inch diameter on 2-inch sapphire substrate without any crack……………..………..…75

Fig. 3-1 Schematic of the temperature ramping GaN growth by HVPE……….....86

Fig. 3-2 A 1.5 inch, 300 μm crack free GaN thick-film grown on sapphire substrate with temperature ramping step……………………………..87

Fig. 3-3 The cross-sectional CL images of temperature ramping layer at various ramping rate……………..……………………………………...88

Fig. 3-4 The CL and Raman spectra of cross-sectional regions of the sample with 1.0^{o}C/min ramping rate…………………..………………………89

Fig. 3-5 The rocking curve of HRXRD and CL image of the freestanding GaN with 1.0 ^{o}C/min ramping rate…………………………………………90

Fig. 3-6 A 2 inch, 360 μm-thick GaN on sapphire substrate before and after LLO Process……………………………………………………..…………91

Fig. 3-7 The CL image of a regrown 600 μm GaN thick-film……………………92

Fig. 4-1 The laser-lift-off process sketch…………………………..………105

Fig. 4-2 The thermally induced decomposition of nitride semiconductors using a heating rate of 0.3 K/s…………………………..…………………106

Fig. 4-3 The relation of decomposition depth caused by a single pulse and absorbed pulse intensity of the Nd:YAG laser……………..………107

Fig. 4-4 The sketch of the laser lift-off system……….………………………108

Fig. 4-5 The SEM images of the backside of GaN films after LLO process..…..109

Fig. 4-6 The plane view Raman spectra of GaN thick-film before and after LLO Process……………………………………………………………110

Fig. 4-7 The cross sectional Raman spectra of GaN thick-film before and after LLO process………………………………………………………...111

Fig. 4-8 The XRD rocking curve of GaN thick-film before and after LLO Process……………………………………………………………112

Fig. 4-9 The SEM images of GaN thick-film after LLO process in air ambient and nitrogen ambient…………………………………………………..113

Fig. 4-10 The experimentally determined epitaxial layer thickness as a function of diameter for fabrication complete GaN wafers……………………114

Fig. 4-11 The temporal and spatial variation of the temperature at GaN/sapphire interface……………..……………………………………………..116

Fig. 4-12 The beam profile of excimer 248 nm KrF and 355 nm Nd:YAG Lasers……………………..………………………..…………....117

Fig. 5-1 Cross sectional structure of the GaN sample prepared for chemical etch…………………………………………...………………..132

Fig. 5-2 Optical microscopic image of GaN EMTs after 30 minutes' etch in

molten KOH at 250 ^{o}C…………………………..……………………..133

Fig. 5-3 Cross sectional SEM images of GaN EMT along the $<1\bar{1}00>$ direction at different temperatures…………………..…………………………...134

Fig. 5-4 Cross-sectional SEM images of GaN EMTs along the $<11\bar{2}0>$ direction at different temperatures…………………..…………………………...135

Fig. 5-5 The bird-view cross-sectional SEM images of EMTs along the $<11\bar{2}0>$ direction and the insert along the $<1\bar{1}00>$ directions………………..136

Fig. 5-6 SEM images of cross section of GaN after the wet chemical etching with different directions…………………………………………………………..137

Fig. 5-7 Plot of the depth of GaN tunnels in different directions…………..……138

Fig. 5-8 Time-dependence of the etching depth of GaN tunnels at various Temperatures……………………………………………………………..139

Fig. 5-9 Cross sectional structure of GaN EMTs, beginning to form well-shaped triangular tunnels and forming larger triangular tunnels upon facet etching……………………………………………………………………140

Fig. 5-10 Arrhenius plot of etching rates of two crystal facets of GaN…..……..141

Chapter 1. Introduction

1.1 History of Gallium Nitride Based Optoelectronic Devices and Properties

1.1.1 History of GaN Devices

Nitride alloys (InN, GaN, AlN) represent the most promising class of optoelectronic materials, as shown in Fig. 1-1. The binaries and their alloys are direct bandgap semiconductors whose energy gaps cover the spectral region from the infrared to deep ultra violet. Nitride devices such as light emitting diodes, field effect transistors and laser diodes have various applications in traffic lights, full color displays, and LCD backlight among others. Most of these applications are based on GaN material and its alloys.

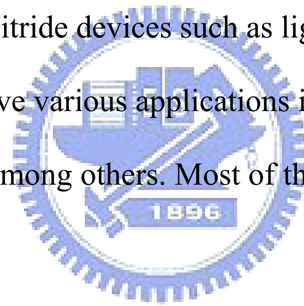

GaN material had been investigated for more than 60 years. However, due to the leak of a suitable substrate, the quality of GaN crystal remained poor until the 90s. In 1940, Juza and Hahn synthesized GaN from ammonia gas and hot gallium. This method produced only small needles and platelets. In 1969, Maruska and Tietjen employed chemical vapor deposition to make a large-area layer of GaN on sapphire substrate. In 1983, Yoshida *et al*. deposited a GaN layer at high temperature AlN buffer layer on sapphire substrate. Akasaki *et al*. first deposited a low-temperature (LT, approximately 600 ^{o}C) AlN buffer layer on sapphire substrate by metal-organic chemical vapor deposition (MOCVD). Then, they grew a high-quality mirror-like GaN after subsequent high temperature (rough 1000 ^{o}C) with an LT AlN buffer layer. In 1991, Nakamura *et al*. of Nichia Corp replaced the LT AlN buffer layer with an LT

GaN buffer layer to form a high-quality mirror-like GaN.

Another problem associated with GaN devices is the difficulty of obtaining p-type doped GaN. This problem was first solved in 1989 by Akasaki *et al*., who used the Cp_2Mg as the source of doping Mg ions in GaN during the growth process, and then employed low-energy electron beam irradiation (LEEBI) to scan the samples to yield p-type GaN. In 1992, Nakamura *et al*. found that an electron beam annealed the sample, breaking the Mg-H bonds. Annealing GaN:Mg at over 750 ^{o}C in N_2 or in a vacuum yielded the same results. All recent works have produced high-brightness visible LEDs, which are available today, and are especially contributed in the blue ray region.

In 1995, Nakamura *et al*. announced the fabrication of a high-quality green LED with InGaN quantum wells (QW) structure as the active layer.[2] It outperformed the blue-green LED whose active layer was fabricated with the double-heterostructure. The color of light of the QW LED can be changed from blue to yellow by changing the In content in InGaN QW. As the In content in InGaN QW increases, the ray color from the LED is shifted from blue to yellow. As the composition of In in InGaN increases, the quality of InGaN decreases. The intensity of InGaN QW LED decreases as the In content in InGaN increases. However, the human eye is more sensitive to green light than to blue light, as shown in Fig 1-2. Even though the intensity of the green LED is less than that of the blue LED, the green LED is brighter than blue LED for human eyes. The brightness of GaN LED increased very much in recent years. Figure 1-3 shows the evolution of lighting. In the future, nitride-based LEDs will be mainstream lighting.

Before 1996, most research groups utilized optical pumping technique to make the GaN laser diodes (LD). In 1996, Nakamura *et al*. of Nichia Corp. first reported a

GaN LD that could operate at room temperature. In the early stage of GaN LD development, the GaN LD was pulse-resonant, rather than continuously wave-lasing. In Dec. 1996, Nichia Corp. announced a continuous wave GaN LD, fabricated on c-plane sapphire substrate with an etched mirror facet. However, its lifetime was only 1s, which was too short for use in any application. The last two decades have seen the extensive development of the GaN LD. A GaN LD with a lifetime of more than 10000 h has been developed and commercialized.

1.1.2 Structure and Properties of GaN

The III-A group elements, B, Al, Ga and In can form the compounds with N, with the composition $A^{III}N$ as shown in Fig. 1-4. Most of the chemical bonds in these III-V compounds are covalent, with tetrahedral bonds at each atom. The GaN and its related III-V compounds can crystallize into the following three crystal structures: (1) zincblende, (2) wurtzite and (3) rock salt structures. However, under ambient conditions, the wurtzite structure is the more common thermodynamically stable phase. The rock salt structural phase transition takes place at high pressure, and the zincblende structure is a metastable. The zincblende and wurtzite structures are very closely related crystallographically. The bonds in zincblende and wurtzite are all tetrahedral. The Bravais lattice of the wurtzite structure is hexagonal and the c-axis is as perpendicularly to the hexagon. In the zincblende structures, the stacking layer is

$Ga_AN_AGa_BN_BGa_CN_CGa_AN_AGa_BN_BGa_CN_CGa_AN_AGa_BN_BGa_CN_C$……

While for the wurtzite structure, it is

$Ga_AN_AGa_BN_BGa_AN_AGa_BN_BGa_AN_AGa_BN_BGa_AN_AGa_BN_BGa_AN_A$……

Figure 1-5 shows the clinographic projection of the wurtzite structure of GaN. The space group of the wurtzite structure is C^4_{6V} ($P6_3mc$). It has two lattice parameters a and c in the ratio c/a = $\sqrt{8/3}$ = 1.633, as shown in Fig. 1-5. The wurtzite structure consists of two hexagonal close-packed (hcp) sublattices with a shift of u = 3/8 in fractional coordinates along the c axis. Every Ga (N) atom is surrounded by four N (Ga) atoms, which are arranged on the edges of a tetrahedron. The two inequivalent atomic positions are $(1/3, 2/3, 0)$ and $(1/3, 2/3, u)$, such that Ga atoms are at both $(0,0,0)$ and $(1/3, 2/3, 1/2)$, while N atoms at $(0,0,u)$ and $(1/3, 2/3, 1/2 + u)$. Yeh *et al*. defined two slightly different bond lengths,[3]

$$\mathrm{Re}(1) = u \times c \qquad \text{E(1-1)}$$

and

$$\mathrm{Re}(2) = a \times [1/3 + (1/2 - u)^2 \times (c/a)^2] \qquad \text{E(1-2)}$$

where u is the dimensionless internal structure parameter. Re(1) equals Re(2) for an ideal wurtzite structure.

Table 1-1 presents the other properties of GaN.

1.2 Introduction to Hydride Vapor Phase Epitaxy

The Hydride Vapor Phase Epitaxy (HVPE) technique was developed more than 30 years ago to grow GaP and GaAsP light emitting diodes (LEDs).[54] The HVPE technique was also applied to grow GaN-based devices. However, for the following

reasons, in the 80s, the attempt to use the HVPE technique to grow GaN was almost abandoned.

1、The leak of a suitable substrate for the homo-epitaxial growth of a GaN device and the large defect density make the quality of GaN devices uncontrollable.

2、The high growth rate of HVPE makes it unfavorable for growing GaN devices.

3、The p-type doping of GaN by HVPE is difficult.[55]

However, the high growth rate of GaN by HVPE can be exploited to produce GaN substrate. In the '90s, the focus of the application of HVPE shifted to the fabrication of a GaN substrate.[56,57]. The GaN substrate cannot be produced by conventional pulling-process synthetics because of the decomposition temperature of GaN is lower than its melting temperature, as shown in Fig. 1-6.[58] Several techniques have been used to prepare the GaN substrate, as shown in Tab. 1-2. In these techniques, HVPE is the most suitable method for preparing high-quality GaN substrates because it supports a high growth rate, and produces no impurity from such organic sources TMGa. In recent years, for reducing defect density including epitaxy lateral overgrowth (ELOG), pendeo and air-bridged techniques have been developed and combined with the HVPE technique for preparing GaN substrate.[59-62] High-quality GaN substrates can be obtained by combining of these techniques.

Figure 1-7 shows an HVPE system. The system consists of several sub-systems, including: a mass flow control system, an oven system, a pressure control system, an exhaust system and others. Figure 1-8 presents the concept that underlies the HVPE reactor. For HVPE GaN growth, the $GaCl_x$ and ammonia gases (NH_3) are used as Ga and nitrogen sources, respectively. $GaCl_x$ is generated by a reaction of gaseous HCl and Ga metal at 850 ^oC. It is then transported into the growth zone with a carrier gas to react with NH_3 gas. The reaction of $GaCl_x$ and NH_3 yields the GaN crystal in the

growth zone. Cadoret *et. al*. developed a theoretical model to explain to the growth mechanism of bulk GaN in HVPE.[63-69] The reactions are as follows.

Adsorption of NH_3 molecules

$$V + NH_{3(g)} \rightleftharpoons NH_3 \quad \text{(R1)}$$

Adsorption of N atoms by NH_3 decomposition

$$2NH_3 \rightleftharpoons 2N + 3H_{2(g)} \quad \text{(R2)}$$

Adsorption of GaCl molecules on N atoms

$$N + GaCl_{(g)} \rightleftharpoons NGaCl \quad \text{(R3)}$$

where the subscript *"g"* refers to gaseous species, and *"V"* is denotes a vacant site.

Two chlorine desorption mechanisms are considered.

H_2 and chlorine desorption mechanism:

$$2NGaCl + H_{2(g)} \rightleftharpoons 2NGa - ClH \quad \text{(R4)}$$

$$NGa - ClH \rightleftharpoons NGa + HCl_{(g)} \quad \text{(R5)}$$

$GaCl_3$ and chlorine desorption mechanism:

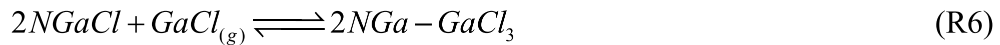

$$2NGaCl + GaCl_{(g)} \rightleftharpoons 2NGa - GaCl_3 \quad \text{(R6)}$$

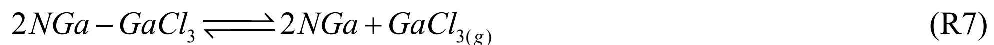

$$2NGa - GaCl_3 \rightleftharpoons 2NGa + GaCl_{3(g)} \quad \text{(R7)}$$

The two overall growth reactions corresponding to H_2 and $GaCl_3$, are as follows.

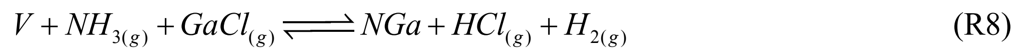

$$V + NH_{3(g)} + GaCl_{(g)} \rightleftharpoons NGa + HCl_{(g)} + H_{2(g)} \quad \text{(R8)}$$

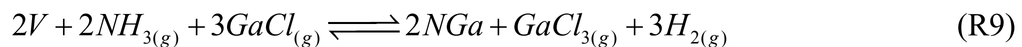

$$2V + 2NH_{3(g)} + 3GaCl_{(g)} \rightleftharpoons 2NGa + GaCl_{3(g)} + 3H_{2(g)} \quad \text{(R9)}$$

The main reactions can be reconstructed as below.

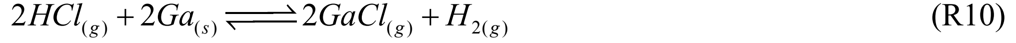

$$2HCl_{(g)} + 2Ga_{(s)} \rightleftharpoons 2GaCl_{(g)} + H_{2(g)} \qquad \text{(R10)}$$

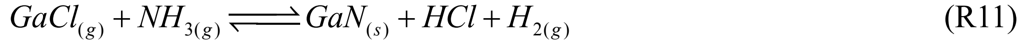

$$GaCl_{(g)} + NH_{3(g)} \rightleftharpoons GaN_{(s)} + HCl + H_{2(g)} \qquad \text{(R11)}$$

The HVPE GaN growth process yields such by-products as $GaCl_x$ and NH_4Cl. NH_4Cl is a white powders, easily coating the reactor or chamber when the temperature was lower than 150 ^{o}C.[70] The reaction is shown as below.

$$NH_{3(g)} + HCl_{(g)} \rightleftharpoons NH_4Cl_{(s)} \qquad \text{(R12)}$$

$$GaCl_{(g)} + 2HCl_{(g)} \rightleftharpoons GaCl_3 + H_2 \qquad \text{(R13)}$$

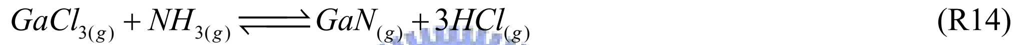

$$GaCl_{3(g)} + NH_{3(g)} \rightleftharpoons GaN_{(g)} + 3HCl_{(g)} \qquad \text{(R14)}$$

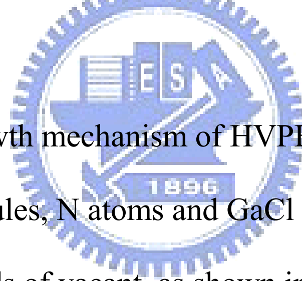

Figure 1-9 presents the growth mechanism of HVPE GaN. The first step includes the adsorptions of NH_3 molecules, N atoms and GaCl molecules. The NH_3 molecules are adsorbed by dangling bonds of vacant, as shown in Fig. 1-9(a)-(b) and the N atoms are produces by the decomposition of NH_3 that is adsorbed by GaCl molecules. The second step involves the H_2 and GaCl mechanisms, according to the one monolayer model of adsorption on the Ga face, as shown in Fig. 1-9(c)-(e). The one monolayer adsorption model and the Bragg-Willams model are adopted to elucidate the growth mechanism, using the surface coverage θ_i of one underlying Ga atom.[63]

$$\theta_V = 1 - \theta_{NH_3} - \theta_N - \theta_{NGaCl} - \theta_{HCl} - \theta_{GaCl_3} - \theta_{NGa} \qquad \text{(R15)}$$

The partial pressure of GaCl and $GaCl_3$ also influences the growth mechanism of HVPE GaN. If the temperature of metal Ga is not sufficiently high, then the HCl and metal Ga will form $GaCl_3$, which is responsible for the low growth rate of HVPE GaN.

However, when the temperature of the metal Ga is sufficiently high, all of the Ga forms GaCl favoring HVPE GaN growth. Figure 1-10 shows the partial pressures of the species involved in HVPE GaN growth. When the temperature exceeds 600 ^{o}C, almost all metal Ga forms GaCl with HCl gas. When the temperature is lower than 400 ^{o}C, the partial pressure of $GaCl_3$ exceeds that of GaCl, reducing the growth rate of HVPE GaN.

1.3 Effect of Strain in Gallium Nitride

The issue of stress during GaN growth is very important in the fabrication of III-nitride semiconductor devices and thick-film epitaxy. Stress in the epitaxial films causes various problems, such as film cracking, reduced etching protection decrease, weakened adhesion between film and substrate, variations in toughness and hardness and a shift in the emission peak. In HVPE GaN thick-film growth, a large strain commonly causes the film to crack and bow. X-ray diffraction (XRD), photoluminescence (PL), cathodluminescence (CL), and Raman spectra are typically adopted to measure the strain of epitaxial films. This section considers the relevant theory, and subsequent chapter will present relevant experimental results.

1.3.1 Calculation of Strain in GaN Epitaxy Film

Stress analysis is necessary to control the growth of a GaN thick-film without any cracks. However, the analysis of stress in a thick film is more complex than that in a thin-film. Stress analysis in a thick film must be consistent with experiment data. This section refers thin-film stress analysis to calculate the stress associated with

hetero-epitaxy.

The stress in an epitaxial film consists of the internal stress σ_I, the external stress σ_E and the thermal stress σ_{TH}. The total stress in epitaxal film is

$$\sigma = \sigma_I + \sigma_E + \sigma_{TH} . \tag{E(1-3)}$$

The internal stress is caused by dislocations, point defects, cracking, boundary layers, stacking fault, and impurities in the crystal. The external stress is normally caused by a lattice mismatch between the epitaxial film and the original substrate, and thermal stress is caused by the difference between the TEC of the epitaxial film and that of the original substrate.

The thermal stress is the main residual stress in the growth of a thick GaN film.

$$\sigma_{TH} = Y_f(\alpha_f - \alpha_s)\Delta T \tag{E(1-4)}$$

After cooling from the growth temperature, if the α_f exceeds α_s, then the epitaxial film is under tensile stress. The epitaxial film and substrate are concave. Otherwise, α_f is less than α_s, and the epitaxial film is under compressive stress. The epitaxial film and substrate are convex form. The relationship between stress and strain is

$$\varepsilon_x = \frac{1}{Y_f}(\sigma_x - v\sigma_y) \tag{E(1-5)}$$

$$\varepsilon_y = \frac{1}{Y_f}(\sigma_y - v\sigma_x) \tag{E(1-6)}$$

$$\varepsilon_z = \frac{-1}{Y_f}(\sigma_x - v\sigma_y) , \tag{E(1-7)}$$

where Y is the Young's Modulus and v is the Poison ratio of the epitaxial film. The equations E(1-5)-E(1-7) can be rewritten as

$$\varepsilon_x + \varepsilon_y = \frac{1+v}{Y_f}(\sigma_x + \sigma_y) \tag{E(1-8)}$$

$$\varepsilon_z = \frac{-v}{1-v}(\varepsilon_x + \varepsilon_y)\,. \qquad \text{E(1-9)}$$

σ_x equals σ_y in a 2-D isotropic system, and

$$\varepsilon_z = \frac{-2v}{1-v}\varepsilon_x\,. \qquad \text{E(1-10)}$$

If the wafer is circular, then $\sigma_x+\sigma_y$ equals σ_r and $\varepsilon_x+\varepsilon_y$ equals ε_r, and equations E(1-8) and E(1-9) can be rewritten as

$$\varepsilon_r = \frac{1-v}{Y}\sigma_r \qquad \text{E(1-11)}$$

$$\varepsilon_z = \frac{-v}{Y}\sigma_r\,. \qquad \text{E(1-12)}$$

The r is the radius of curvature of a bowing epitaxial film, and d is the length of the curve in the no-stress plane. The maximum strain is Δd/d, as shown in Fig 1-11.

$$\frac{d}{r} = \frac{\Delta d}{t_f/2} \quad \text{or} \quad \frac{1}{r} = \frac{\Delta d/d}{t_f/2} = \frac{\varepsilon_{\max}}{t_f/2} \qquad \text{E(1-13)}$$

The strain in the no-stress plane is zero, and the stress linearly increases with distance z, as shown in Fig. 1-11. Therefore,

$$\frac{\varepsilon_f(z)}{z} = \frac{\varepsilon_{\max}}{t_f/2} = \frac{1}{r} \qquad \text{E(1-14)}$$

Equations E(1-14) to E(1-11) yield the stress of the epitaxial film.

$$\sigma_f(z) = \left(\frac{Y}{1-v}\right)_f \varepsilon_f(z) = \left(\frac{Y}{1-v}\right)_f \frac{z}{r} \qquad \text{E(1-15)}$$

1.3.2 Effect of Emission in GaN on Strain

In hetero-epitaxy GaN films, a large lattice mismatch and a difference between the thermal expansion coefficients of GaN alloy and the foreign substrate lead to strain in

the lateral plane of GaN. Residual biaxial strains are known to change the valence band structure, which change is reflected in the optical spectra near the band gap. However, the strain reduces the density of states of the topmost valence bands for the laser action.

Calculations of the effect of strain in the valence band of GaN that are required to analyze the experimental data are presented, which summarize the strain ε_{zz} dependence of the A, B, C exciton resonance energizers.

Consider the valence band near the Γ point in the Brillouin zone under biaxial strain.

$$\varepsilon_{xx} = \varepsilon_{yy} = -\frac{1}{2}\frac{C_{33}}{C_{13}}\varepsilon_{zz} \qquad \text{E(1-16)}$$

and

$$\varepsilon_{yz} = \varepsilon_{zx} = \varepsilon_{xy} = 0 \qquad \text{E(1-17)}$$

where C_{ij} denote the constant components of the elastic stiffness. The Hamiltonian for wurtzite GaN is given by the following 6×6 matrix.

$$H_{6\times6} = \begin{pmatrix} H_{11} & H_{12} \\ H_{21} & H_{22} \end{pmatrix} \qquad \text{E(1-18)}$$

where

$$H_{11} = \begin{pmatrix} F & 0 & -H^* \\ 0 & G & \Delta \\ -H & \Delta & \lambda \end{pmatrix} \qquad \text{E(1-19)}$$

$$H_{12} = \begin{pmatrix} 0 & K^* & 0 \\ -H^* & 0 & K^* \\ 0 & I^* & 0 \end{pmatrix} \qquad \text{E(1-20)}$$

$$H_{21} = \begin{pmatrix} 0 & -H & 0 \\ K & 0 & I \\ 0 & K & 0 \end{pmatrix} \qquad \text{E(1-21)}$$

$$H_{22} = \begin{pmatrix} \lambda & \Delta & I^* \\ \Delta & G & 0 \\ I & 0 & F \end{pmatrix} \quad \text{E(1-22)}$$

The symbols are defined as follows.

$\Delta = \sqrt{2}\Delta_3$, $H = i(A_6 k_z k_+ + D_6 \varepsilon_{z+} + A_7 k_+)$, $I = i(A_6 k_z k_+ + D_6 \varepsilon_{z+} - A_7 k_+)$

$F = \Delta_1 + \Delta_2 + \lambda + \theta$, $G = \Delta_1 - \Delta_2 + \lambda + \theta$, $K = A_5 k_+^2 + D_5 \varepsilon_+$

$\lambda = A_1 k_z^2 + A_2 k_\perp^2 + D_3 \varepsilon_{zz} + D_4 \varepsilon_\perp$, $\theta = A_3 k_z^2 + A_4 k_\perp^2 + D_3 \varepsilon_{zz} + D_4 \varepsilon_\perp$

with

$k_+ = k_x + i k_y$, $k_\perp^2 = k_x^2 + k_y^2$

$\varepsilon_{z+} = \varepsilon_{xz} + i\varepsilon_{yz}$, $\varepsilon_\perp = \varepsilon_{xx} + \varepsilon_{yy}$, $\varepsilon_+ = \varepsilon_{xx} - \varepsilon_{yy} + 2i\varepsilon_{xy}$

The *k, ε, Ai* (*i*=1-7) and *Di* (*i*=1-6) represents the wave vector, the strain, the valence band parameter and the deformation potential constants, respectively. Δ_1 is the crystal-field splitting and the $3\Delta_2$ is typically set equal to $3\Delta_3$ which is called the spin-orbit splitting, as shown in Fig. 1-12. For simplicity, the quantities Δ_i, A_i, and D_i were approximated as follows.[75]

$\Delta_2 = \Delta_3$, $4A_5 - \sqrt{2}A_6 = -A_3$, $2A_4 = -A_3 = A_1 - A_2$, $A_7 = 0$, $4D_5 - \sqrt{2}D_6 = -D_3$

$2D_4 = -D_3 = D_1 - D_2$,

In determining the eigenvalue of Eq. E(18), the energies at the Γ point, *k*=0, are

$$E_A^0 = \Delta_1 + \Delta_2 \quad \text{E(1-23)}$$

$$E_{B,C}^0 = \frac{1}{2}(\Delta_1 - \Delta_2) \pm [\frac{1}{4}(\Delta_1 - \Delta_2)^2 + 2\Delta_2^2]^{1/2} \quad \text{E(1-24)}$$

for the strain-free crystal, and

$$E_A^1 = E_A^0 + (D_1 - \frac{C_{33}}{C_{13}} D_2)\varepsilon_{zz} + (D_3 - \frac{C_{33}}{C_{13}} D_4)\varepsilon_{zz} \quad \text{E(1-25)}$$

$$E_{B,C}^{1} = \frac{1}{2}[\Delta_1 - \Delta_2 + (D_3 - \frac{C_{33}}{C_{13}} D_4)\varepsilon_{zz}] + (D_1 - \frac{C_{33}}{C_{13}} D_2)\varepsilon_{zz} \pm \{\frac{1}{4}[\Delta_1 - \Delta_2 + (D_3 - \frac{C_{33}}{C_{13}} D_4)\varepsilon_{zz}]^2 + 2\Delta_2^2\}^{1/2} \quad \text{E(1-26)}$$

for the crystal under the biaxial strain. Here, the subscripts correspond to the plus and minus signs in Eq. E(24) and E(16), respectively. C_{13} and C_{33} are the elastic constants.

Figure 1-13 shows the A, B, and C exciton ground state resonance energies and the first excited resonance energy of A exciton as a functions of ε_{zz}. The resonance energies E_A, E_B, E_C, and $E_{A,n=2}$ increase with ε_{zz} increasing. The ground state binding energy of the A-exciton, $E_{ex,A}$ is independent of strain.[76] The least square fit to the data of E_A and $E_{A,n=2}$ yields

$$E_A = 3.478 + 15.4\varepsilon_{zz} \quad \text{E(1-27)}$$

$$E_{A,n=2} = 3.498 + 15.4\varepsilon_{zz} \quad \text{E(1-28)}$$

The difference between the E_A and $E_{A,n=2}$, $E_{ex,A}$, is calculated to be 26 meV. The curve of the A-exciton is linear and the slope is 15.4 eV. The nonlinear least-square method yields Δ_1, Δ_2=Δ_3, and

$$D_3 - \frac{C_{33}}{C_{13}} D_4 = 23.6eV\ . \quad \text{E(1-29)}$$

1.3.3 Strain and Raman Spectrum in GaN

Raman scattering spectroscopy is an effective method for studying molecular vibration. Raman scattering was discovered by Raman in 1928. However, before the ‘60s, Raman spectra were very weak because high-power and highly pure light sources were unavailable. Such a source, the laser, was developed in that decade, and was a suitable light source for producing Raman spectra.

When incident photons exchange energy with the phonons, Raman scattering

occurs. When the incident photons do not exchange energy with the phonons, Rayleigh scattering occurs. Figure 1-14 presents Raman and Reyleigh scatterings. Raman spectroscopy measures the change of the photons upon scattering with phonons, as follows (where the wavenumber, Δω, is measured in Δcm^{-1}.)

$$\Delta\omega = \frac{\Delta E}{hc} \qquad E(1.30)$$

When the scattering photons obtain energy from the phonons, Stokes scattering occurs, and is evident in the Raman spectrum: otherwise, the scattering is anti-Stokes scattering. Raman spectra are typically obtained from Stokes scattering because the signal intensity of Stokes scattering exceeds that from anti-Stoke scattering.

Phonons in wurtzite structure at the Γ point (k=0) have eight modes - $2A_1+2E_1+2E_2+2B_1$. One of the A_1 and one of the E_1 modes are acoustic phonon modes. The remaining six phonon modes, $A_1+E_1+2E_2+2B_1$, are optical. Figure 1-15 schematically presents the atomic displacement associated with these optical phonon modes. The B1 modes are silent modes in both Raman and IR spectra because the plus and minus directions of ionic vibration are the same, and so on dipole moment is not generated to interact with the photons. If the atomic displacement is parallel to the wavevector $\vec{k}$, then the optical phonon modes are called longitudinal optical modes (LO). Otherwise, the atomic displacement is perpendicular to the wavevector $\vec{k}$, then the optical phonon modes are called transverse optical (TO) modes. The Raman spectrum from a wurtzite structure has six active optical phonon modes A_1(LO), A_1(TO), E_1(LO), E_1(TO), E_2(low) and E_2(high). The Raman spectrum is sensitive to the polarization of the incident and scattered photons in a manner that determines the selection rules of the Raman spectral measurement, which, along with familiar values are presented in Tables 1-3 and 1-4.[6-8]

Phonon transport in crystal is limited by the mean free path of phonons and the stress. The mean free path of phonon vibration in a crystal is called the confinement length, L, which decreases as the density of defects and dislocations, N, increases.

$$L = \frac{1}{\sqrt[3]{N}} \qquad \text{E(1.31)}$$

Reducing L broadens and shifts the Raman phonon frequency signal. Another factor that affects the Raman phonon frequency shift is the strain. However, in most cases of strain analysis by Raman spectroscopy of wurtzite GaN, the effect of L is neglected, because the strain of GaN caused by the hetro-epitaxy is large and the difference between TEC values is large in most cases.[80-83] The residual thermal strain can therefore be estimated using the expression for the Raman spectrum shift,

$$\Delta\omega_\lambda = [a_1\varepsilon_{zz} + a_2(\varepsilon_{xx} + \varepsilon_{yy})] + [b_1\varepsilon_{zz} + b_2(\varepsilon_{xx} + \varepsilon_{yy})] \qquad \text{E(1.32)}$$

where a_1, a_2, b_1 and b_2 are the deformation constants. In the wurtzite structure, the equation E(1.3.30) can be rewritten as

$$\Delta\omega_\lambda = [\frac{C_{33}}{(C_{11} + C_{12})C_{33} - 2C_{13}{}^2}(2p_\lambda + q_\lambda r)]\sigma_{xx} \equiv K_\lambda^R \sigma_{xx} \qquad \text{E(1.33)}$$

where $q_\lambda = a_1 + b_1$, $p_\lambda = a_2 + b_2$, and $r = \frac{\varepsilon_{zz}}{\varepsilon_{xx}} = \frac{-2C_{13}}{C_{33}}$. K_λ^R is defined as the coefficient of σ_{xx}. Table 1-5 summarizes of K_λ^R, which is defined as the Raman calibration factor, obtained by various research groups. K_λ^R can be used to calculate the stress of GaN from the Raman phonon frequency shift.

1.4 References

1 M. S. Shur, and R. F. Davis, GaN-BASED MATERIALS AND DEVICES: Growth, Fabrication, Characterization and Performance, World Scientific, **33** (2004).

2 S. Nakamura, M. Senoh, N. Iwasa, S. Nagahama, T. Yamada, and T. Mukai, *Jpn. J. Appl. Phys.* **34**, L1332 (1995).

3 C. Y. Yeh, Z. W. Lu, S. Froyen, and Alex Zunger, *Phys. Rev. B.* **46**, 10086 (1992).

4 J. I. Pankove, and T. D. Moustakas, Gallium Nitride (GaN) I: Semiconductors and Semimetals, Acdemic Press (1998).

5 S. Nakamura et al., The Blue Laser Diode: The Complete Story, Springer (2000).

6 S. Nakamura et al., Introduction to Nitride Semiconductor Blue Lasers and Light Emitting Diodes, Taylor and Francis (2000).

7 V. W. L. Chin, T. L. Tansley, and T. Osotchan, *J. Appl. Phys*. **75**, 7365(1994).

8 H. Harima, *Journal of Physics: Cond. Matter.* **14**, R967 (2002).

9 S. N. Mohammad, and H. Morcoc, *Prog. Quant. El.*, **20**, 361 (1996).

10 Monemar, *J. Material Sci.: materials in Electronics*, **10**, 227 (1999).

11 S. Strite, H. Morcoc, *J. Vac. Sci. Technol. B.*, **10**, 1237 (1992).

12 R. Goldhan, S. Shokhovets, in III-nitride semiconductors optical properties II, M. O. Manasreh, H. X. Jiang, editors, Taylor&Francis, 73 (2002).

13 I. Vurgaftman, J.R. Meyer, L.R. Ram-Mohan, *J. Appl. Phys.*, **89**, 5815 (2001).

14 V. M Bermudez, C.-I. Wu, A.Khan, *J. Appl. Phys.*, **89**, 1991 (2001).

15 V. YU. Davydov,Yu. E. Kitaev, I. N. Goncharuk, A. N. Smirnov, J. Graul, O. Semchinova, D. Uffmann, M. B. Smirnov, A. P. Mirgorodsky, and R. A. Evarestov, *Phys. Rev.B.*, **58**, 12899(1998).

16 W. J. Moore, J. A. Freitas, Jr., S. K. Lee, S. S. Park, and J. Y. Han, *Phys. Rev. B.*,

65, 081201/1 (2002).

17 M. Wraback, H. Shen, J. C. Carrano, T. Li, J. C. Campbell, M. J. Schurman, and I. T. Ferguson, *Appl. Phys. Lett.*, **76**, 1155 (2000).

18 M. Fanciulli, T. Lei, T. D. Moustakas , *Phys. Rev. B.*, **48**, 15144 (1993).

19 R. Stepniewski, A. Wysmolek, K. P. Korona, and J. M. Branowski, in III-nitride semiconductors optical properties I, M. O. Manasreh, H. X. Jiang, editors, Taylor & Francis, 197 (2002).

20 M. Leszczynski, H. Teisseyre, T. Suski, I. Grzegory, M. Bockowski, and J. Jun, *Appl. Phys. Lett.*, **69**, 73 (1996).

21 B. Heying, I. Smorchkova, C. Poblenz, C. Elsass, B.Fini, S. Den Baars, U. Mishra, and J.S. Speck, *Appl. Phys. Lett.*, **77**, 2885 (2000).

22 D. C. Look, C. E. Stutz, R. J. Molnar, K. Saarinen and Z. Liliental-Weber, Solid State Comm. **117**, 571 (2001).

23 S. Nakamura, T. Makui, and M. Senoh, *J. Appl. Phys.*, **71**, 5543 (1992).

24 J. G. Kim, A. C. Frenkel, H. Liu and R. M. Park, *Appl. Phys. Lett.*, **65**, 91 (1994).

25 D. K. Gaskill, L. B. Rowland, K. Doverspike, (in Properties of Group III Nitrides, Ed. by J. Edgar), EMIS Datareviews series No. **11**, 101 (1995).

26 D. J. As, D. Schikora, A. Greiner, M. Lubbers, J. Mimkes, and K. Lischka, *Phys. Rev. B.*, **54**, R11118 (1996).

27 J. R. L. Fernandez, V. A. Chitta, E. Abramof, A. Ferreira da Silva, J. R. Leite, A. Tabata, D. J. As, T. Frey, D. Schikora, and L. Lischka, (in: GaN and Related Alloys - 1999. Symposium (Materials Research Society Symposium Proceedings Vol.595); Warrendale, PA, USA : Mater. Res. Soc. (2000).

28 J. F. Muth, J. D. Brown, M. A. L. Johnson, Zhonghai Yu, R. M. Kolbas, J. W. Cook, Jr., J. F. Schetzina, *MRS Internet J. Nitride Semicond. Res.*, **4S1**, G5.2

(1999).

29 G. Yu, G. Wang, H. Ishikawa, M. Umeno, T. Soga, T. Egawa, J. Watanabe, and T. Jimbo, *Appl. Phys. Lett.*, **70**, 24, 3209 (1997).

30 S. Bloom, G. Harbeke, E. Meier, I. B. Ortenburger, *phys. stat. Solidi.*, **66,** 161 (1974).

31 R. Dingle, D. D. Sell, S. E. Stokowski, P. J. Dean and B. Zetterstrom, *Phys. Rev. B.*, **3**, 497500 (1971).

32 X. Zhang, Y. T. Hou, Z. C. Feng, and J. L. Chen, *J. Appl. Phys.*, **89**, 6165 (2001).

33 O. Ambacher, W. Rieger, P. Ansmann, H. Angerer, T. D. Moustakas and M. Stutzman, *Sol. State Comm.*, **97**, 365 (1996).

34 J. F. Muth, J. H. Lee, I. K. Shmagin, R. M. Kolbas, H. C. Casey, Jr., B. P. Keller, U. K. Mishra, and S. P. DenBaars, *Appl. Phys. Lett.*, **71**, 2572 (1997).

35 T. J. Schmidt, J. J. Song, in III-nitride semiconductors optical properties II, M. O. Manasreh, H. X. Jiang, editors, Taylor&Francis, p.3 (2002).

36 R. F. Davis, A. M. Roskowski, E. A. Preble, J. S. Speck, B. Heying, J. A. Freitas, Jr. Glaser, E. R., and W.E. Carlos, Proceedings of the IEEE **90**, 993 (2002).

37 H. X. Jiang, J. Y. Lin, and W. W. Chow, in III-nitride semiconductors optical properties I, M. O. Manasreh, H. X. Jiang, editors, Taylor&Francis, p960 (2002).

38 B. Monemar, J. P. Bergman, H. Amano, I. Akasaki, T. Detchprohm, K. Hiramatsu, N. Sawaki, Int. Symp. on Blue Laser and Light Emiting diodes, Chiba Univ., Japan, March 5 (1996).

39 J. Holst, L. Eckey, A. Hoffmann, I. Broser, B. Schottker, D. J. As, D. Schikora and K. Lischka, *Appl. Phys. Lett.*, **72**, 1439 (1998).

40 J. Wu, H. Yaguchi, K. Onabe, in III-nitride semiconductors optical properties II, M. O. Manasreh, H. X. Jiang, editors, Taylor&Francis, p.363 (2002).

41 J. C. Nipko, C. K. Loong, C. M. Balkas, R. F. Davis, *Appl. Phys. Lett.*, **73**, 3435(1998).

42 I. Barin, O. Knacke, and O. Kubaschewski, Thermochemical properties of inorganic substances, Springer-Verlag, Berlin-Heidelberg-New York (1977).

43 D. I. Florescu, V. M. Asnin, F. H. Pollak, R. J Molnar, and C. E. C. Wood, *J. App. Phys.*, **88**, 3295 (2000).

44 Kotchetkov, D. J. Zou, A. A. Balandin, D. I. Florescu, and F. H Pollak, *Appl. Phys. Lett.*, **79**, 4316 (2001).

45 E. K. Sichel, J. I. Pankove, *J. Phys. Chem. Solids.*, **38,** 330 (1977).

46 J. Zou, D. Kotchetkov, A. A. Balandin, D. I. Florescu, and F. H. Pollak, *Journal of Applied Physics.*, **92**, 2534 (2002).

47 A. Polian, M. Grimsditch, and I. Grzegory, *J. Appl. Phys.*, **79**, 3343 (1996).

48 A. F. Wright, *J. Appl. Phys.*, **82**, 2833 (1997).

49 F. Bernardini, V. Fiorentini, *Appl. Phys. Lett.*, **80**, 4145 (2002).

50 A. D. Bykhovski, B. L. Gelmont, and M. S. Shur, *J. Appl. Phys.*, **81**, 6332 (1997).

51 I. L. Guy, S. Muensit, E. M. Goldys, *Appl. Phys. Lett.*, **75**, 4133 (1999).

52 A. Zoroddu, F. Bernardini, P. Ruggerone, V. Fiorentini, *Phys. Rev. B.*, **64**, 045208/1 (2001).

53 M. S. Shur, B. Gelmont and A. Khan, J. Electronic Materials **25**, 777 (1996).

54 H. Maruka et. al, Appl. Phys. Lett. **15**, 327 (1969).

55 R. J. Molnar et. al, J. Cryst. Growth **178**, 147 (1997).

56 K. Naniwae, S. Itoh, H. Amano, K. Itoh, K. Hiramatsu, and I. Akasaki, J. Cryst. Growth **99**, 381 (1990).

57 S. T. Kim, Y. J. Lee, D. C. Moon, C. H. Hong, T. K. Yoo, J. Cryst. Growth **194**,

37 (1998).

58 W. Utsumi, H. Saitoh, H. Kaneko, T. Watanuki, K. Aoki and O. Shimomura, Nature Mater. **2**, 735 (2003).

59 T. S. Zheleva, S. A. Smith, D. B. Thomson, T. Gehrke, K. J. Linthicum, P. Rajagopal, E. Carlson, W. M. Ashmawi, and R. F. Davis, MRS Internet J. Nitride Semicond. Res. **4S1**, G3.38 (1999).

60 N. N. Morgan, Y. Zhizhen, X. Yabou, Materials Science and Engineering **B90**,201 (2002).

61 B. Beaumont, M. Vaille, G. Natat, A. Bouillé, J. C. Guillaume, P. Vénnègues, S. Haffouz, and P. Gibart, MRS Internet J. Nitride Semicond. Res. **3**, 20 (1998).

62 Y. Chen, R. Schneider, S. Wang, R. S. Kern, C. H. Chen, and C. P. Kuo, Appl. Phys. Lett. **75**, 2062 (1999).

63 R. Cadoret, et al, J. Cryst. Growth **205**, 123 (1999).

64 E. Aujol, J. Napierala, A. Trassoudaine, E. Gil-Lafon, R. Cadoret, J. Cryst. Growth **222**, 538 (2001).

65 R. Cadoret, and A. Trassoudaine, J. Phys. Condens. Matter **13**, 6893 (2001).

66 A. Trassoudaine, R. Cadoret, E. Gil-Lafon, J. Cryst. Growth **260**, 7 (2004).

67 E. Aujol, A. Trassoudaine *, D. Castelluci, R. Cadoret, Mater. Sci. Eng. **B 82**, 65 (2001).

68 A. Trassoudaine1, E. Aujol, P. Disseix, D. Castelluci, and R. Cadoret, Phys. Stat. b Sol. (a) **176**, 425 (1999).

69 R. Cadoret, A. Trassoudaine1, and E. Aujol, Phys. Stat. Sol. (a) **183**, 5 (2001).

70 R. J. Molnar, et al, J. Cryst. Growth **178**, 147 (1997).

71 H. Lee, j. S. Harris, Jr. J. Cryst. Growth **169**, 689 (1996).

72 D. K. Schroder, Semiconductor material and Device characterization, 2nd, John

Wiley & Sons (1998).

73 H. Luth, Surface and Interfaces of Solid materials, 3rd, Springer Verlag, Berlin Heidelberg (1995).

74 K. N. Tu, J. W. Mayer, L. C. Feldman, Electronic Thin Film Science: For Electrical Engineers & Material Scientists, Macmillan college publishing company (1992).

75 G. L. Bir, G. E. Pikus, Symmetry and Strain-Induced Effects in Semiconductors, John Wiley & Sons, New York, USA (1974).

76 J. J. Hopfield, *J. Phys. Chem. Solids* **15**, 97 (1960).

77 H. Harima, *J. Phys.: Condens. Matter* **14**, R967 (2002).

78 T. Azuhata, T. Sota, K. Suzuki, and S. Nakarmura, *J. Phys.: Condens. Matter.* **7**, L129 (1995).

79 H. Siegle, L. Eckey, A. Hoffmann, C. Thomsen, B. K. Meyer, D.Schikora, M. Hankeln, and K. Lischka, *Solid State Comm.* **96**, 943 (1995).

80 F. C. Wang, C. L. Cheng, Y. F. Chen, C. F. Huang, and C. C. Yang, *Semicond. Sci. Technol.* **22**, 896 (2007).

81 J. M. Wagner, F. Bechstedt, *Phys. Rev. B* **66**, 115201 (2002).

82 S. Tripathy, R. K. Soni, H. Asahi, K. Iwata, R. Kuroiwa, K. Asami, S. Gonda, *J. Appl. Phys*. **85**, 8386 (1999).

83 P. Puech, F. Demangeot, J. Frandon, C. Pinquier, M. Kuball, V. Domnich, Y. Gogotsi, *J. Appl. Phys*. **96**, 2853 (2004).

84 F. Bertram, T. Riemann, J. Christen, A. Kaschner, A. Hoffmann, K. Hiramatsu, T. Shibata, and N. Sawaki, *Meterials Science and Engineering B* **59**, 117 (1999).

85 M. Kuball, M. Benyoucef, B. Beaumont, and P. Gibart, *J. Appl. Phys.* **90**, 3656 (2001).

86 T. Kozawa, T. Kachi, H. Kano, H. Nagase, N. Koide, K. Manabe, *J. Appl. Phys*. **77**, 4389 (1995).

87 C. Kisielowski, J. Kruger, S. Ruvimov, T. Suski, J. W. Ager, E. Jones, Z. L. Weber, M. Rubin, E. R. Weber, M. D. Bremser, R. F. Davis, *Phys. Rev. B* **54**, 17745 (1996).

88 V. Yu. Davydov, N. S. Averkiev, I. N. Goncharuk, D. K. Nelson, I. P. Nikitina, A. S. Polkovnikov, A. N. Smirnov, M. A. Jacobson, and O. K. Semchinova, *J. Appl. Phys*. **82**, 5097 (1997).

89 F. Demangeot, J. Frandon, P. Baules, F. Natali, F. Semond, J. Massies, *Phys. Rev. B* **69**, 155215 (2004).

90 S. Nakamura, and S. F. Chichibu, Introduction to Nitride Semiconductor Blue Lasers and Light Emitting Diodes, Taylor & Francis (2000).

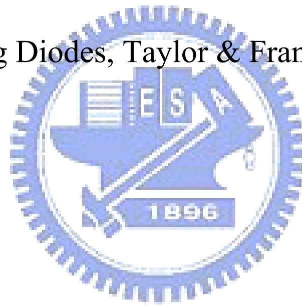

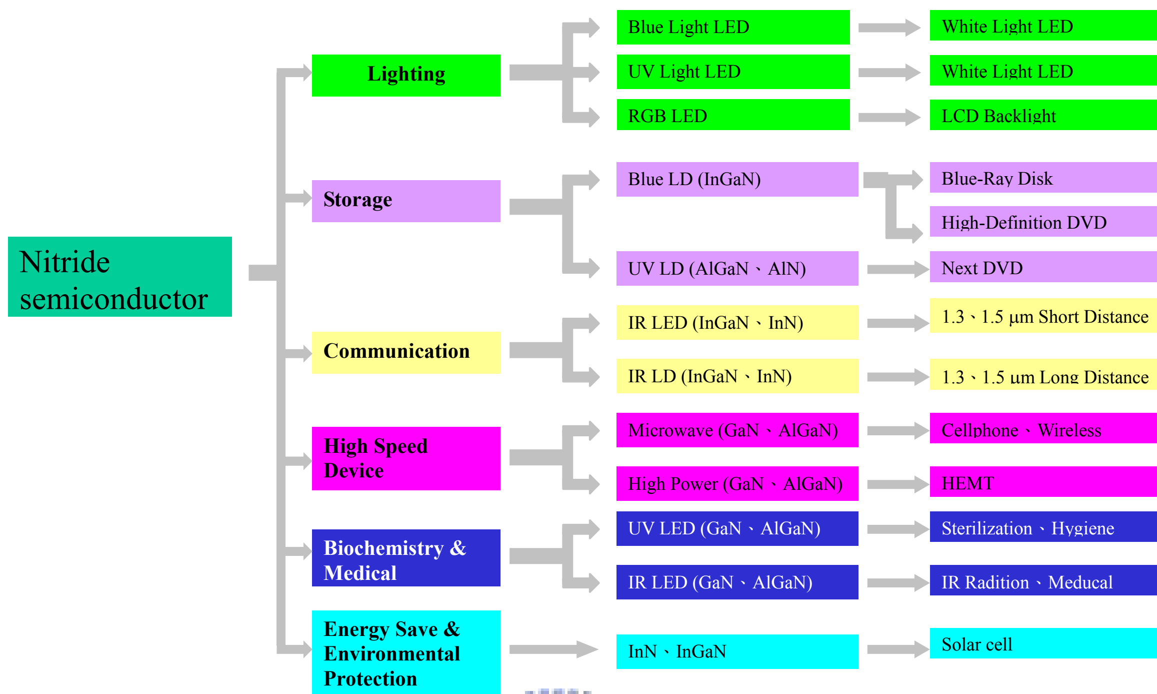

Fig. 1-1 The applications of nitride base optoelectronic devices

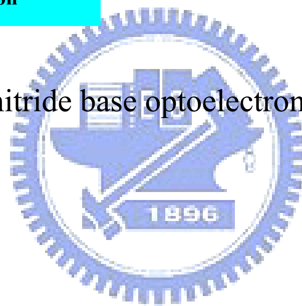

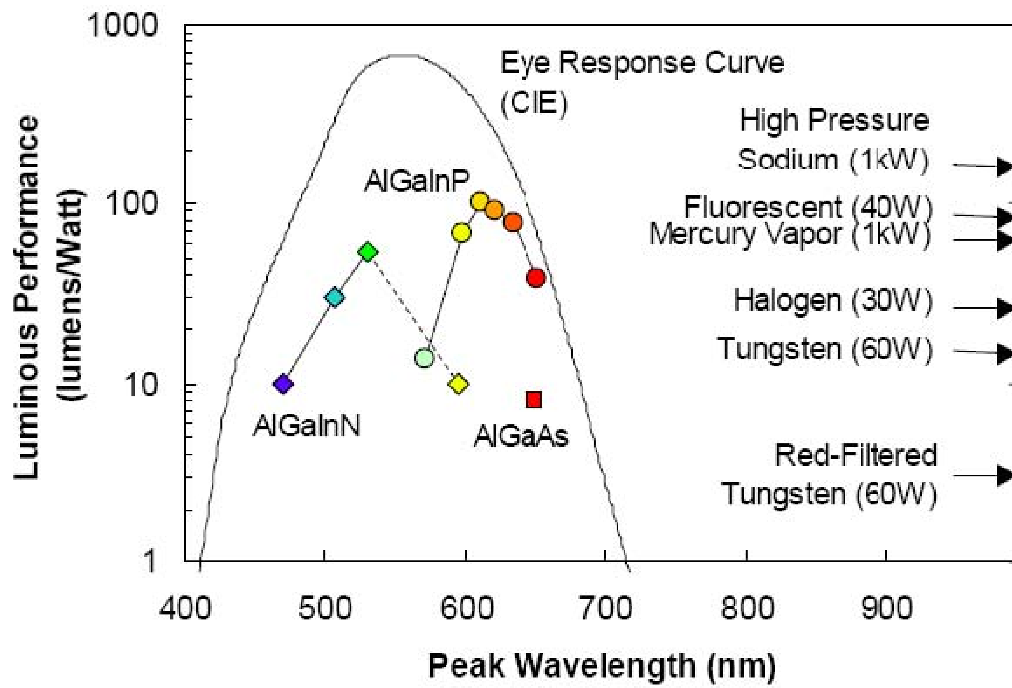

Fig. 1-2 The optimum transform efficiency of different material in visible region. The black real line is the CIE curve for human's eye.[Lumileds lighting Company]

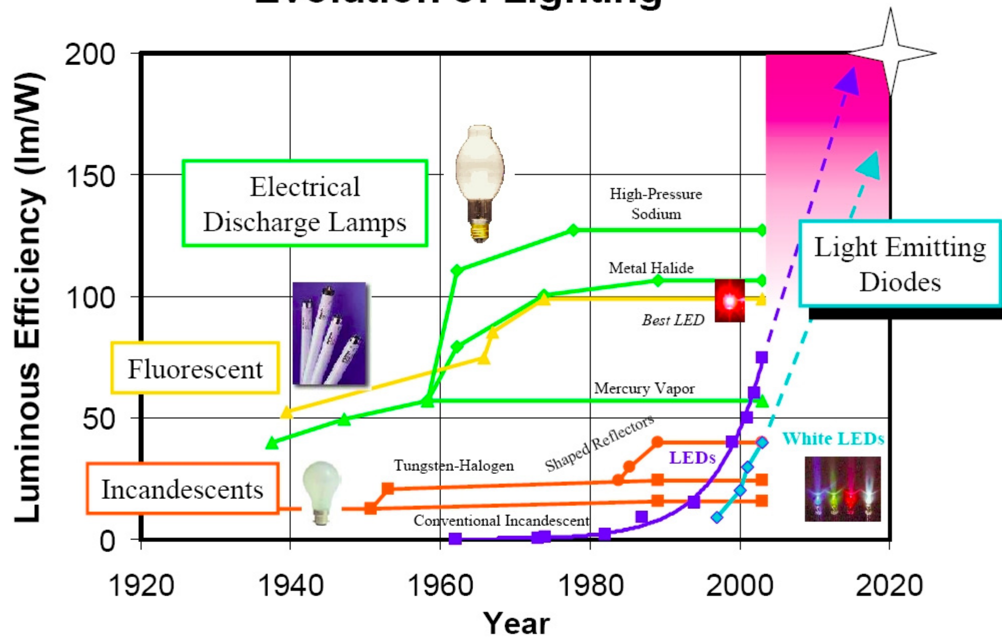

Fig. 1-3 The evolution of solid state lighting from 1920, the efficiency of LED increasing several multiples.[Lumileds lighting Company]

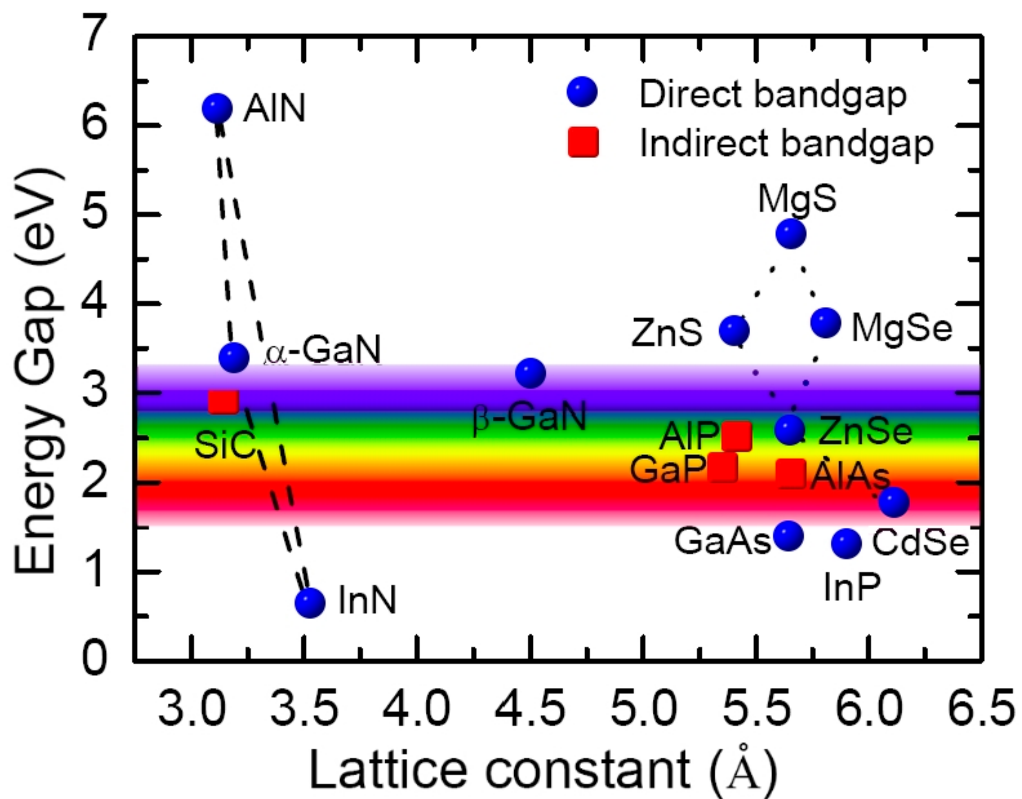

Fig. 1-4 The relationship of lattice constant and energy gap of different compound semiconductors.

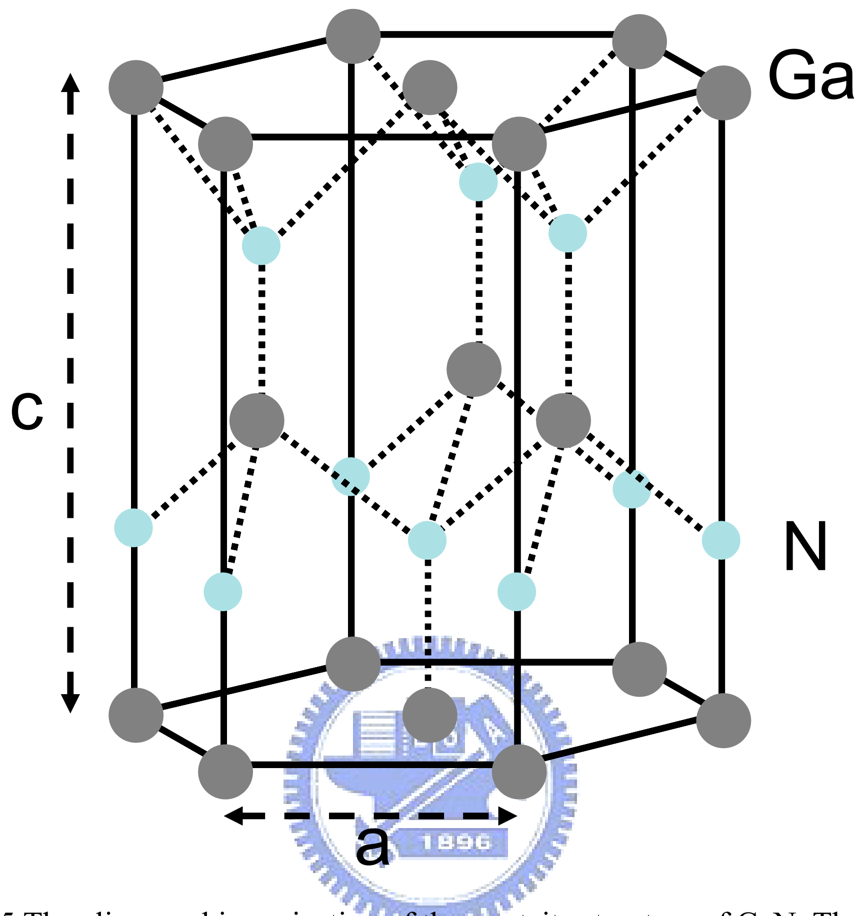

Fig. 1-5 The clinographic projection of the wurtzite structure of GaN. The c and a are the lattice constant.

Tab. 1-1 The properties of gallium nitride (Shur *et al*.[1])

Crystal structure	Wurtzite	Zincblende
Group of symmetry	$C_{6V}^4 P6_3mc$	T_d^2-F$\underline{4}$3m
Density (g/cm^3)	6.15[7,8]	
Dielectric constant		
static	8.9-9.5[8,9,10,11]	9.7
high frequency	5.35[12,8,9,10,11]	5.3[12]
Lattice constants (A)	a = 3.189[13] c = 5.185[14,13]	4.52[8]-4.50[10,13]
Optical phonon energy (meV)	91.8[15,8]	91.9[8]
Band structure		
Energy gap (eV)	3.5[13]	3.3[13]
Temperature dependence of the energy gap 0<T<600	$3.57-7.4\times10^{-4} \times T^2/(T+600)$	$3.37-7.4\times10^{-4} \times T^2/(T+600)$
Conduction band		
Effective electron mass (in units of m_o)	0.22[16,13,17]	0.15[18]
Effective conduction band density of states (cm^{-3})	2.6×10^{18}	1.4×10^{18}
Ionization energies of shallow donors		
Si (eV)	0.012-0.03	
O (eV)	0.004-0.01	
Valence band		
Energy of spin-orbital splitting E_{SO}(eV)	0.011-0.018[19,13]	0.017[13]
Energy of crystal-field splitting E_{cr} (eV)	0.011-0.022[19,13]	
Effective hole mass (in units of m_o)		
heavy	1.0[13]	1.3[18,20]

Effective valence band density of states (cm^{-3})	2.5×10^{19}	4.1×10^{19}
Ionization energies of shallow acceptors		
Mg (eV)	0.14-0.21	
Zn (eV)	0.21	
Native defect V_{Ga} (eV)	0.14	
Electrical properties		
Breakdown field (Vcm^{-1})	$\sim5\times10^{6}$ [8]	$\sim5\times10^{6}$
Mobility ($cm^{2} V^{-1}s^{-1}$)		
Electrons	~1000[21,22,8223]	≤1000[24]
Holes	≤ 200[25]	≤ 350[26,27]
Diffusion coefficient($cm^{2}s^{-1}$)		
Electrons	25	25
holes	5	9
Optical properties		
Infrared refractive index	2.3[8]	
Refractive index spectra	[28,29]	[12]
Reflectance spectra	[30,31,19,32]	
Absorption spectra	[33,31,12,28,34,35]	
Photoluminescence spectra	[36, 37,38, 19,35]	[39,40]
	820[41]	
Specific heat at 300K ($Jg^{-1}°C^{-1}$) 298<T<1773 (see also [83])	0.49[41] $0.456+0.107\times10^{-3}T$[42]	
Thermal conductivity ($Wcm^{-1}°C^{-1}$)	>1.95 [43,44,45,46]	
Thermal diffusivity ($cm^{2}s^{-1}$)	0.65	
Thermal expansion, linear ($°C^{-1}$)	$\alpha_a = 5.59\times10^{-6}$ [8]	
	$\alpha_c = 3.17\times10^{-6}$ [8]	

Mechanical properties		
Elastic constants (GPa)		
C_{11}	390±15[47]	293[48]
C_{12}	145±20[47]	159[48]
C_{13}	106±20[47]	
C_{33}	398±20[47]	
C_{44}	105±10[47]	155[48]
Piezoelectric constants (cm^{-2}) [49,50,51,13,52]		
e_{15}	−0.30	
e_{31}	(−0.3)−(−0.55)	
e_{33}	0.6−1.12 1.27	
e_{14}		0.4[53]

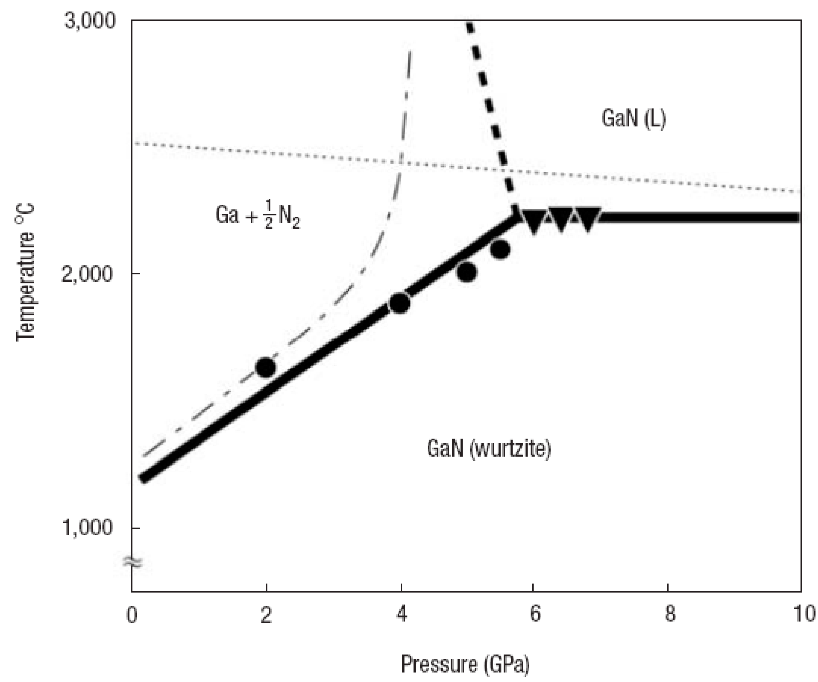

Fig. 1-6 The phase diagram of GaN.[58]

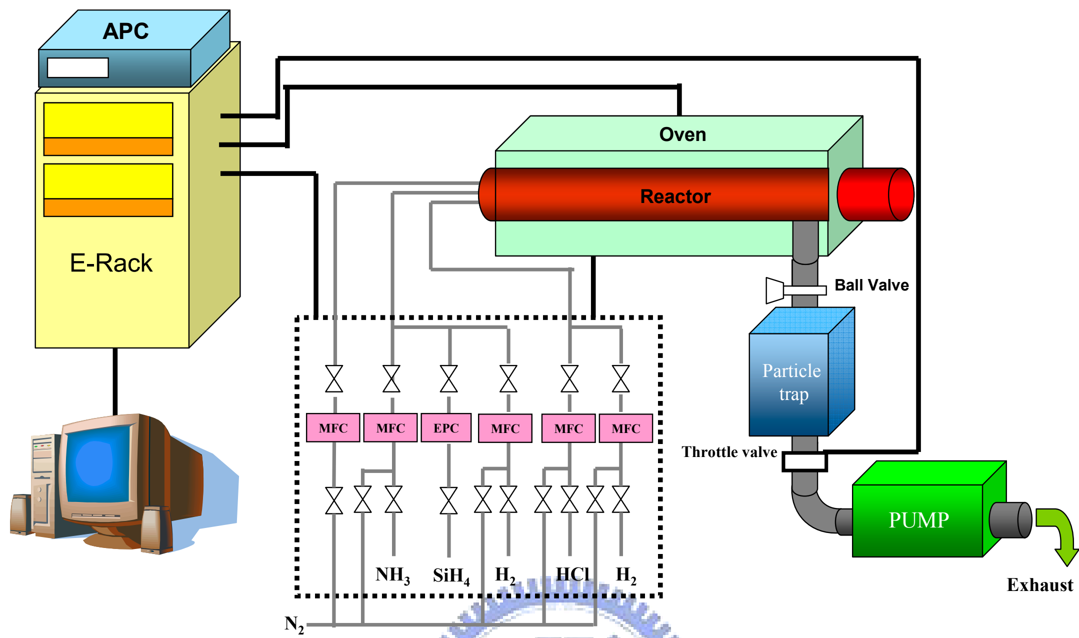

Fig. 1-7 The sketch of HVPE system.

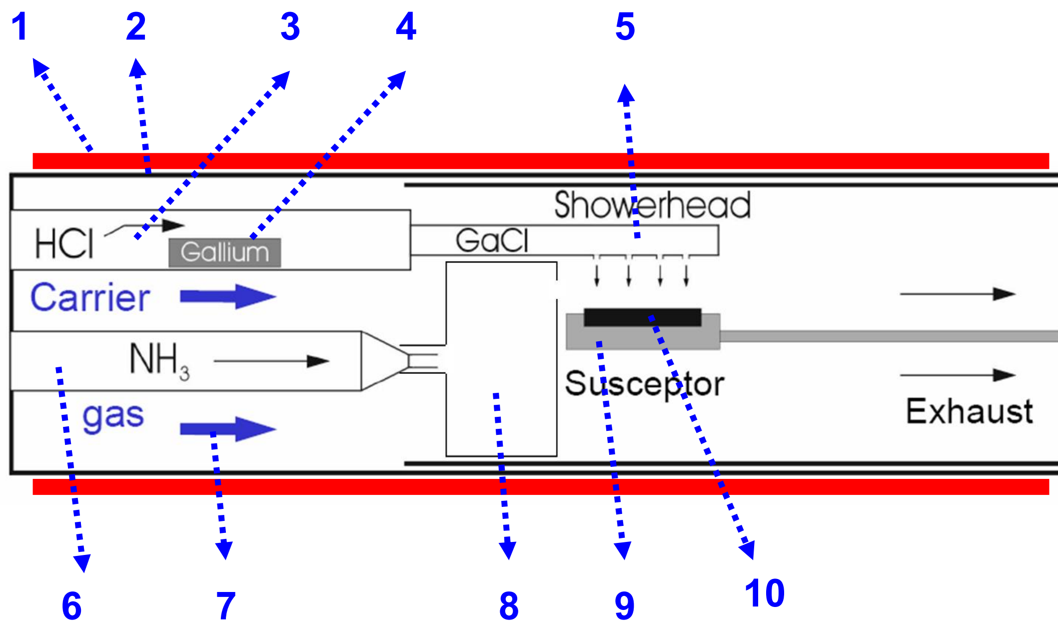

Fig. 1-8 The reactor of HVPE system. Including:

1. Oven
2. Quartz tube
3. HCl line
4. Gallium boat
5. Shower head
6. NH_3 line
7. Ambient gases line
8. Mixing box
9. Susceptor
10. Wafer holder

Tab. 1-2 The methods of bulk GaN growth (IWN 2006)

Methods of Bulk GaN Growth				
	Na flux (LPE)	Ammonothermal	N_2 high pressure	HVPE
Temperature	500~800 °C	400~600 °C	1400~1550 °C	1000 °C
Pressure	50~100 atm	< 1500 atm	15000 atm	~ 1 atm
Size	45 mm	1”	Several mm	> 2”
Character	No bulk porduct	The same technique as hydro-thermal method with mass production results	The setup is large an expensive	Sunstrate Complexity (expensive)
Organization	Tohoku Univ. Cornell Univ. Osaka Univ. NGK	Tohoku Univ. Naval research (USA) Air Force (USA) UCSB (USA) Ammon (Poland) Nichia (with Ammon)	Unipress (Poland) Japan energy Yamaguchi Univ.	Sumitomo Hitachi Cable Mitsubishi Chemical Lumilog ITRI **Chiao-Tung Univ.**
Mass production			No!	OK!
reference	JJAP 45, L1136 (2006)	J. Cryst. Growth **260**, 67 (2004)	J. Cryst. Growth **274**, 55 (2005)	

(a)

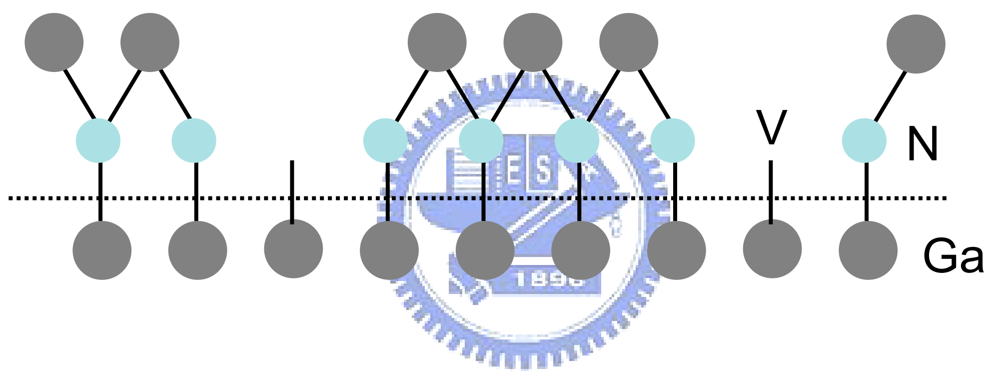

(b)

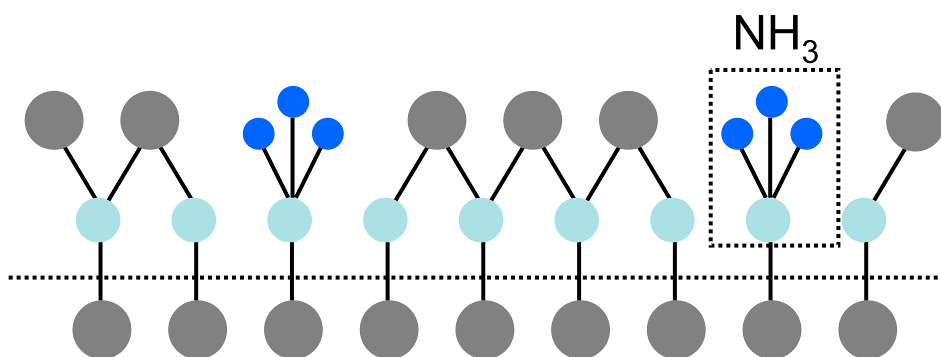

(c)

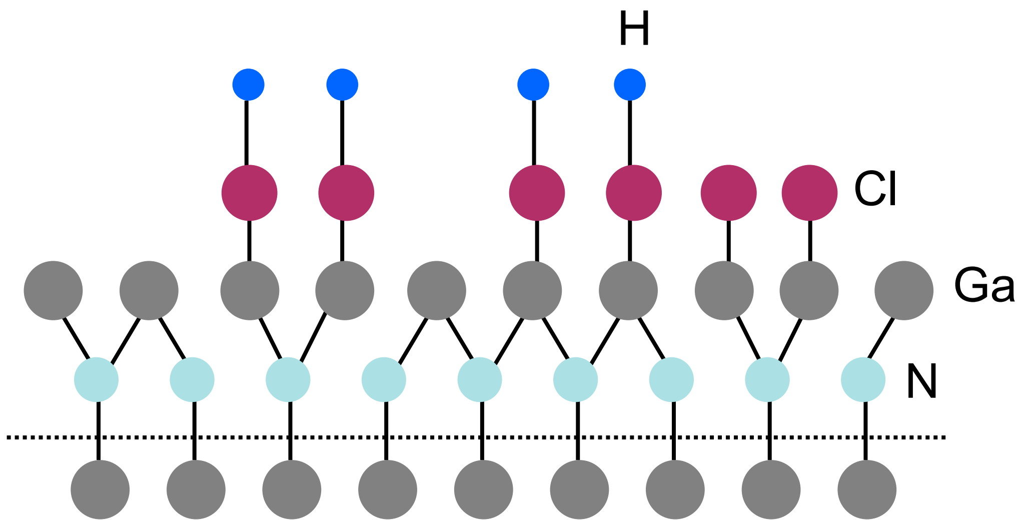

(d)

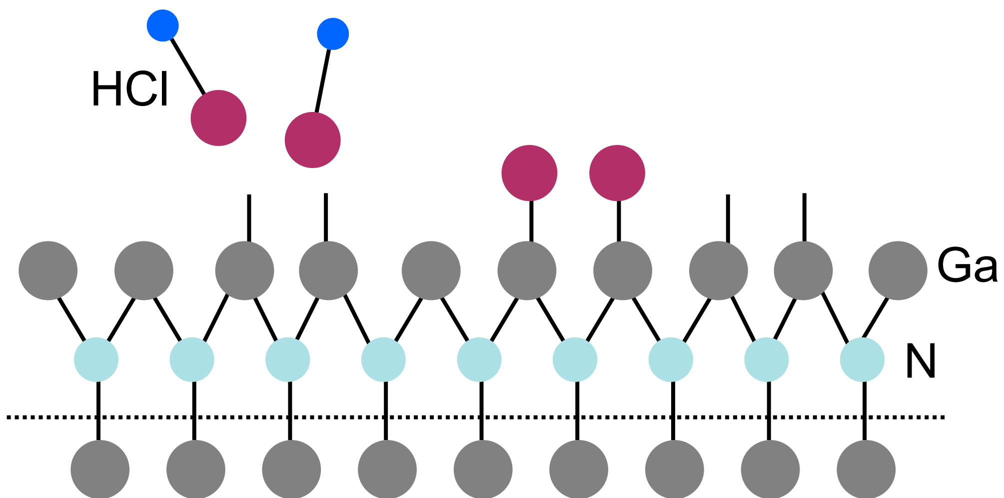

(e)

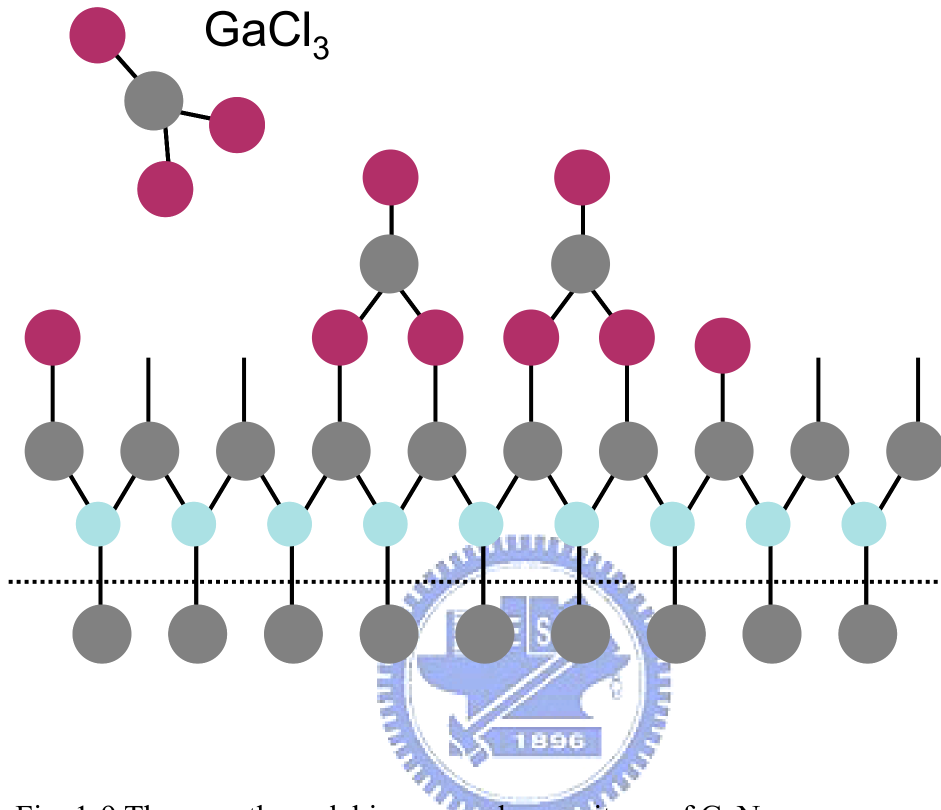

Fig. 1-9 The growth model in vapor phase epitaxy of GaN.

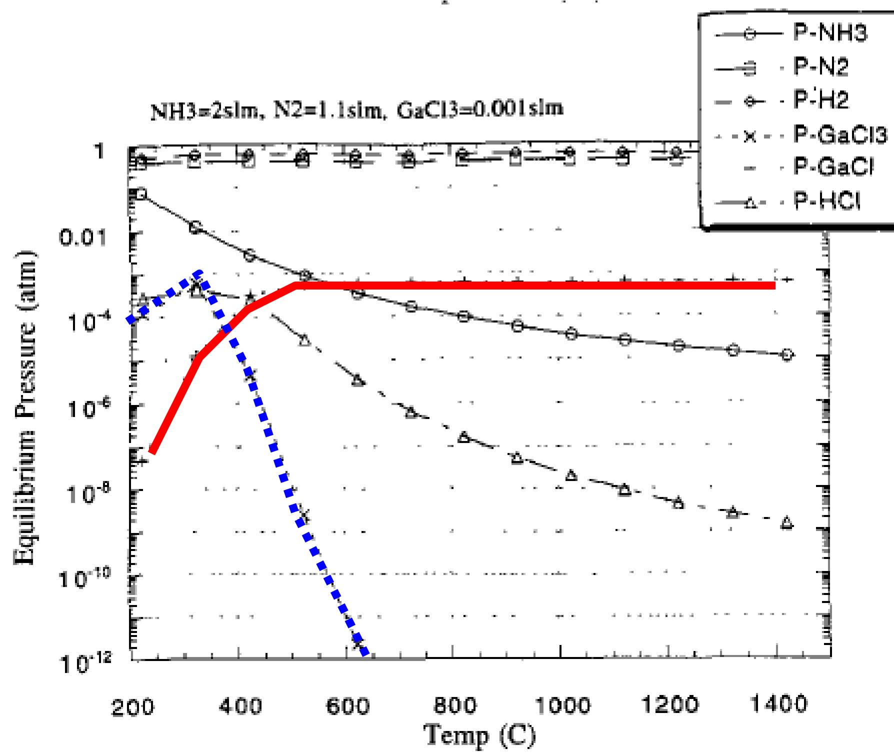

Fig. 1-10 Equilibrium partial pressures of gaseous species inside the reactor.[71]

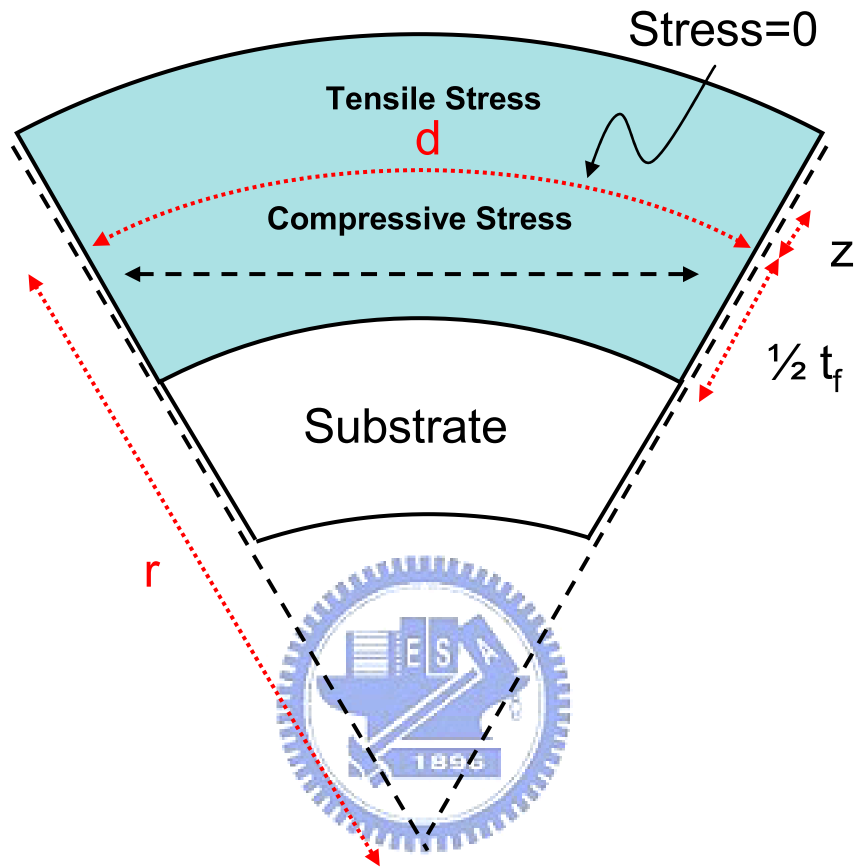

Fig. 1-11 The Stress distribution in thick-film with substrate. The r denotes the curvature radius of bowing film.

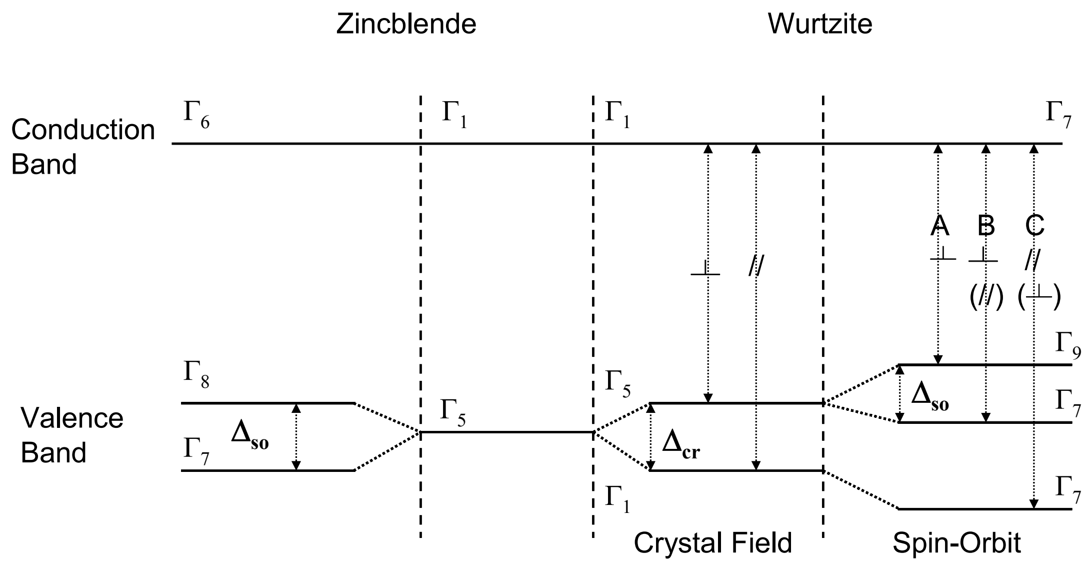

Fig. 1-12 The Band structures and respective transition in GaN. The indications ⊥ and // show the transition is allowed for the polarization perpendicular and parallel to the optic axis, respectively. The value Δ_{so} and Δ_{cr} are the spin-orbit and crystal-field splittings, respectively.[80]

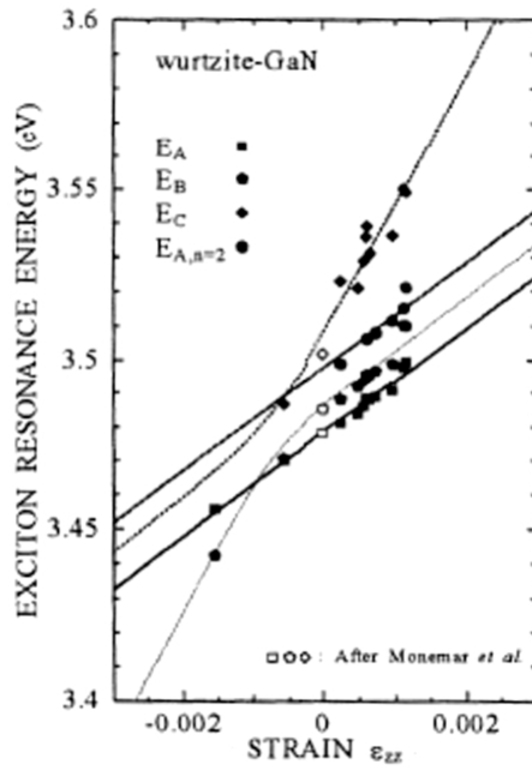

1896

Fig. 1-13 Strain dependence of the free exciton resonance energies in wurtzite GaN. $\varepsilon_{zz}=(c-c_0)/c_0$ denotes the strain along the z-axis.[80]

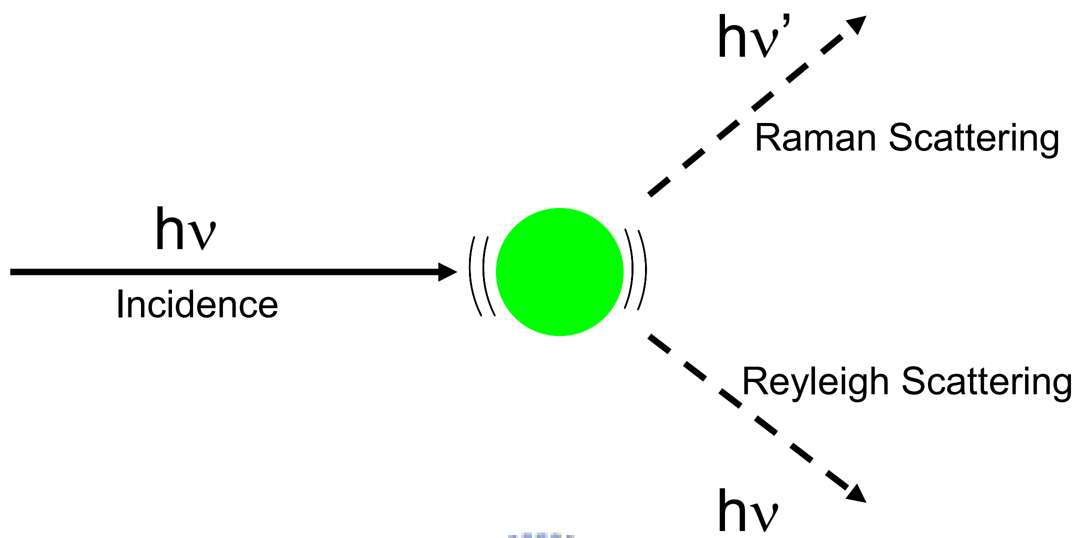

Fig. 1-14 The scheme of Raman and Reyleigh scattering. In the Raman scattering, the photons have energy exchange with the phonons.

ES A 1896

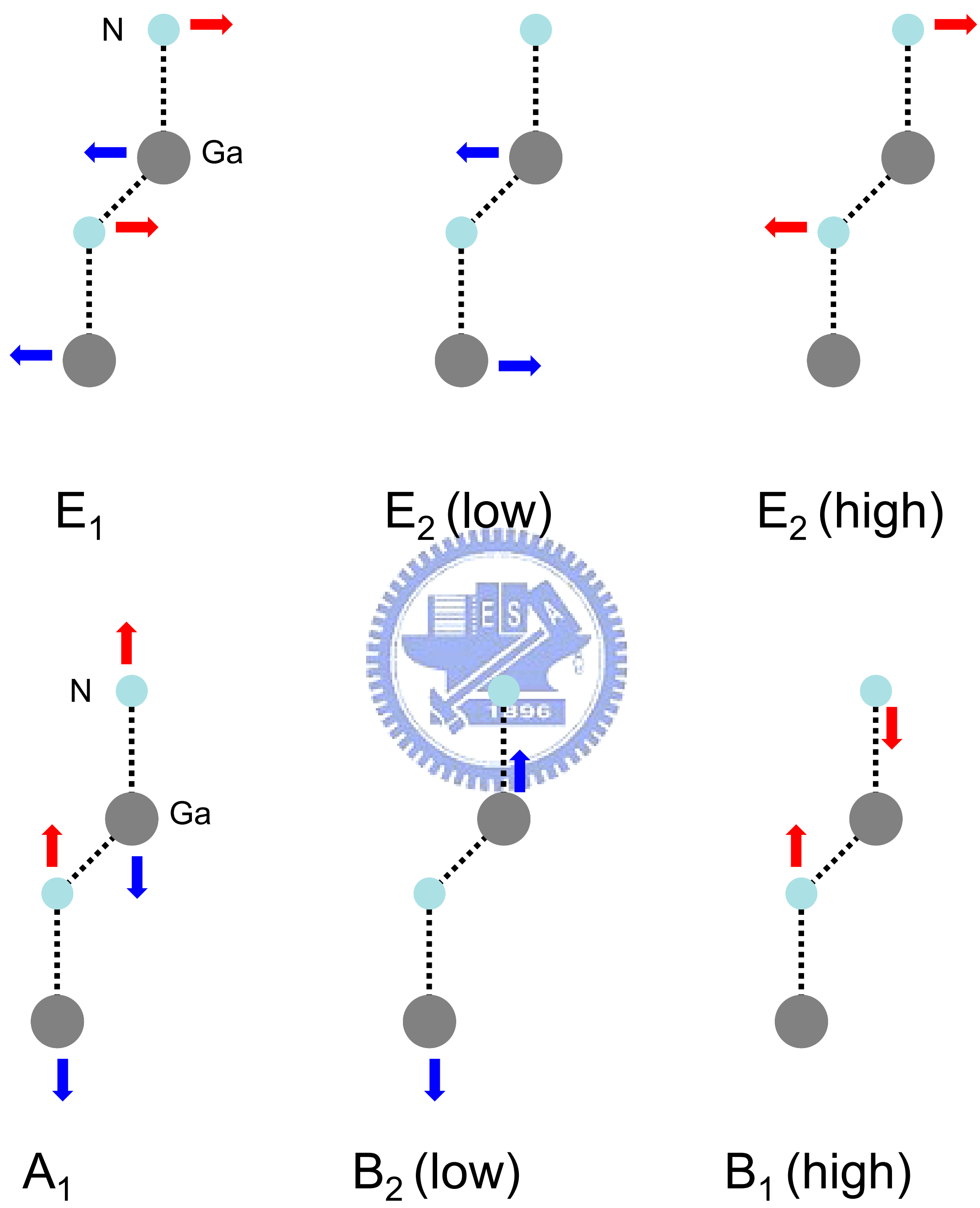

Fig. 1-15 Optical phonon modes in wurtzite structure crystal.

Tab. 1-3 Raman selection rule for optical phonon in wurtzite structure (x//a)

Scattering Configurations		Allowed Modes
$y(x,x)\bar{y}$		A_1(TO)、E_2(high)、E_2(low)
$y(z,z)\bar{y}$		A_1(TO)
$y(z,x)\bar{y}$		E_1(TO)
$z(x,x)\bar{z}$		A_1(TO)、E_2(high)、E_2(low)
$z(x,y)\bar{z}$		E_2(high)、E_2(low)
$z(y,y)\bar{z}$		A_1(LO) 、E_2(high)、E_2(low)
$z(\bar{y},\bar{y})\bar{z}$		A_1(TO) 、E_2(high)、E_2(low)
$z(\bar{y},\bar{x})\bar{z}$		E_1(TO)、E_1(LO)

Tab. 1-4 Familiar Raman phonon frequency values in wurtzite structure of GaN

E_1(low)	A_1(TO)	E_1(TO)	E_2(high)	A_1(TO)	E_1(LO)	
144	531.8	558.8	567.6	734	741	[77]
144	533	561	569	735	743	[78]
	533	561	570	735	742	[79]

Tab. 1-5 Raman calibration factor

Group	Growth Method	Substrate	K_{λ}^{R} [$GPa^{-1}cm^{-1}$]
T. Kozawa *et al.* (1995)[86]	MOCVD	sapphire	6.2
C. Kisielowski *et al.* (1996) [85, 87]	HVPE	sapphire	4.24
V. Yu. Davydov *et al.* (1997)[88]	MOCVD	6H-SiC	2.7
S. Tripathy *et al.* (1999)[82]	MBE	sapphire	4.86
M. Kuball *et al.* (2001)[85]	MOCVD	sapphire	2.9
F. Demangeot *et al.* (2004)[91]	MBE	Si(111)	2.43
F. C. Wang *et al.* (2007)[80]	MOCVD	sapphire	2.56

Chapter 2. Air-bridged Epitaxial Lateral Overgrowth

The epitaxial lateral overgrowth (ELOG) technology was applied to produce high quality GaN with at least one order of magnitude reducing of threading dislocation density. Numerous modifications of ELOG process have been proposed in order to improve it, such as pendeo ELOG, facet controlled ELOG, air-bridged ELOG, and patterned substrate ELOG. For relaxing the thermal stress and developing self-separation technology of bulk GaN, two kind of trenched ELOG structures were investigated in this chapter, called high-void air-bridged ELOG and dot air-bridged ELOG. These structures can reduce the thermal stress and dislocation density of bulk GaN, indeed, self-separated it from sapphire substrate.

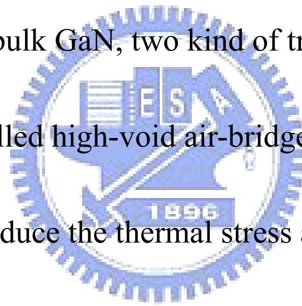
E S A
1896

2.1 High-Void Air-Bridged Technique

2.1.1 Introduction of Air-Bridged technique

Most current nitride-based devices are hetero-epitaxially grown on lattice-mismatched substrates, such as sapphire, Si, GaAs, and SiC. The large mismatches between the lattice constants of substrates and epitaxial films generate

high dislocation densities. Furthermore, differences between the thermal expansion coefficients (TEC) of the substrates and the epitaxial films as shown in Tab. 2-1 cause large warp or bowing of the epi-layers. Selective epitaxial techniques, such as lateral epitaxial overgrowth (LEO) and pendeo epitaxy (PE) have been demonstrated to be extremely effective in reducing threading dislocations (TDs) density by over two orders of magnitude in two to several steps of laterally grown GaN films on sapphire and SiC substrates.[1-4] However, c-axis tilting in the wing region, of commonly 0.2^{o}-1°, are normally observed in both LEO and pendeo structures in an azimuth perpendicular to the LEO or PE stripe direction. When wing tilt is present, the coalescence of nearby stripes may yield arrays of dislocations, reducing the defect-free region of overgrown GaN.[5] Kidoguchi *et al.*, proposed a new method of lateral growth called air-bridged LEO to improve the wing tilting of conventional selective epitaxy.[6-8] The dry etching and standard photolithography technique were employed to produce trenches in a GaN template, and the sidewall of GaN trenches was covered with a dielectric mask such as SiN_x or SiO_2 in air-bridged LEO structure. After the regrowth of GaN, the voids of the air-bridged structure were buried in the coalesced GaN wings. Currently, however, the effect of the voids height in an air-bridged structure is still not clearly understood, especially in the stress distribution caused by the difference between the TECs of the epitaxial films and the substrate in

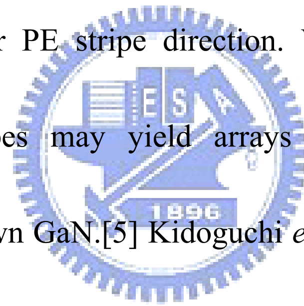

thick GaN films.

2.1.2 Experiment

In this investigation, a specially designed air-bridged structure with high voids was developed to grow thick GaN layers using HVPE. The quality of the GaN layers grown by this technique was compared to that of GaN layers that were prepared by a more conventional pendeo growth process with lower voids. The HVAB structure with the higher voids is proposed to reduce the density of TDs, the residual stress induced by the difference between TECs, and to obtain the self-separated freestanding GaN wafer from the sapphire substrate.[9]

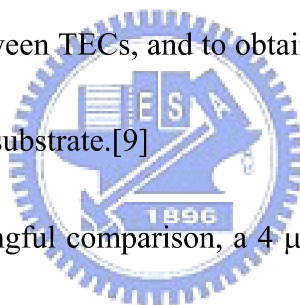

To provide a meaningful comparison, a 4 μm-thick GaN layer was initially grown on a c-plane sapphire substrate by metal-organic chemical vapor deposition (MOCVD). Then, a standard photolithographic technique was applied to fabricate a pattern of 4 μm-wide GaN seed stripes and 6 μm-wide grooves between adjacent stripes in the $<1\bar{1}00>$ direction of GaN. Dry etching was employed to form the trenches with 0.2 μm-deep etched into the sapphire. The GaN template was then sliced into two half-wafers. One of the half-wafers (pendeo structure) remained without any additional treatment. The other half-wafer (HVAB structure) was passivated with a thin oxide layer on the sidewall of the GaN seed. The two

half-wafers were then mounted side by side in an HVPE reactor to grow 30-μm GaN. Figures. 2-1(a) and (c) schematically depict the conventional pendeo and the HVAB structures after the HVPE regrowth, respectively. For the HVPE regrowth, NH_3 gas was used as a nitrogen source and GaCl generated by 850 ^{o}C liquid gallium with HCl gas, was used as a gallium source. The ambient of the carrier gas was a mixture of H_2 and N_2. The growth was performed using an AIXTRON 800064 horizontal reactor at approximately 1050 ^{o}C. The GaN growth was separated into two steps under different pressures; the first step was at 500 mbar for lateral overgrowth and the second step was at 900 mbar for 3D growth. The HVPE GaN was characterized by scanning electron microscopy (SEM), cathodeluminescence (CL), high resolution X-ray diffraction (HRXRD), micro-Raman spectroscopy, and etch pit density (EPD) measurements.

2.1.3 Result and Discussion

Figures 2-1(b) and (d) show the cross-sectional SEM images of the GaN films from conventional pendeo and HVAB structures. Conventional pendeo and HVAB structures form voids of different heights underlying HVPE GaN at the coalescence boundary of the wing region; neither structures included small tapered voids. The heights of the voids in the pendeo and the HVAB structures are 0.2 and 3

μm, respectively. The heights of the voids in the HVAB structure is much higher than that of the conventional air-bridged LEO.[6-8]

Figure 2-2 shows the cross-sectional and plane-view CL images of conventional pendeo and HVAB structures. The cross-sectional CL images of Fig. 2-2(a) and 2(c) explain the GaN growth mechanism of pendeo and HVAB structures. The bright region of the conventional pendeo and HVAB structures is the selective epitaxial growth region. TDs are more likely to propagate to the GaN surface in the conventional pendeo structure than in the HVAB structure in the seed region. Figures 2-2(b) and (d) show the plane-view CL images of conventional pendeo and HVAB structures. The density of TDs in the GaN surface can be calculated from the CL image. On both samples, most of the TDs were confined in the coalescence region. However, the dislocation density in the HVAB structure sample was much lower than that in the conventional pendeo structure sample. EPD measurements supported similar conclusions. The TDs densities of HVAB and conventional pendeo structures in the wing region are approximately 10^7 and 10^8 cm^{-2}, respectively. In another experiment, the width of the grooves in the HVAB structure is increased to more than 10 μm, the density of TDs can be reduced to 10^6 cm^{-2} in the wing region.

Figure 2-3 schematically depicts the propagation of TDs in conventional pendeo and HVAB structures. Since the sidewalls of GaN seeds were passivated with

oxide in the HVAB structure, the GaN regrowth by HVPE could start only from the top of the GaN seeds forming triangularly ELOG GaN in the initial state of regrowth. The TDs would then have a better chance to bend and coalesce. In conventional pendeo regrowth, the sidewalls of the GaN seeds did not have passivation and, therefore, the GaN started to grow from the sidewall as well as from the top, rapidly coalescing immediately above the groove region. The TDs did not have enough opportunity to coalesce and propagated to the surface of the GaN thick film.

Figure 2-4 shows the full-width-at-half-maximum (FWHM) of HRXRD rocking curves of GaN symmetric (002) and asymmetric (102) peaks. In the symmetric measurement, the directions of incidence X-ray were parallel to the stripes (azimuth $\phi=0^o$) and perpendicular to the stripes ($\phi=90^o$) for the GaN (002) peak. In the asymmetric measurement, the incidences of the X-ray were aligned to $\phi=0^o$ and $\phi=60^o$ for the GaN (102) peak. No clear evidence of wing tilt was observed in either conventional pendeo and HVAB structures in 30-μm-thick GaN films. The result that thick GaN films can reduce wing tilt was consistent with the report by Ishibashi *et al.*[10] The wing tilt causes stress in the coalescent region, which disfavors the growth of high quality GaN thick films by HVPE. The FWHM of (002) and (102) X-ray rocking curves show the high quality of the samples in both conventional pendeo and HVAB structures. The FWHM of the (102) peak is broadened by screw, mixed, and

edge dislocations.[11, 12] The FWHM value of the rocking curve of as low as 204 arcsec in HVAB GaN (102) peak at the 60° azimuth shows that the number of all types TDs can be reduced in the HVAB structure, even in the direction of lateral overgrowth.

Figure 2-5 shows the HRXRD reciprocal space maps around the (006) Al_2O_3 reciprocal point of conventional pendeo and HVAB structures. The (002) GaN peak of the HVAB structure is considerably broadened in the direction parallel to surface plane and very narrow normal to the surface. The broadened (002) GaN peak in RSM is the characteristic of a relaxed single crystalline film with a distorted lattice related to misfit relaxation of dislocations and bending of lattice.[13-15] In this case, the lattice distortion may be caused by the difference between the TECs of the GaN film and the sapphire substrate.

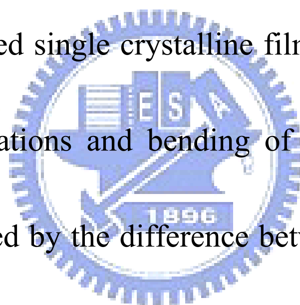

The residual strain of these samples was measured by micro-Raman scattering pectroscopy using the E_2(high) phonon frequency. Figure 2-6 shows the cross-sectional and in-plane Raman spectra of conventional pendeo and HVAB structures. The difference between the TECs of GaN and sapphire substrate causes compressive stress normally observed in the GaN film under hetero-epitaxial growth on the sapphire substrate. With an E_2(high) mode phonon wavenumber of 567.0 cm^{-1} as the reference value for strain-free GaN, a wavenumber blue shift of the Raman

E_2(high) mode of 4.24 cm^{-1} would correspond to a stress of 1 GPa.[16, 17] The compressive stress in the surface of the HVAB structure is 165 MPa less than the conventional pendeo structure, above both the window and the wing regions, and this result is similar to that in the cross-sectional region of these samples. Therefore, the relaxation of residual stress in the HVAB structure is greater than that in the conventional pendeo structure.

2.1.4 Conculsion

In conclusion, the growth mechanism of the high-void air-bridged structure differs from that of the conventional pendeo structure because of the formation of high voids by the sidewall passivation of the GaN seed. CL, HRXRD, EPD, and Raman spectra show that the HVAB growth process substantially improves GaN quality. The relaxation of the residual stress of the HVAB structure exceeds that in the conventional pendeo structure, which factor is an important factor for the growth of a GaN thick film by HVPE.

2.2 Strain reduced GaN thick film grown by hydride vapor phase epitaxy utilizing dot air-bridged structure

2.2.1 Introduction

The difference between the TEC of foreign substrate and epitaxial GaN films causes large bowing of the epi-layers and the substrates. The bowing usually induces large residual strain in epitaxial GaN film, especially, in GaN thick-film grown by HVPE. The large residual strain normally makes GaN thick-film crack in epitaxy or in cooling down process from the growth the temperature to room temperature. When crack occured it is impossible to get the complete GaN wafer from the foreign substrate, e.g. with laser lift-off or self-separation techniques. However, only few methods can be used in reducing thermal stress for GaN epitaxial procedure. Dam *et al*., reported a gallium treatment step technique to grow crack-free GaN layer on sapphire substrate with varying buffer thickness of metal-organic chemical vapor deposition (MOCVD) GaN template.[18] In this investigation, a specially designed epitaxial lateral overgrowth (ELOG) process, called dot air-bridged growth, has been developed to grow thick GaN layers by HVPE system, which could reduce the residual thermal stress of GaN and foreign substrate. The stress was estimated according to the E_2(high) phonon frequency using micro-Raman scattering spectroscopy.

2.2.2 Experiment

Figure 2-7 illustrates the HVPE GaN fabrication process of dot air-bridged structure. First, a 3 μm-thick GaN template was grown by MOCVD on 330 μm-thick c-plane sapphire substrate in 2 inch diameter for HVPE regrowth. A thin SiN_x layer was deposited on MOCVD GaN template by plasma enhanced chemical vapor deposition (PECVD). Then, conventional photolithographic technique was applied to fabricate a hexagonally aligned dot pattern of 3-μm-wide square seed regions and 4-μm-wide grooves between adjacent square regions. These dot patterns worked as hard mask for subsequent inductively coupled plasma (ICP) dry etching. The 3-μm-wide square GaN seed and 4-μm-wide grooves with 0.2 μm depth etched into the sapphire substrate was formed after the ICP dry etching as shown in Fig. 1(b). After the dot air-bridged pattern was defined, a 200 nm dielectric layer was deposited on the sidewall of GaN seed region by PECVD as shown in Fig. 2-7(c). Then, the sample was mounted in HVPE reactor to grow GaN thick-film as shown in Fig. 2-7(d). For HVPE GaN thick-film growth, the NH_3 gas was used as a nitrogen source and GaCl generated by liquid gallium with HCl gas at 850 ^{o}C was used as a gallium source. The ambience of the carrier gas was a mixture of H_2 and N_2. The growth was performed by an Aixtron 800064 horizontal reactor at approximately 1050 ^{o}C under 900 mbar with a growth rate about 150 μm/h. The HVPE GaN was characterized by

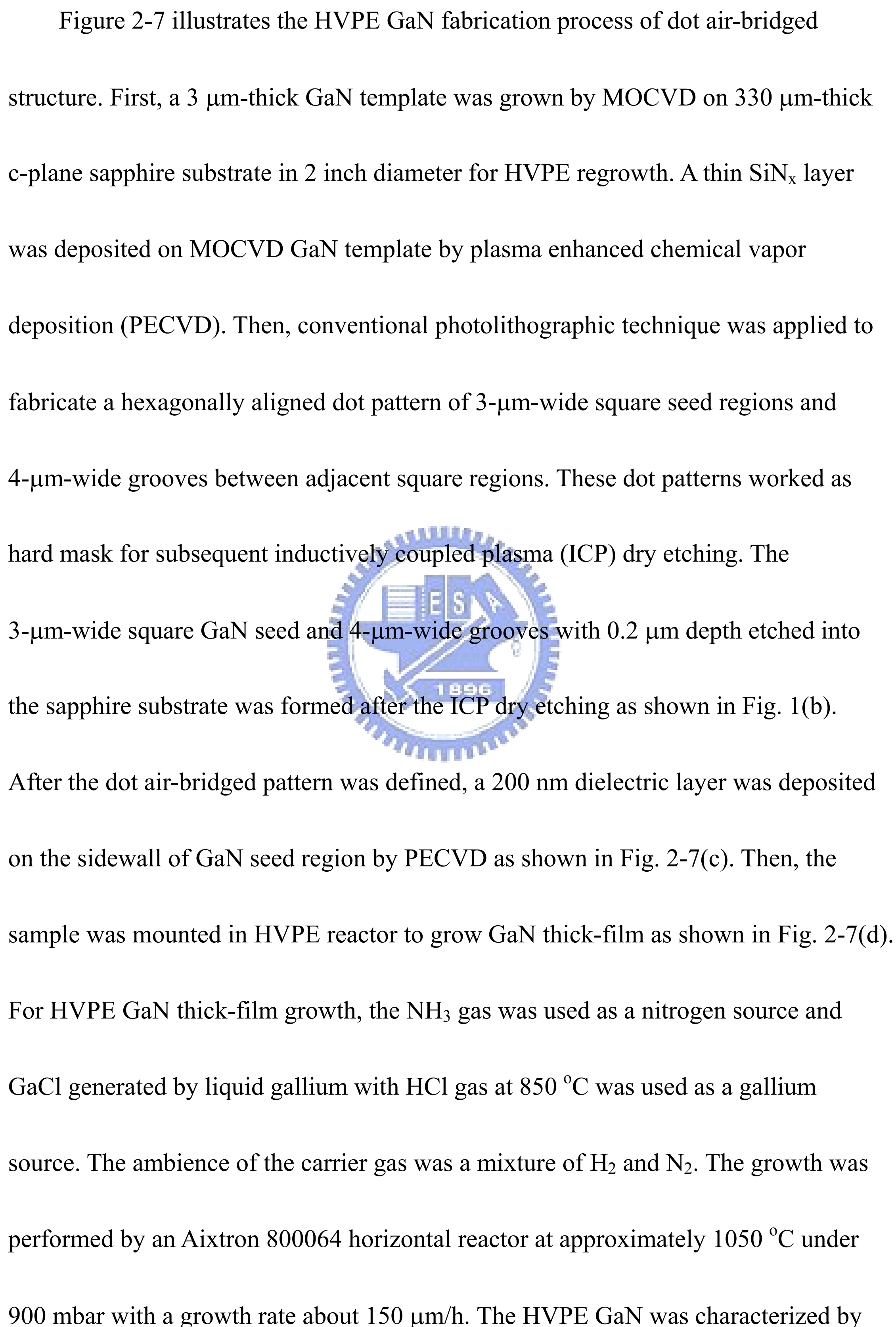

scanning electron microscopy (SEM), cathodeluminescence (CL), and micro-Raman spectroscopy.

2.2.3 Result and Discussion

Figure 2-8(a) shows the bird's-eye view SEM image of GaN template of dot air-bridged structure. The region of GaN seeds was isolated clearly and arrayed in hexagonal geometry. Figure 2-8(b) shows the bird's-eye view SEM image of initial growth for 2 min by HVPE. The morphology of the initial state of the dot air-bridged structure in GaN seed region formed a pyramid shape. The shape and the size distribution of the pyramid-shaped GaN islands were uniform. The pyramid-shaped GaN islands were formed by the $\{10\bar{1}1\}$ crystal facets, which were stable and the growth rate of this facet was very slow due to the low surface energy.[19, 20] The stability of these crystal facets makes the GaN epitaxial layer harder to coalesce along the $<10\bar{1}0>$ direction than along the $<11\bar{2}0>$ direction, which was the normal coalesced direction for ELOG. If the distance of the groove region is too large, the GaN film is very hard to coalesce to form a complete thick-film. Then, polycrystalline GaN will grow in the large groove region. The dot air bridged-structure was not as good as stripe air-bridged structure in large groove distance in dislocation reduction. However, the dislocation density of dot air-bridged structure was still observed a large

decrease compared with no-structure samples. Figure 2-9(a) shows the plane view CL image of the dot air-bridged structure after the HVPE thick-film regrowth. The dark spots indicated the position of dislocations with the density of 1.8×10^{7} cm^{-2}, which is much smaller than the direct growth GaN on sapphire substrate without any structure of patterns. The full-width-at-half-maximum (FWHM) of CL spectra at 300 K of the dot air-bridged sample was also measured. The FWHM measured from the surface of the dot air-bridged sample was 77 meV without observed yellow band. Figure 2-9(b) shows the cross-sectional SEM image of the pyramid-shaped GaN islands. The dashed line of GaN islands indicated a special growth region in Fig. 2-9(b). In these regions, the GaN was grown toward the $<000\bar{1}>$ direction and the high index crystal facets were observed. This phenomenon was resulted from the slow growth rate of the $\{10\bar{1}1\}$ crystal facets of pyramid-shaped GaN islands, which make the GaN have enough time to grow toward $<000\bar{1}>$ direction in the dash line regions before the pyramid-shaped GaN islands coalesced together. The GaN grown toward $<000\bar{1}>$ direction changed the height in the void of the dot air-bridged structure. The height of the void in the dot air-bridged structure could determine whether the HVPE GaN thick-film can self-separate from the sapphire substrate or not. If the HVPE GaN growth conditions and the process of fabricating dot air-bridged structure were controlled well, the GaN growth toward $<000\bar{1}>$ direction would be much

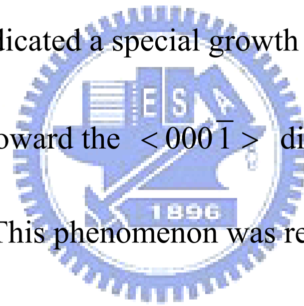

decreased, and the GaN thick-film would be easily separated from the sapphire substrate. Otherwise, the HVPE GaN thick-film would remain on the sapphire without separation. Even if the GaN thick-film was not separated from the sapphire, the residual stress was still relaxed without cracking the GaN. Crack free freestanding GaN wafer can still be fabricated by laser lift-off technique. In this paper, the discussion mainly focuses on the samples without separation from the sapphire substrate, and the self-separation technique will be discussed on the other paper.

To understand the residual stress distribution, a 100 μm-thick GaN sample with the dot air-bridged structure on sapphire substrate was cleaved to measure the cross-section stress variation. Figure 2-10(a) shows the cross-sectional CL image of the dot air-bridged structure. The height of voids in this sample between the interface of the GaN and the sapphire was roughly 0.4 μm, which was due to the $<000\bar{1}>$ growth of the GaN. The bright region of CL image indicated the high free carrier density region.[21] The stress in the dot air-bridged structure was measured by micro-Raman spectroscopy with E_2(high) phonon mode as shown in Fig. 2-10(b). Different regions of micro-Raman spectroscopy were measured as in the bottom, the middle, and the top of the cross section of the dot air-bridged sample. Compressive stress is normally observed in heteroepitaxy such as GaN/sapphire. A 4.24 cm^{-1} wavenumber blue shift of Raman E_2(high) mode would correspond to a stress of 1

GPa. Taking the E_2(high) mode phonon frequency at 567.0 cm^{-1} as the reference value for strain-free GaN,[22] the compressive stress of the dot air-bridged sample upon the interface is 0.04 GPa, which is much smaller than standard ELOG samples.[23, 24]

Figure 2-11(a) show the photograph of a 1.5 inch diameter 300 μm GaN thick-film on 2 inch sapphire substrate. No crack was found either the GaN thick-film or the sapphire substrate. The surface of the GaN was mirror-like and the structure of GaN/sapphire was bowed. Figure 2-11(b) shows the photograph of 1.5 inch diameter, 300 μm-thick freestanding GaN wafer, which was separated from the sapphire substrate by the laser lift-off technique with an Nd:YAG 355 nm laser. These results show that the dot air-bridged structure is a promising technique for the growth of crack-free and thick GaN film.

2.2.4 Conculsion

We have demonstrated the crack-free GaN thick-film with the dot air bridged structure by HVPE growth. This technique can be used in relaxing the residual stress caused by different TECs and lattice constants between the GaN and the sapphire substrate. The 300 μm-thick freestanding GaN wafer in 1.5 inch diameter was fabricated by dot the air-bridged structure and the laser lift-off technique. The dislocation density was 1.8×10^{7} cm^{-2} and the FWHM of CL spectrum at 300 K was 77

meV which indicated the good quality of the HVPE GaN.

In addition, the strain reduced structure has been developed for GaN thick-film growth by HVPE. The compressive stress could be reduced to as small as 0.04 GPa to prevent the crack in the epitaxial process of GaN growth. This technique could obtain large area GaN thick-film which can be used for the fabrication of freestanding GaN wafer.

2.3 References

1 T. S. Zheleva, S. A. Smith, D. B. Thomson, T. Gehrke, K. J. Linthicum, P. Rajagopal, E. Carlson, W. M. Ashmawi, and R. F. Davis, MRS Internet J. Nitride Semicond. Res. **4S1**, G3.38 (1999).

2 N. N. Morgan, Y. Zhizhen, X. Yabou, Materials Science and Engineering **B90**,201 (2002).

3 B. Beaumont, M. Vaille, G. Natat, A. Bouillé, J. C. Guillaume, P. Vénnègues, S. Haffouz, and P. Gibart, MRS Internet J. Nitride Semicond. Res. **3**, 20 (1998).

4 Y. Chen, R. Schneider, S. Wang, R. S. Kern, C. H. Chen, and C. P. Kuo, Appl. Phys. Lett. **75**, 2062 (1999).

5 C. Roder, H. Heinke, D. Hommel, T. M. Katona, J. S. Speck, and S. P. Denbaars, J. Phys. D: Appl. Phys. **36**, A188 (2003).

6 I. Kidoguchi, A. Ishibashi, G. Sugahara, and Y. Ban, Appl. Phys. Lett. **76**, 3768 (2000).

7 I. Kidoguchi, A. Ishibashi, G. Sugahara, A. Tsujimura, and Y. Ban, Jpn. J. Appl. Phys. **39**, 453(2000).

8 A. Ishibashi, Y. Kawaguchi, G. Sugahara, T. Shimamoto, T. Yokogawa, Y. Yamada, Y. Ueki, K. Nakamura, and T. Taguchi, Phys.Stat. Sol. (b) **241**, 2730 (2004).

9 S. Bohyama, H. Miyake, K. Hiramatsu, Y. Tsuchida, and T. Maeda, Jpn. J. Appl. Phys. **44**, 24 (2005).

10 A. Ishibashi, G. Sugahary, Y, Kawaguchi, and T. Yokogawa, Jpn. J. Appl. Phys. **42**, L1248 (2003).

11 B. Heying, X. H. Wu, S. Keller, Y. Li, D. Kapolnek, B. P. Keller, S. P. Denbaars, and . S. Speck, Appl. Phys. Lett. **68**, 643 (1996).

12 H. Heinke, V. Kirchner, S. Einfeldt, and D. Hommel, Appl. Phys. Lett. **77**, 2145 (2000).

13 V. Darakchieva, J. Birch, M. Schubert, T. Paskova, S. Tungasmita, G. Wagner, A. Kasic, and B. Monemar, Phys Rev **B70**, 045411 (2004).

14 V. Darakcheva, J. Birch, P. P. Paskov, S. Tungasmita, T. Paskova, and B. Monemar, phys. stat. sol. (a) **190**, 59 (2002).

15 P. F. Fewster, Crit. Rev. Solid State Mater. Sci. **22**, 69 (1997).

16 M. Kuball, M. Benyoucef, B. Beaumont, and P. Gibart, J. Appl. Phys. **90**, 3656 (2001).

17 A. kaschner, A. Hoffmann, C. Thomsen, F. Bertram, T. Riemann, J. Christen, K. Hiramatsu, T. Shibata, and N. Sawaki, Appl. Phys. Lett. **74**, 3320 (1999).

18. C. E. C. Dam, A. P. Grzegorczyk, P. R. Hageman, P. K. Larsen, J. Cryst. Growth 290 (2006) 463.

19. S. Haffouz, B. Beaumont, P. Gibart, MRS Internet J. Nitride Semicond. Res.3 (1998) 8.

20. J. E. Northrup, J. Neugebauer, Phys. Rev. B, 60 (1999) R8473.

21. S. Bohyama, H. Miyake, K. Hiramatsu, Y. Tsuchida, T. Maeda: Jpn. J. Appl. Phys. 44 (2005) L24.

22. A. R. Goñi, H. Siegle, K. Syassen, C. Thomsen, J.-M. Wagner, Phys. Rev. B 64 (2001) 035205.

23. F. Bertram, T. Riemann, J. Christan, A. Kaschner, A. Hoffmann, K. Horamatsu, T. Shibata, N. Sawaki, Meterials Science and Engineering B 59 (1999) 117.

24. M. Kuball, M. Benyoucef, B. Beaumont, P. Gibart, Jpn. J. Appl. Phys. 90 (2001) 3656.

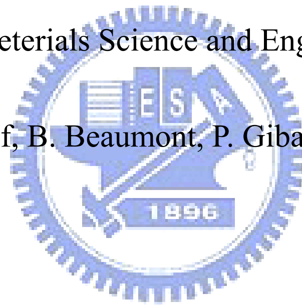

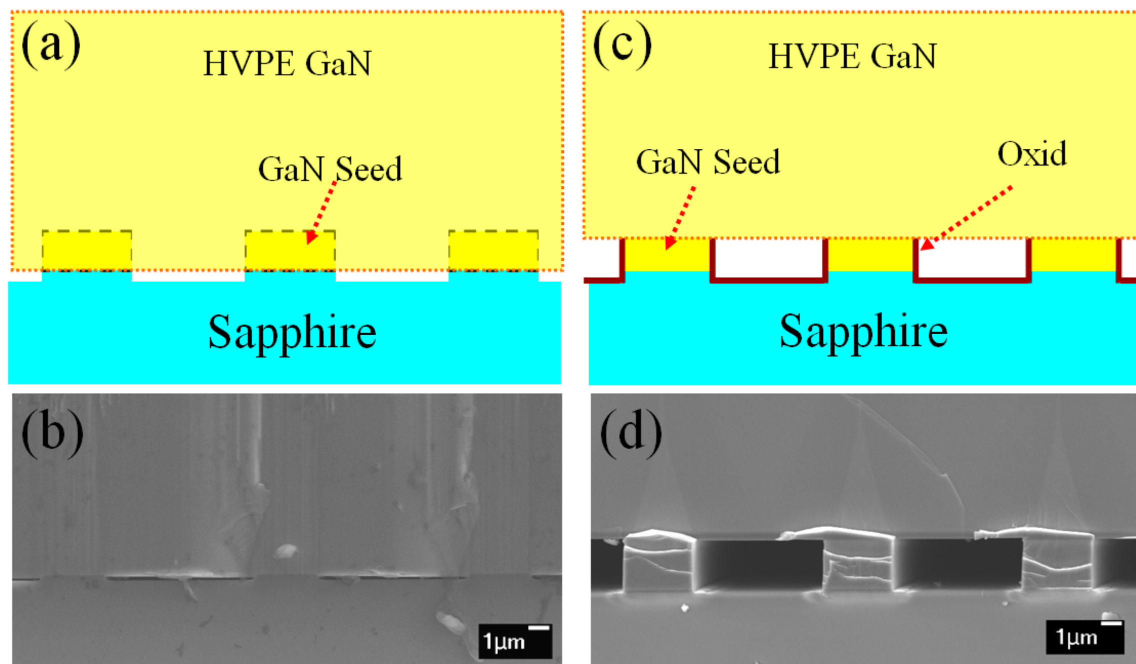

Fig. 2-1 Schematics and SEM images of the conventional pendeo and the HVAB structures after HVPE regrowth. (a) Schematic of the conventional pendeo structure. (b) SEM image of (a) after the HVPE regrowth. (c) Schematic of the HVAB structure. (d) SEM image of (c) after the HVPE regrowth.

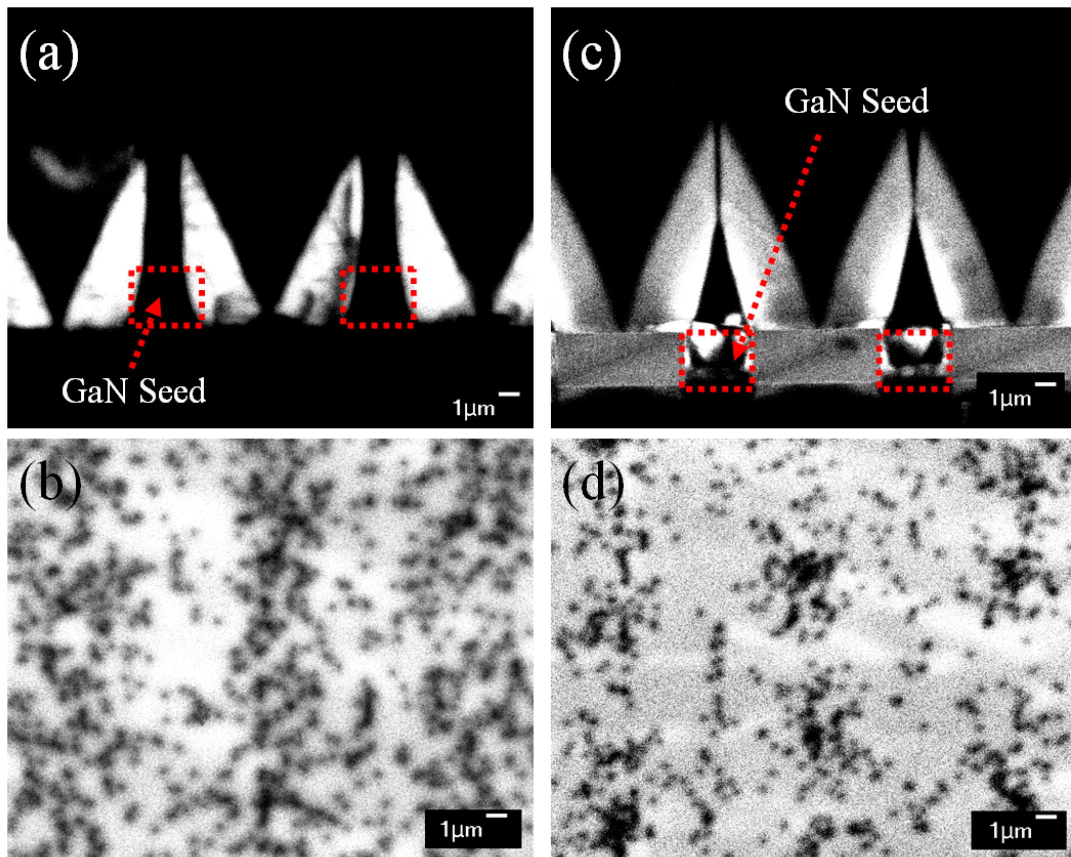

Fig. 2-2 Plane and cross-sectional CL images of the conventional pendeo and the HVAB structures. (a) Cross-sectional image of the conventional pendeo structure. (b) Plane-view of the conventional pendeo structure. (c) Cross-sectional image of the HVAB structure. (d) Plane-view of the HVAB structure.

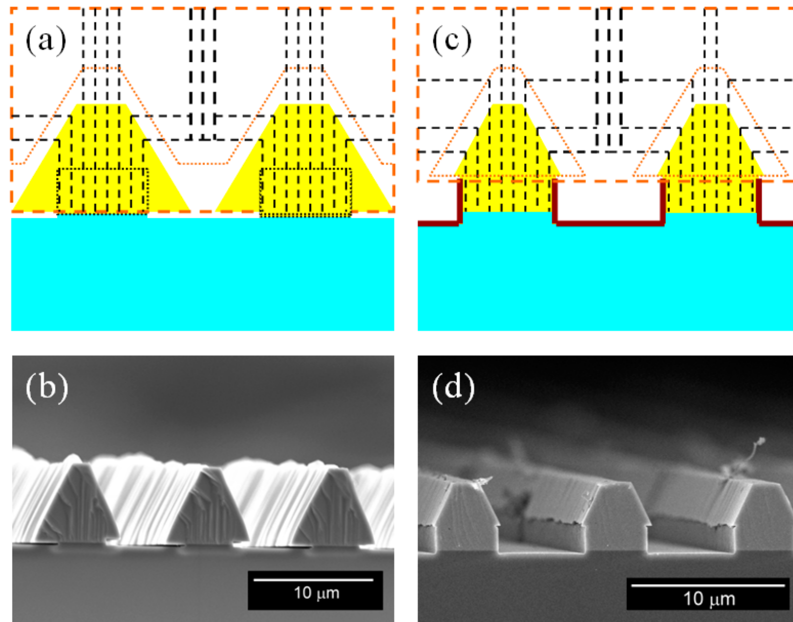

Fig. 2-3 Schematics of growth mechanism and SEM images of initial state of the HVPE regrowth in the conventional pendeo structure and the HVAB structures. (a) Schematic growth mechanism of the conventional pendeo structure. (b) Schematic of growth of the conventional pendeo structure. (c) SEM image of the initial growth of the HVAB structure. (d) SEM image of the initial growth of the HVAB structure.

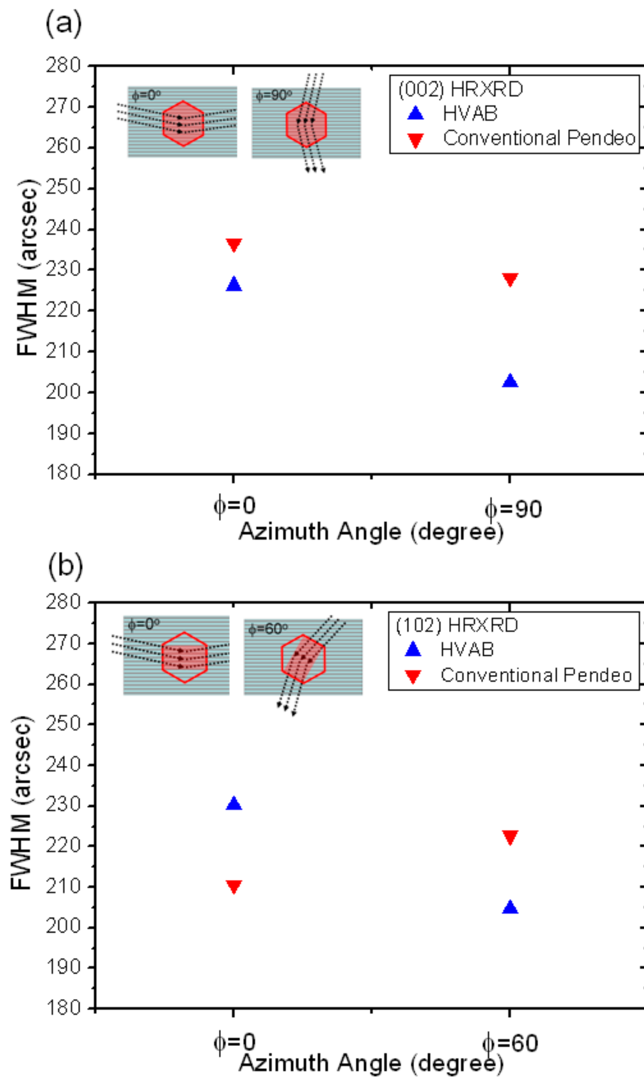

Fig. 2-4 Azimuthal dependence of the FWHM of (a) GaN (002) and (b) (102) HRXRD rocking curve of the conventional pendeo and the HVAB structures.

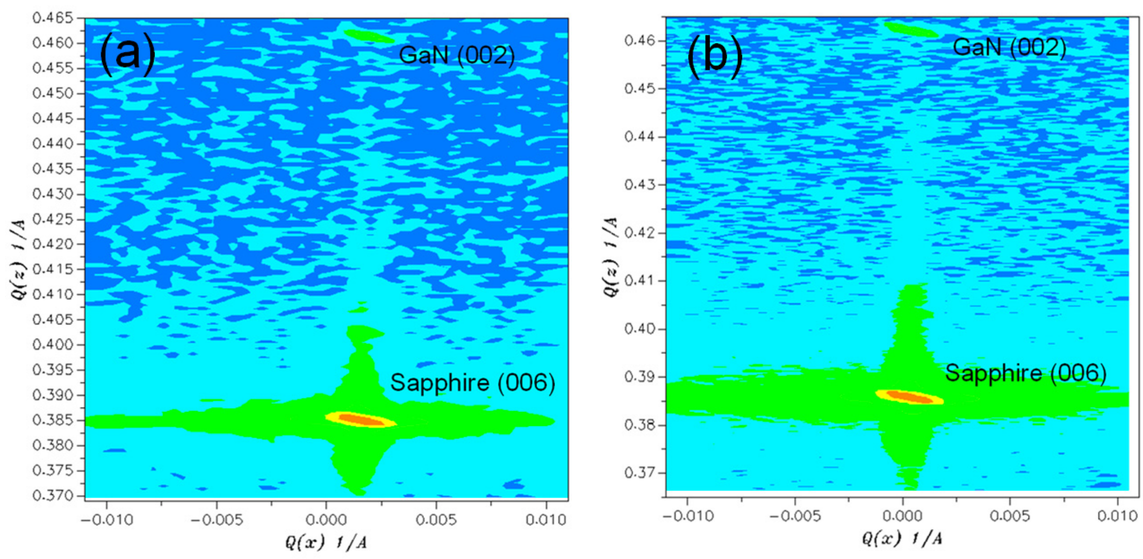

Fig. 2-5 Reciprocal space maps around the (002) point of c-plane GaN grown by HVPE in (a) conventional pendeo and (b) HVAB structures.

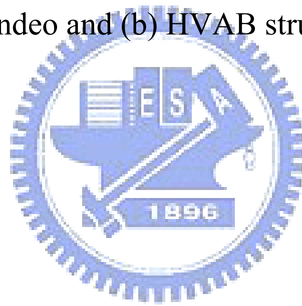

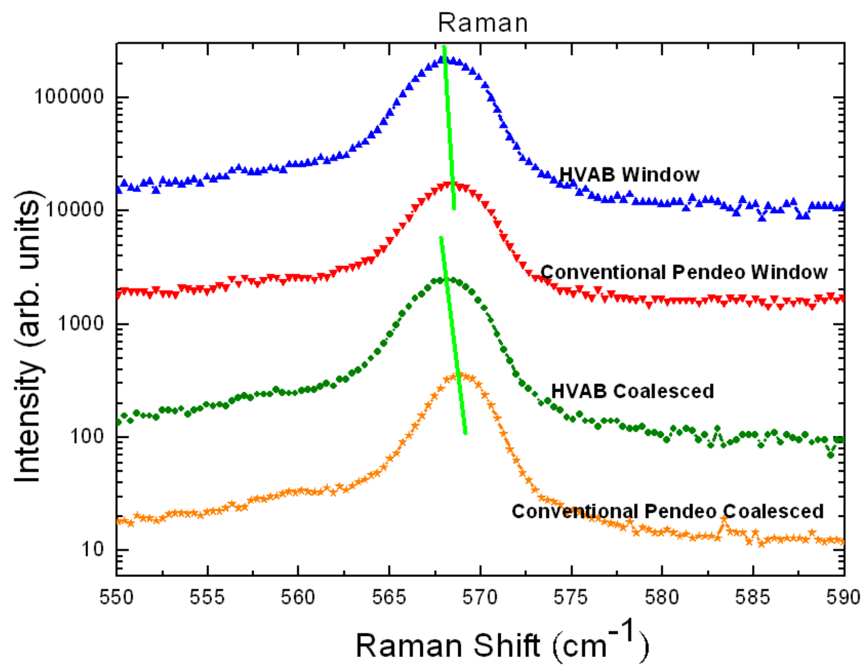

Fig. 2-6 Raman spectra of E_2(high) phonon frequency of the conventional pendeo and the HVAB structures in window and in wing regions.

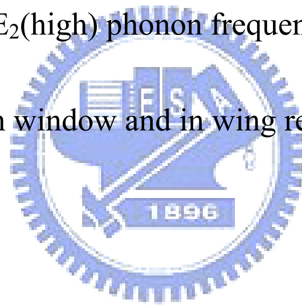

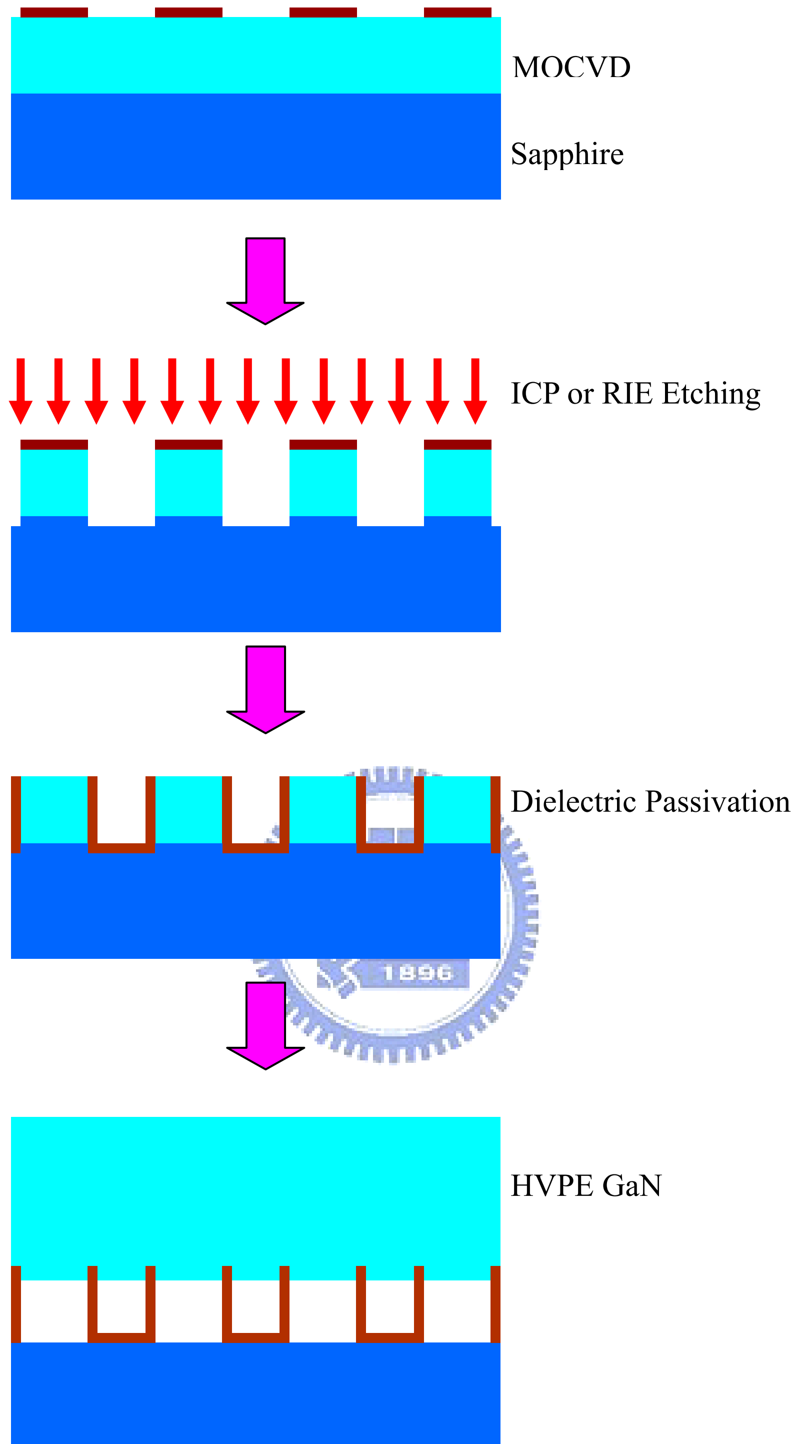

Fig. 2-7 Schematic of the GaN thick-film fabrication process with the dot air-bridged structure by HVPE. (a) MOCVD GaN template with SiN_x hard mask. (b) Dry etching process by ICP. (c) The sidewall passivation of GaN seed regions. (d) GaN thick-film regrowth by HVPE.

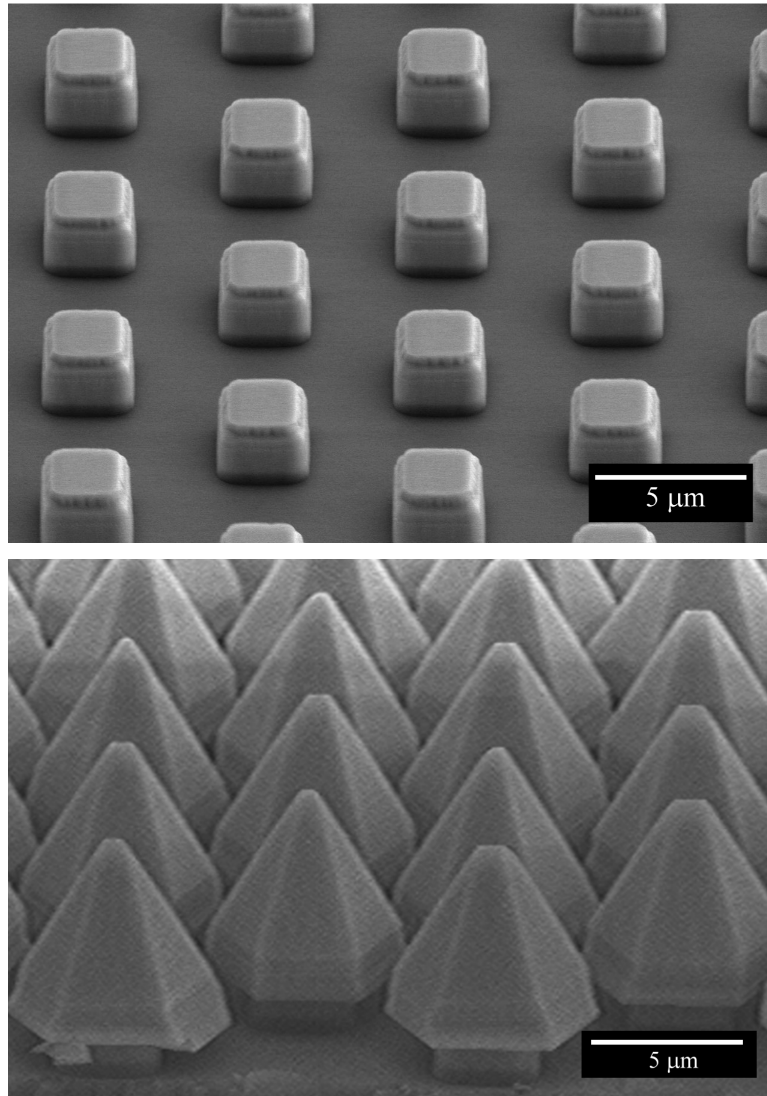

Fig. 2-8 (a) The bird's-eye view SEM image of the dot air-bridged structure. (b) The SEM image of 2 min initial growth state of the dot air-bridged structure by HVPE.

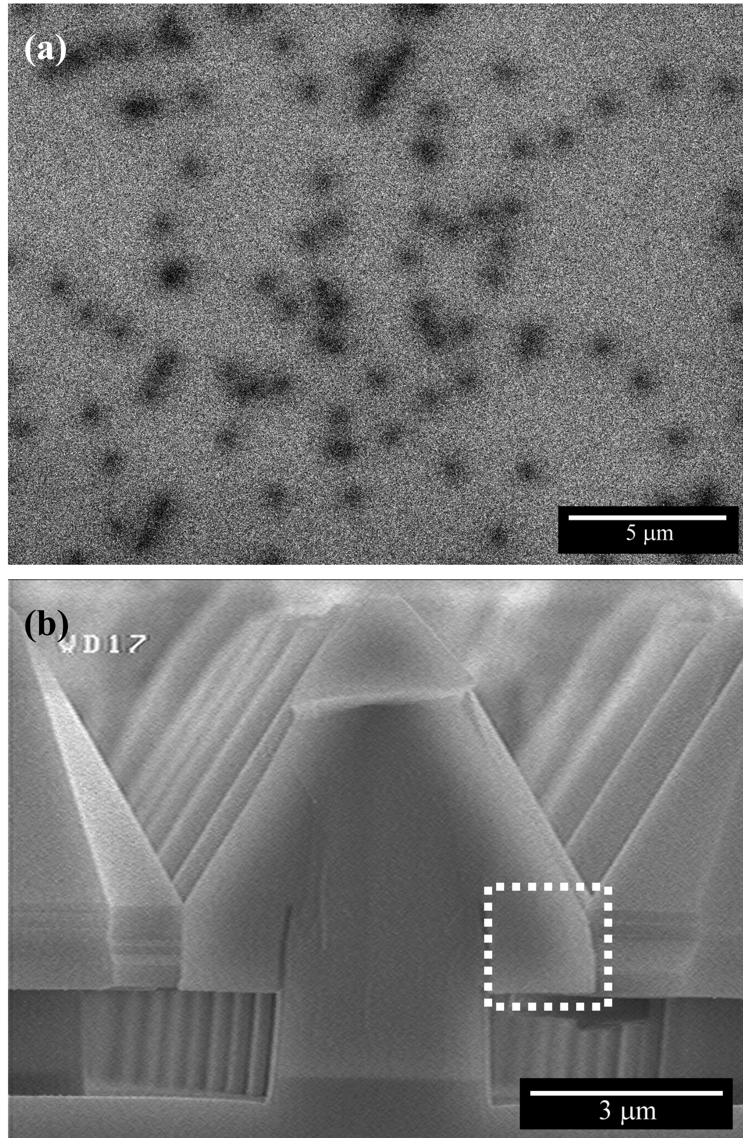

Fig. 2-9 (a) The plane view CL image of GaN thick-film of the dot air-bridged structure by HVPE. (b) The cross-sectional SEM image of GaN islands of the dot air-bridged structure. The dash line region indicated the GaN grown toward $< 000\overline{1} >$ direction.

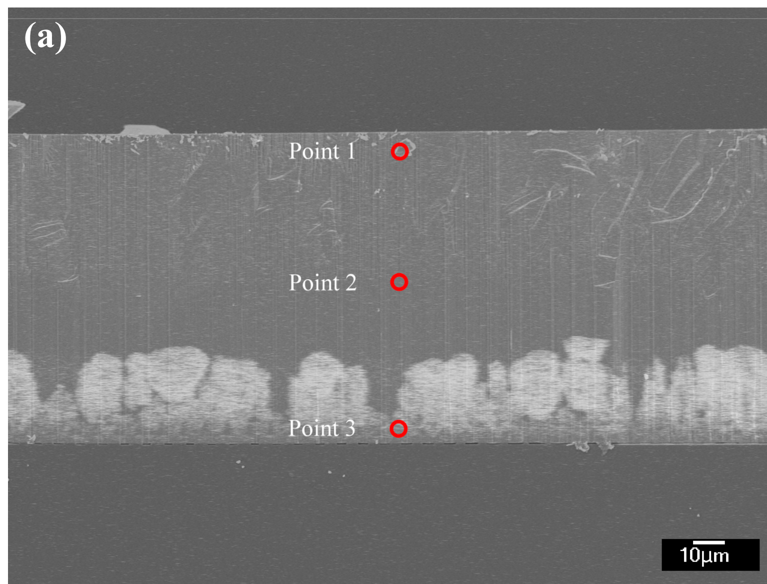

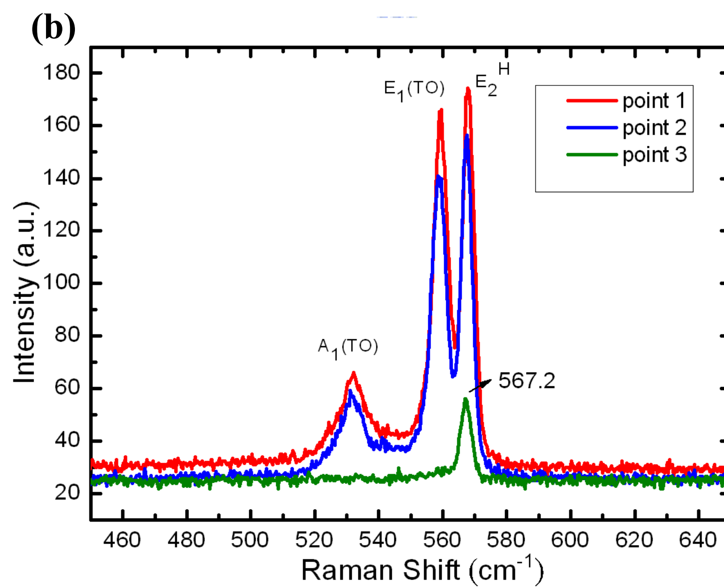

Fig. 2-10 (a) Cross section CL image of the dot air-bridged sample. (b) Raman spectra recorded on point 1, 2, and 3 of (a).

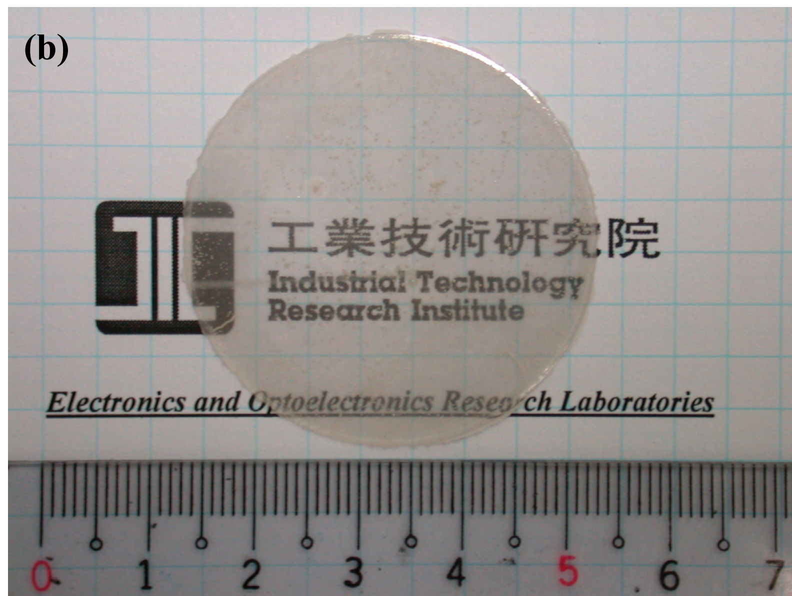

Fig. 2-11 (a) A 300 μm GaN thick-film in 1.5-inch diameter on 2-inch sapphire substrate without any crack. (b) The 300 μm freestanding GaN wafer in 1.5-inch diameter without any crack. The GaN wafer is transparent.

Tab. 2-1 Thermal expansion coefficient of wurtzite materials

(Wurtzite)	Thermal expansion coefficient (10^{-6}/K)	Room T ~600℃	600~1000℃
GaN	5.45	0.3 %	0.55 %
AlN	5.3	0.32 %	0.53 %
InN	5.7	0.34 %	0.57 %
6-H SiC	4.46	0.27 %	0.45 %
Si (111)	2.62	0.16 %	0.26 %
$LiAlO_2$	15	0.9 %	1.5 %
$LiGaO_2$	6	0.36 %	0.6 %
Al_2O_3	7.5	0.45 %	0.75 %
ZnO	2.9	0.16 %	0.3 %
GaAs(cubic)	6.0	0.36%	0.6%

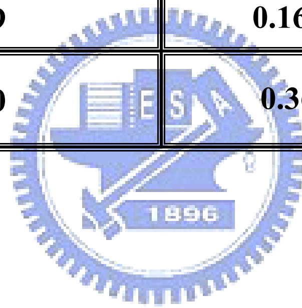

Chapter 3 Using Temperature Ramping Technique to Grow Crack-Free GaN Thick-Film by Hydride Vapor Phase Epitaxy

3.1 Introduction

The low decomposition temperature compared with the melting temperature of GaN makes it very challenging to obtain GaN by liquid-phase growth technology.[1] HVPE is the most effective method of fabricating a GaN substrate owing to its fast GaN growth rate.[2-5] In most cases of HVPE GaN growth, the foreign substrate used is a sapphire substrate owing to its reliability and low cost. The lattice mismatch and the difference in TEC between sapphire and GaN are 16% and roughly 2×10^{-6}/K, respectively.[6-8] If the growth temperature of HVPE GaN is near 1000 ^{o}C, the difference in TEC between sapphire and GaN is 0.2%, which results in the GaN/sapphire structure bending and cracking during the cooling process.

Several groups have developed self-separation techniques for producing freestanding GaN thick films by HVPE via several methods such as void-assisted separation, facet-controlled separation, and $WSiN_x$ epitaxial lateral overgrowth techniques.[9-12] These self-separation techniques can prevent GaN thick films from

cracking; however, they require excess processing, which increases the cost of GaN thick-film epitaxy. In addition, the yield of self-separation techniques for obtaining complete freestanding GaN wafers without any cracks is still very low.

3.2 Experiment

In this investigation, a very simple technique without complex processes was developed to prevent cracks caused by differences in TEC between GaN and original substrates for HVPE growth.

A 4-μm-thick GaN layer was initially grown on a c-plane sapphire substrate as template for the HVPE GaN thick-film regrowth by MOCVD. The GaN template was mounted a horizontal HVPE reactor to grow a 300-μm-thick GaN film. The HVPE GaN growth temperature was started at a low temperature (LT) of 950 ^{o}C and ramped to a high temperature (HT) of 1050 ^{o}C at a ramping rate of about 1 ^{o}C/min. After the temperature ramping, GaN growth temperature was maintained at 1050 ^{o}C until the thickness of the GaN film exceeded 300 μm. In the GaN growth process, NH_3 gas was used as the nitrogen source, and GaCl, generated by liquid gallium and HCl gas at 850 ^{o}C, was used as the gallium source. The ambient of the carrier gas was a mixture of H_2 and N_2, and pressure was maintained at 900 mbar throughout the GaN growth process. To provide a significant comparison, another GaN sample was directly grown

on the MOCVD template at 1050 ^{o}C without the temperature ramping step and LT layer.

3.3 Result and Discussion

Figure 3-1 shows the full structure of the GaN film grown with the temperature ramping step. The HVPE GaN growth process was started at 950 ^{o}C for rough 50 μm GaN growth. Then, the growth temperature was ramped at 1 ^{o}C/min until it reached 1050 ^{o}C. The thicknesses of the GaN film grown with temperature ramping and at HT were roughly 120 μm and over 130 μm, respectively.

As can be seen in Fig. 3-2(a), the sample grown with the temperature ramping step shows crack-free and mirrorlike features on the surface. However, the sample grown without the temperature ramping step and LT layer was cracked, as shown in the inset of Fig. 3-2(a). The 1.5 in. crack-free sample was separated by a laser lift-off process using a 355 nm Nd:YAG laser, as shown in Fig. 3-2(b). The HVPE GaN was characterized by scanning electron microscopy (SEM), cathodoluminescence (CL) measurement, high-resolution X-ray diffraction (HRXRD) analysis, micro-Raman spectroscopy, and etch pit density (EPD) measurement. The sample for the EPD experiment was etched at 220 ^{o}C for 20 min in a mixture of H_3PO_4 and H_2SO_4 at a ratio of 1:3. To understand the stress distribution, the CL and Raman measurements

were carried out on the GaN thick films samples without separation from the sapphire substrate. The XRD analysis was carried out before and after the laser lift-off process.

Figure 3-3 shows the cross-sectional CL contrasted images of the HVPE GaN samples grown at different ramping rates. A bright band was clearly observed in these samples with different thicknesses. Several reports have mentioned that the bright band corresponds to free carriers, which result from defects and impurities.[11, 13] Figure 3-3(a) shows the sample grown with a ramping rate of 3.3 ^{o}C/min, and the thickness of the bright region is 90 μm. Figures 3-3(b)-3(d) show the samples with ramping rates of 1.7, 1, and 0.8 ^{o}C/min, respectively. As the ramping rate decreases, the ramping process needs more time to achieve HT growth. This means that thicker HVPE GaN was grown during the lower-temperature process than during the HT, high-quality growth process, as ramping time was increased. The of LT growth and ramping growth regions were like a large buffer layer that relaxed the thermal stress to prevent the cracking of GaN thick films grown on sapphire substrate. In this paper, the discussion mainly focuses on the sample of 1 ^{o}C/min ramping rate; results obtained with different ramping rates will be compared and discussed in the future.

Figure 3-4(a) shows the low-temperature CL spectra of a cross-sectional region of the sample grown with a 1 ^{o}C/min ramping rate at 15 K. The CL spectrum data were measured at the bottom, middle, and top regions of the cross-sectional sample.

The middle and top regions corresponded to the ramping layer and HT growth layer, respectively. Near-band-edge emission peaks were observed at 358 nm (3.46 eV), 358 nm, and 357 nm (3.47 eV), which correspond to the bottom, ramping, and HT regions, respectively, for HVPE GaN growth. A biaxial stress of one GPa would shift the near-band-edge peak by 27 $\pm$ 2 meV. Tensile or compressive stress can be calculated with reference to the strain-free emission peak at 3.467 eV.[14] If the near-band-edge emission energy was less than 3.467 eV, the presence of tensile stress would be expected; on the other hand, larger values would indicate that the stress was compressive. On the basis of the report by Kisielowski *et al.*,[14] the stress in the bottom, ramping, and HT regions of the GaN/sapphire structure could be calculated. The bottom and ramping regions showed a small tensile stress of 0.1 GPa, and the HT region showed a compressive stress of 0.2 GPa. Normally, compressive stress would be observed in GaN/sapphire structures; the presence of tensile stress at the bottom and ramping regions may be in the error range of the CL measurement.

Raman scattering spectra were also measured at the same positions as CL spectra at room temperature, as shown in Fig. 3-4(b). The peaks of the E_2 (high) mode phonon frequency were observed at 567.5, 567.5, and 567.3 cm^{-1} in the bottom, ramping, and HT regions, which corresponded to compressive stresses of 0.12, 0.12, and 0.07 GPa, respectively.[15] The E_2 (high) mode phonon frequency of the sample

grown without ramping and the LT layer was observed at 569.2 cm^{-1} in the bottom region of GaN, which indicated a larger compressive stress of 0.5 GPa.

From the results of the CL and Raman spectrum analyses, we determined that residual stress could be relaxed in the structure of GaN thick films without separation from the sapphire substrate by the temperature ramping technique. The relaxation of thermal stress is useful for preventing the cracking of the GaN/sapphire structure. This is very important for successfully fabricating GaN substrates by HVPE.

Figure 3-5(a) shows the full width at half maximum (FWHM) of the HRXRD rocking curve of the GaN symmetric (002) plane before and after the laser lift-off process. The FWHM of GaN on the sapphire substrate is 847.2 arcsec. This large value is due to the bowing of the GaN/sapphire structure. The FWHM of the freestanding GaN thick film is 156.7 arcsec, which could be more improved after the LT growth region was removed. Figure 3-5(b) shows a top-view CL image of the 300 μm free-standing GaN. The dislocation density is about 1×10^{7} cm^{-2} by the calculation of both the CL image and the EPD measurement. The random distribution of dark spots in the CL image shows that there is no additional designed-patterned structure applied to reduce dislocation density in these samples.

Figure 3-6(a) shows the picture of 2 inch GaN thick-film on sapphire with 360 μm-thick. The curvature radius of the GaN wafer is about 0.4 m before lift-off from

sapphire substrate. Figure 3-6(b) shows the picture of freestanding GaN wafer after LLO process. The curvature radius of freestanding GaN wafer is large than 2 m. The ring of the outer was caused by higher power density of the laser pulse.

Figure 3-7 shows the CL image of regrown GaN thick-film with the thickness about 600 μm. The dislocation density is about 4×10^{6} cm^{-2}. It demonstrates that the increasing of GaN thickness can reduce to dislocation density. Tablet 3-1 shows the properties of GaN thick-film by the temperature ramping technique.

3.4 Conclusion

In summary, a very simple technique without complex processes for preventing cracks in GaN thick films grown by HVPE is developed. High-quality 1.5 in. large-area freestanding GaN films with thicknesses of over 300 μm can be obtained by this technique after the consequent lift-off process. The FWHM of HRXRD of GaN (002) is 156.7 arcsec and the dislocation density is about 1×10^{7} cm^{-2}. No additional designed-patterned structure was required in these samples to reduce dislocation density and thermal stress.

3.5 References

1) W. Utsumi, H. Saitoh, H. Kaneko, T. Watanuki, K. Aoki, and O. Shimomura: Nat. Mater. **2**, 735 (2003).

2) M. K. Kelly, R. P. Vaudo, V. M. Phanse, L. Görgens, O. Ambacher, and M. Stutzmann: Jpn. J. Appl. Phys. **38**, L217 (1999).

3) S. S. Park, Il-W. Park, and S. H. Choh: Jpn. J. Appl. Phys. 3**9**, L1141 (2000).

4) K. Motoki, T. Okahisa, N. Matsumoto, M. Matsushima, H. Kimura, H. Kasai, K. Takemoto, K. Uematsu, T. Hirano, M. Nakayama, S. Nakahata, M. Ueno, D. Hara, Y. Kumagai, A. Koukitu, and H. Seki: Jpn. J. Appl. Phys. **40**, L140 (2001).

5) D. Gogova, H. Larsson, A. Kasic, G. R. Yazdi, I. Ivanov, R. Yakimova, B. Monemar, E. Aujol, E. Frayssinet, J. P. Faurie, B. Beaumont, and P. Gibart: Jpn. J. Appl. Phys. **44**, 1181 (2005).

6) R. D. Vispute, V. Talyansky, S. Choopun, R. P. Sharma, T. Venkatesan, M. He, X. Tang, J. B. Halpern, M. G. Spencer, Y. X. Li, L. G. Salamanca-Riba, A. A. Iliadis, and K. A. Jones: Appl. Phys. Lett. **73**, 348 (1998).

7) S. Hearne, E. Chason, J. Han, J. A. Floro, J. Figiel, J. Hunter, H. Amano, and I. S. T. Tsong: Appl. Phys. Lett. **74**, 356 (1999).

8) T. Detchprohm, K. Hiramatsu, K. Itoh, and I. Akasaki: Jpn. J. Appl. Phys. **31**,

L1454 (1992).

9) Y. Oshima, T. Eri, M. Shibata, H. Sunakawa, K. Kobayashi, T. Ichihashi, and A. Usui: Jpn. J. Appl. Phys. **42**, L1 (2003).

10) Y. Oshima, T. Suzuki, T. Eri, Y. Kawaguchi, K. Watanabe, M. Shibata, and T. Mishima: J. Appl. Phys. **98**, 103509 (2005).

11) S. Bohyama, H. Miyake, K. Hiramatsu, Y. Tsuchida, and T. Maeda: Jpn. J. Appl. Phys. **44**, L24 (2005).

12) C. Hennig, E. Richter, M. Weyers, and G. Tränkle: J. Cryst. Growth **310**, 911 (2008).

13) T. B. Wei, P. Ma, R. F. Duan, J. X. Wang, J. M. Li, and Y. P. Zeng：Chin. Phys. Lett. **24**, 822 (2007).

14) C. Kisielowski, J. Krüger, S. Ruvimov, T. Suski, J. W. Ager III, E. Jones, Z. Liliental-Weber, M. Rubin, E. R. Weber, M. D. Bremser, and R. F. Davis: Phys. Rev. B **54**, 17745 (1996).

15) A. R. Goñi, H. Siegle, K. Syassen, C. Thomsen, and J.-M. Wagner, Phys. Rev. B **64**, 035205 (2001).

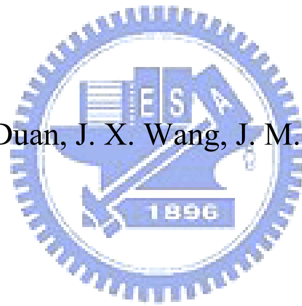

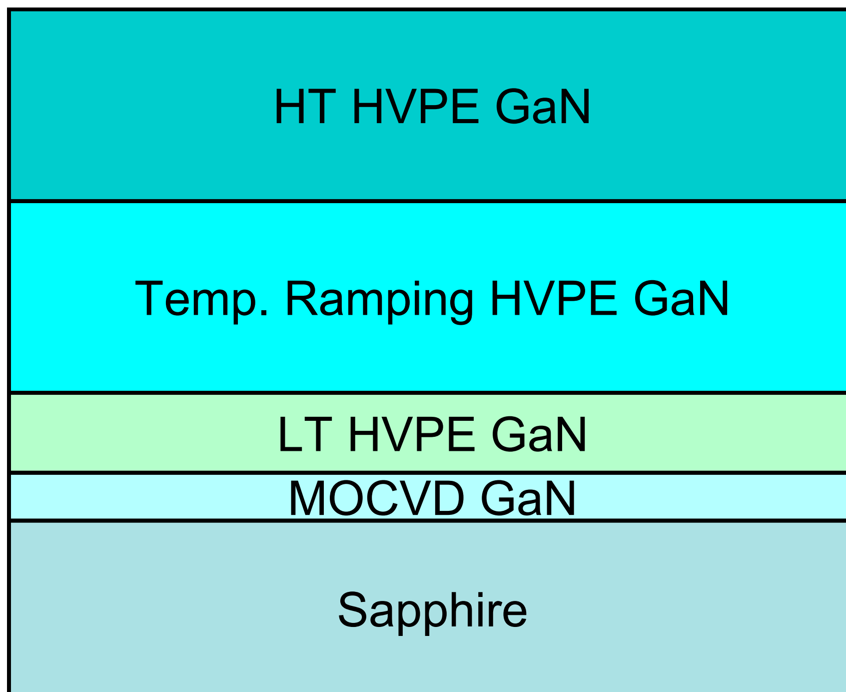

Fig. 3-1 Schematic of the temperature ramping GaN growth structure by HVPE.

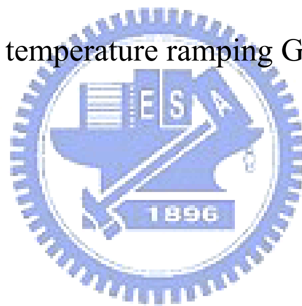

Fig. 3-2 (a) A 1.5 inch 300 μm crack free GaN thick-film grown on sapphire substrate with temperature ramping step. The inset is the cracked GaN without any temperature ramping step. (b) A 300 μm crack free freestanding GaN separated by laser lift-off process.

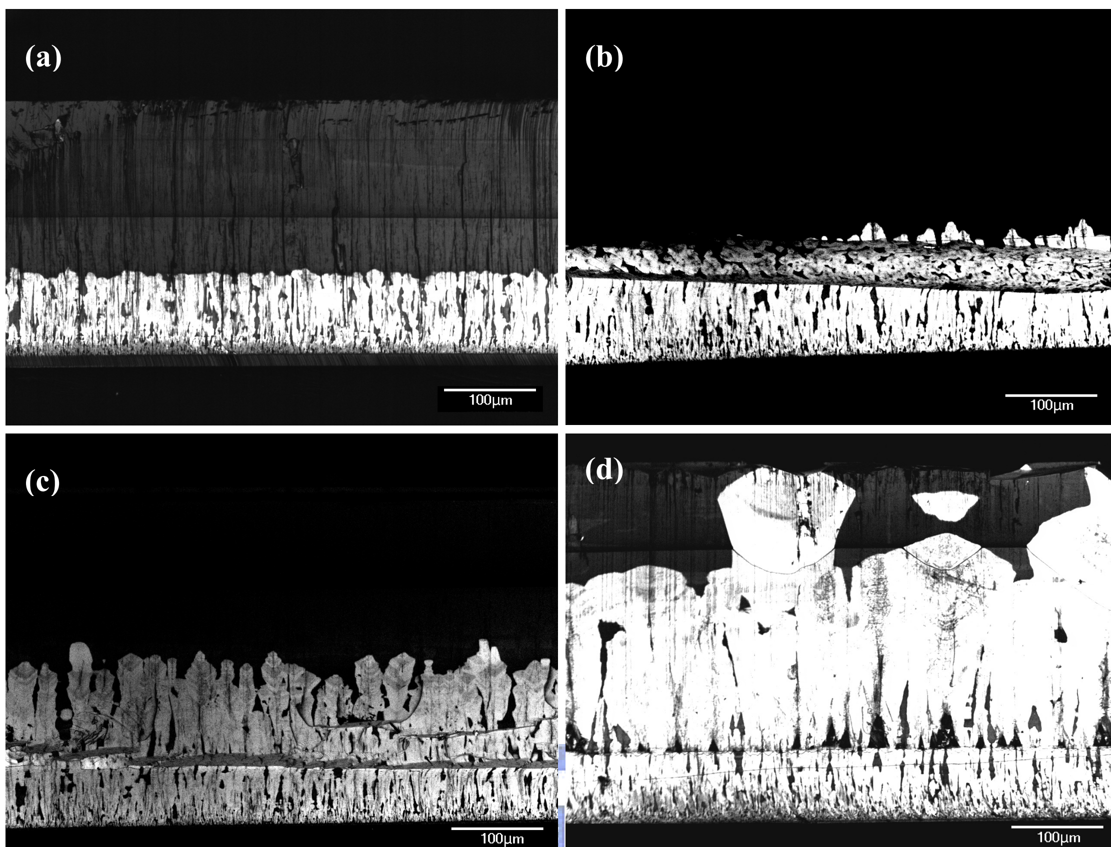

Fig. 3-3 The cross-sectional CL images of temperature ramping layer at various ramping rate. (a) 3.3 °C/min. (b) 1.7 °C/min. (c) 1.0 °C/min. (d) 0.8 °C/min.

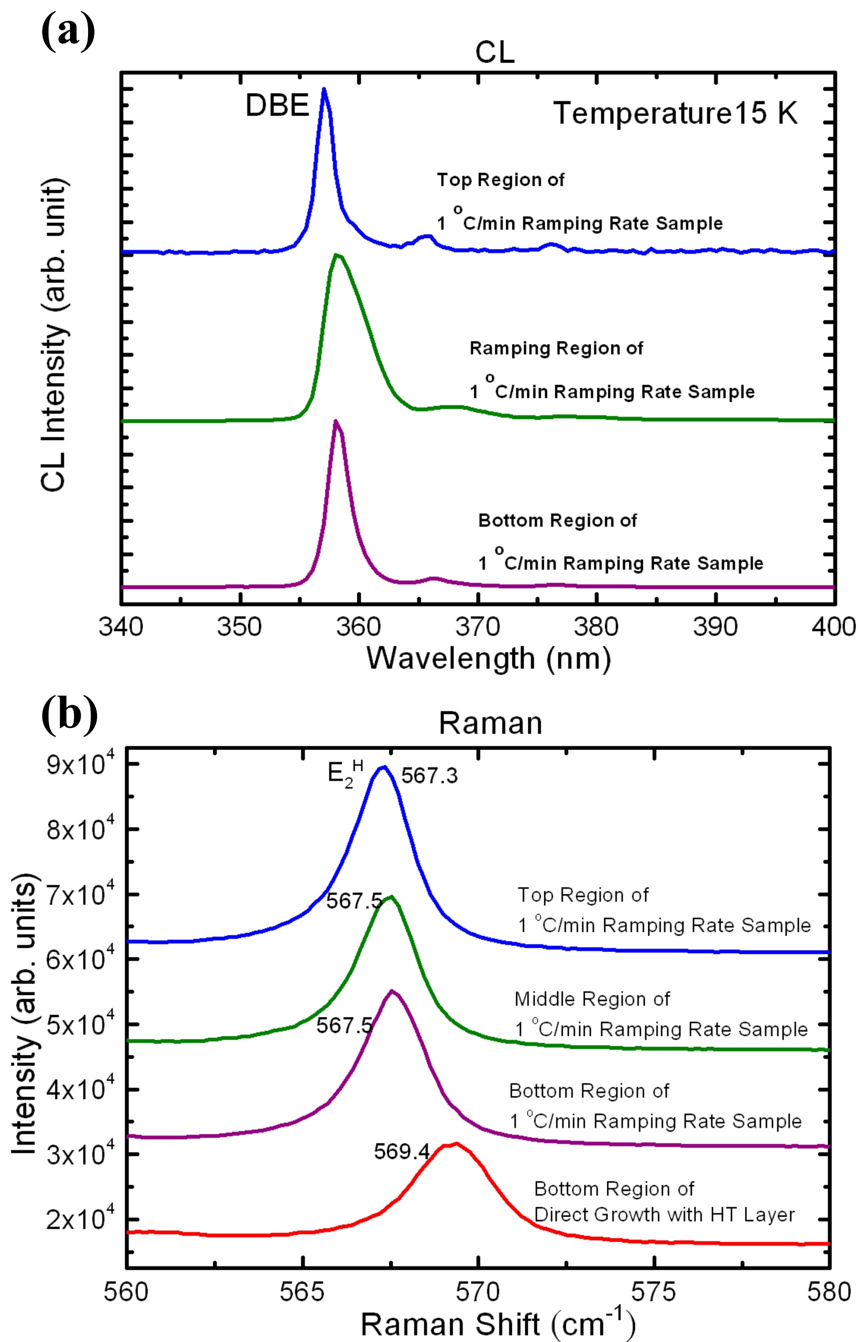

Fig. 3-4 (a) The CL spectra of cross-sectional regions of the sample with 1.0 °C/min ramping rate. The spectra were measured at the bottom, the ramping, and the HT regions. (b) The Raman spectra of cross-sectional regions of the same sample as (a). The spectra were measured at the bottom, the ramping, and the HT regions.

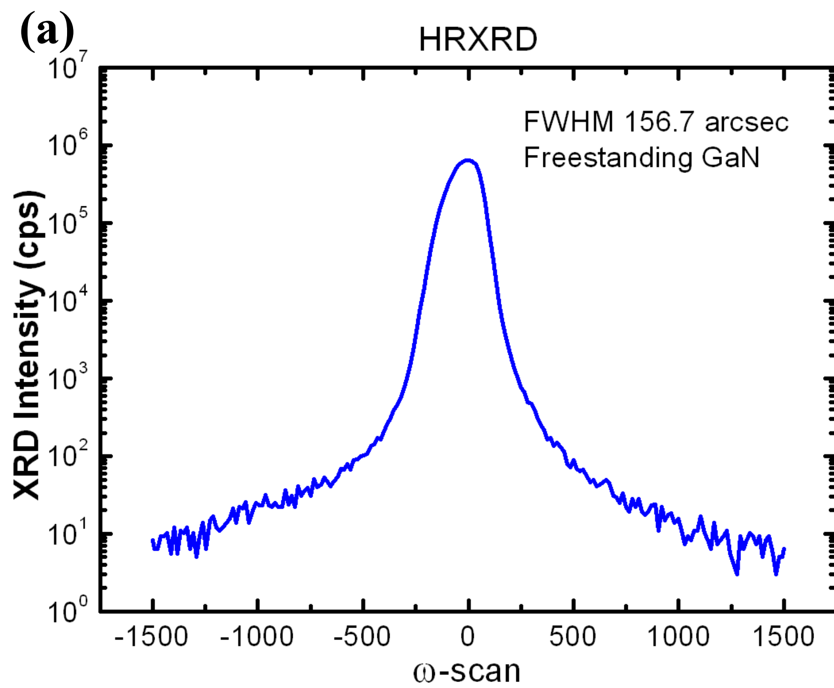

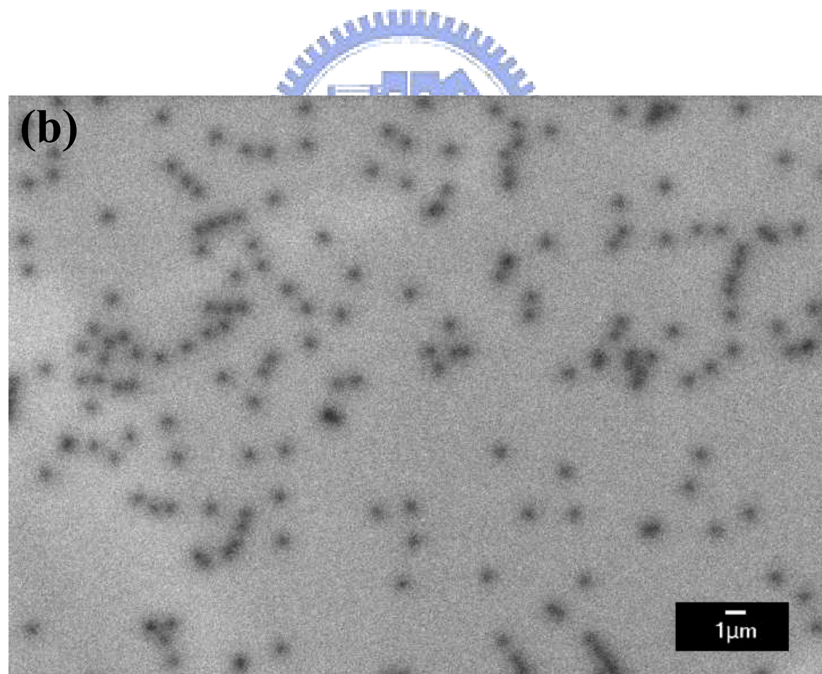

Fig. 3-5 (a) The rocking curve of HRXRD of the freestanding GaN with 1.0 °C/min ramping rate. The value of FWHM is 156.7 arcsec. (b) The top view CL image of freestanding GaN wafer. The dark spots show the position of dislocations.

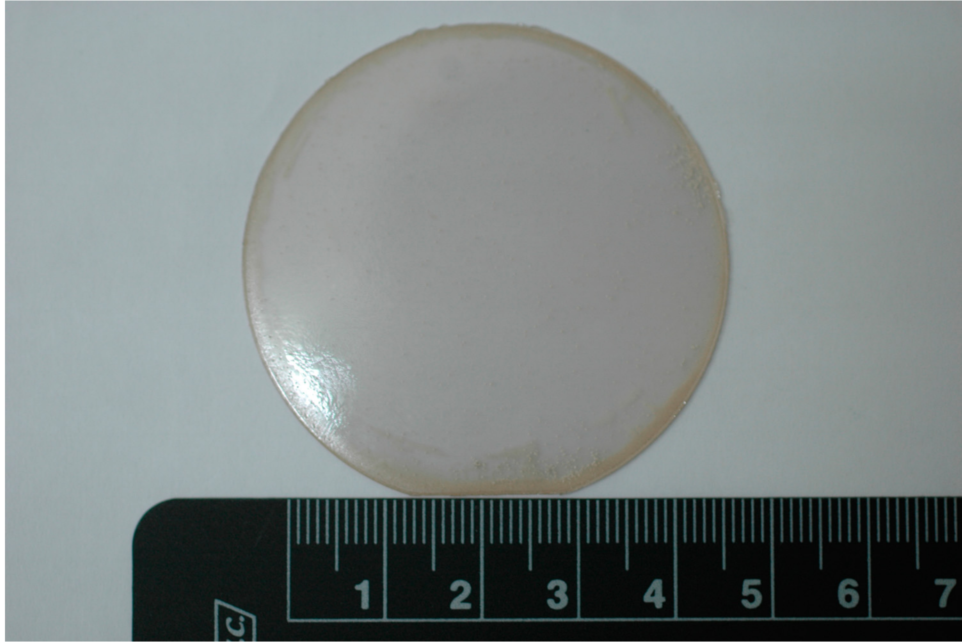

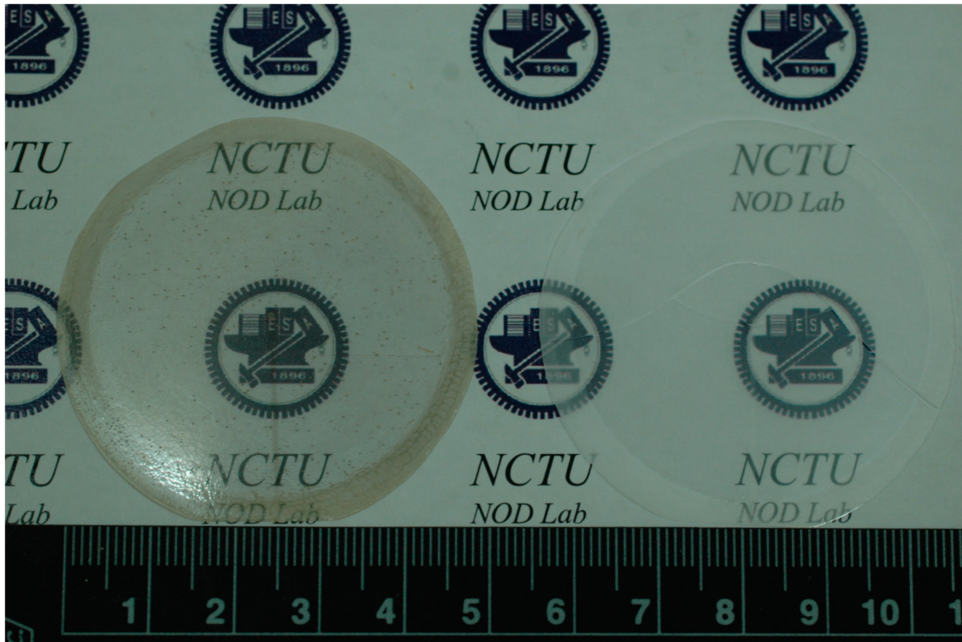

Fig. 3-6 (a) A 2 inch, 360 μm-thick GaN on sapphire substrate before LLO process. (b) Freestanding GaN wafer from (a) after the LLO process. The right hand side is the sapphire substrate and the left hand side is the GaN wafer.

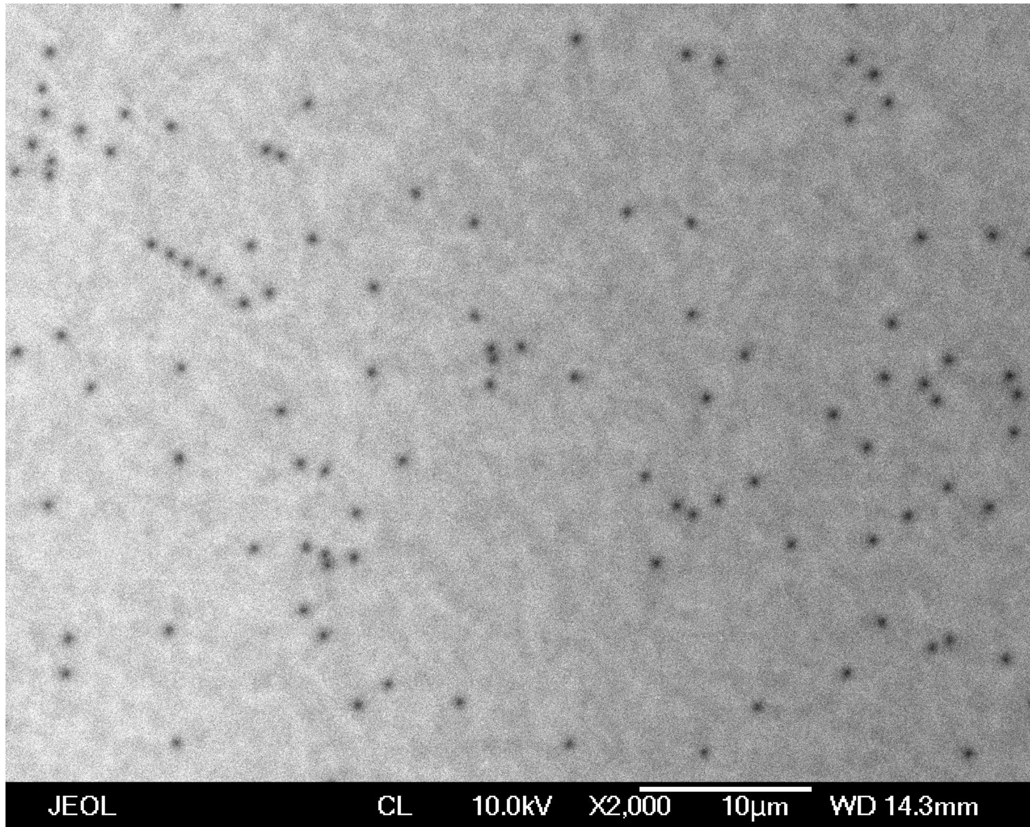

Fig. 3-7 The CL image of a regrown 600 µm GaN thick-film. The dislocation density is about 4×10^6 cm^{-2}.

Tab. 3-1 The properties of GaN wafer of NOD Lab

Wafer Size	**1.5 to 2 inch**	
Wafer Thickness	**250 to 350 μm**	
Crystal Orientation	**(001) c-axis**	
Crystal Structure	**Wurtzite**	
Growth Face	**Ga-Face**	
FWHM of XRD w-sacn	**~150 arcsec (free-standing GaN)**	
Resistivity	**0.09 Ω-cm**	
Carrier Type	**n-Type**	
Carrier Concentration	**1.60 x 10^{17} cm^{-3}**	
Mobility	**437 cm^2/V-s**	
Surface roughness (RSM)	**3.25 nm**	
Dislocation Density	**4×10^{6} to 1×10^{7} cm^{-2}**	

Chapter 4 Introduction to Laser Lift-Off

4.1 Introduction to Laser Lift-Off

After a GaN thick-film has been grown by HVPE, the most difficult problem in obtaining a freestanding GaN wafer is the separation of the GaN thick-film from the foreign substrates such as GaAs, Si, Ga_2O_3, or 6H-SiC.

Various methods have been adopted to remove the foreign substrates, such as selective chemical etching, self-separation, lapping, dry etching and laser induced lift-off. Selective chemical etching depends on the deposition of a sacrificial layer between the foreign substrate and the GaN thick-film. Then, the selective chemical etching properties of the sacrificial layer are exploited to maintain the GaN thick-film and remove the sacrificial layer to separate the GaN from the foreign substrate. Another approach involves using a selective chemical etchant to etch the foreign substrate and leave GaN as, for example, a GaN thick-film grown on an GaAs substrate. The second approach is the developed epitaxial procedure by which the GaN film is caused to self-separation from its foreign substrate during cooling from the growth temperature by the accumulation of thermal stress between GaN and its

foreign substrate. Chapter 2 described in detail epitaxial self-separation methods. The third and fourth approaches are lapping and dry etching to remove the substrate. The fifth approach is the laser lift-off (LLO) technique, which is extremely flexible and significantly faster than the aforementioned methods. In 1996, Kelly *et al*. reported upon the pulse laser-assisted thermal decomposition of GaN using a Q-switched Nd:YAG laser with a wavelength of 355 nm.[1, 2] This technique can be used in the fabrication of freestanding bulk GaN, thin-GaN, or flip chip LEDs.

In the LLO process, the GaN layer is separated from the substrate by irradiating the substrate-film interface through the transparent substrate at a wavelength that can be transmitted in the substrate in a high-power laser pulse. The sapphire substrate is the most suitable substrate for using in LLO technique. The advantages of the LLO process over the other aforementioned methods are,[3]

1、 Sapphire substrate is a readily available, well developed and reasonably priced.

2、 The LLO technique does not depend on any specific sacrificial layers in the growth process.

3、 The rate of removing by the LLO technique is quite fast and can be easily scaled up.

4、 The LLO process can also occur immediately after the epitaxial process

that involves GaN in the deposition reactor before cooling to room temperature. It prevents bending induced by the difference between the TECs of GaN and the foreign substrate.[7]

5、 The yield of the LLO process is more stable than that of the other aforementioned lift-off methods.

The absorption of the laser pulse energy of GaN in LLO process causes rapid thermal decomposition of the irradiated GaN interfacial layer into gaseous N_2 and metallic Ga, as shown in Fig. 4-1.

$$2GaN \rightleftharpoons N_{2(g)} + 2Ga_{(s)} \qquad \text{(R4-1)}$$

High-intensity laser pulses enter the GaN/sapphire interface via the side of the sapphire. The shock wave decomposes the thin GaN layer. The samples are placed on sapphire powder to dampen the laser pulse. An additional hot plate is used to raise the temperature to relax the bowing that is caused by difference between the TECs of GaN and substrate during the LLO process. The most suitable laser systems in the case of GaN/sapphire are the third harmonic of the Q-switch Nd:YAG laser and the excimer KrF laser.[8-10] The wavelengths for GaN/sapphire LLO of Nd:YAG and KrF lasers are 355 and 248 nm, respectively. In this experiment, the chosen laser system is an Nd:YAG 355 nm laser.

Figure 4-2 plots the thermal decomposition rate of GaN as a function of temperature. The flux of nitrogen molecules can be a significant index of the GaN decomposition rate. The nitrogen flux increases exponentially with the temperature above 850 ^{o}C.[3]

$$\Phi(N_2) = 1.2\times 10^{31} e^{-3.9eV/kT} (s^{-1}cm^{-2}) \qquad \text{Eq(4-1)}$$

Therefore, GaN can be decomposed efficiently by thermal decomposition when the temperature exceeds 850 ^{o}C. The 355 nm Nd:YAG or 248 nm excimer KrF pulse lasers can locally heat the GaN/sapphire interface to increase the temperature over 850 ^{o}C to decompose GaN. Figure 4-3 shows the depth of decomposition that is caused by the signal pulse Nd:YAG laser in GaN at room temperature at different absorbed laser power densities. The threshold laser power density was approximately 250 mJ/cm^2 in the experiment of Miskys *et al*. However, in this experiment, the threshold laser power density of GaN decomposition was less than 200 mJ/cm^2.

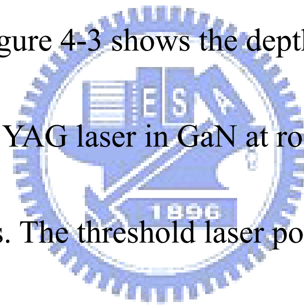

4.2 Laser Lift-Off System

Figure 4-4 schematically depicts the LLO system, which consists of various parts, including the UV laser main body, mirrors, a laser power meter, a hot plate, the x-y 2-dimension stage, a controlling computer and others.

The laser was a pulsed UV laser with a photon energy above the GaN bandgap (3.42 eV), such as that of the third harmonic of the Nd:YAG laser at 355 nm, or an excimer laser. The duration time of the laser pulse was short to localize the heating close to the GaN/sapphire interface. Typically, the duration time of the excimer KrF laser is several tens of nanoseconda, which is probably acceptable for an LLO system. However, the duration time of a Q-switched Nd:YAG laser pulse is in the range of several nanoseconds, which is better for an LLO system, because it requires less energy and causes a thinner region of the interface of GaN/sapphire to be decomposed. Less nitrogen gas is thus released, shocking to the film less.

1896

The mirrors used in the LLO system include the reflective mirrors; the system also includes a half-wave retarding plate, a polarizing beam splitter and a beam sampler. The coating of the reflective mirrors should be rated for high energy pulse lasers with a wavelength of 355 nm at an angle of incidence of 45°. The half-wave retarding plate is used to rotate the polarization of the laser beam. It is made of crystal quartz and is mounted in a rotating holder. The half-wave retarding plate is specified for 355 nm and has a high energy rated pulse antireflection coating on both sides. The polarizing beam splitter realized using a Glan-Taylor prism, which passes the 355 nm UV pulse and refracts the others to the beam dump. Combining the half-wave retarding plate and the polarizing beam splitter enables, the power and polarization of

a 355 nm UV pulse to be adjusted and controlled. The beam sampler and laser power meter set in the LLO system are used to monitor *in-situ* the laser pulse energy. The front side of the beam splitter is uncoated and has about 5 % reflectivity, and the backside is an antireflection coating.

The x-y stage used in the LLO system transfers the wafers. Since the laser light trace is fixed in the LLO system and hard to move to scan ove the samples, a high resolution x-y stage is necessary to scan the laser pulse uniformly on the plate of the samples. The resolution of the x-y stage system is 0.1 μm. The hot plate in the LLO system is used to heat GaN/sapphire homogeneously during the LLO process, to reduce its bending, which is caused by the difference between the TECs of GaN and sapphire. The bowing of GaN can be significantly reduced when the temperature is above 600 ^{o}C.[3, 4] Ideally, the temperature of homogeneous heating of the GaN/sapphire should be close to the growth temperature, or else *in-situ* lift-off in the HVPE reactor would be the preferred means of preventing bending and cracking.

4.3 Results and Discussion

Figure 4-5(a) shows a bird's eye view SEM image of the interface of the GaN thin-film that is separated from the sapphire by the LLO process. The 3 μm-thick GaN

thin-film was initially bonded to the GaAs substrate with the Ti/Al/Ti/Au metals, and then, the samples were separated using an Nd:YAG laser. Ga droplets were observed on the underside of freestanding GaN films. The GaN film remained on the GaAs submount without flaking. Figure 4-5(b) shows a plane-view SEM image of the underside of a 250 μm-thick freestanding GaN. Small voids and GaN droplets were observed on its surface. No cracks were found in the freestanding GaN thick-film. The GaN droplets on the n-face GaN were removed by HCl solution at room temperature. Figure 4-6 shows the Raman spectra of a GaN thick-film before and after the LLO process. The stress was analyzed by examining the E_2(high) phonon mode of the Raman spectrum. The E_2(high) mode of GaN thick-film after the LLO process is shifted by 0.5 cm^{-1} shift from that before the process, indicating that a 120 mPa of compressive stress in the top of the GaN thick-film was relieved after the LLO process. The stress of the GaN thick-film on sapphire is much smaller than that of the GaN thin-film on sapphire, but the LLO process relieves more of residual stress. Figure 4-7 shows the cross-sectional Raman spectra of the GaN thick-film before and after LLO process. The stress of the GaN thick-film on sapphire is a large compressive stress near the interface and small compressive stress near the top. After the LLO process, the compressive stress was relaxed both near the interface and at the top: 0.59 GPa stress of the GaN thick-film was relaxed near the interface of the

GaN/sapphire. Notably, the stress measured from the Raman spectrum in the cross sectional region is little less than that from the plane view because of the presence of the bi-axial stress. Figure 4-8 plots the XRD rocking curve of the ELOG GaN thick-film before and after the LLO process. Earlier chapter presents other samples without an ELOG structure. The LLO process significantly improves the FWHM of (002) GaN. The FWHM from the GaN thick-film on sapphire of the ELOG sample was 450 arcsec, which was reduced to 166 arcsec after the separation from the sapphire substrate. The quality of the GaN thick-film was significantly improved by the LLO process, in terms of both the FWHM and the intensity of XRD.

However, the LLO process of the GaN thick-film still has some disadvantages. Homogeneous heating is used in the LLO process to prevent the bending of GaN/sapphire. Heating to high temperature causes the surface of GaN (Ga-face) to decompose, oxidize and reform in air ambient, as shown in Fig. 4-9(a). To eliminate the aforementioned problems, the GaN wafer was placed in N_2 ambient. The experimental results obtained from LLO in N_2 ambient reveal that the surface of GaN neither decomposed nor was reconstructing, as shown in Fig. 4-9(b). However, in the results of an advanced experiment show that the surface of GaN in the LLO process in N_2 ambient was slightly decomposed, inhibiting the regrowth of the GaN wafer after the LLO process. The best solution to these problems is to implement the

homogeneous LLO process in the HVPE growth reactor. Figure 4-10 plots the experimental relationship between the thickness and diameter in the successful fabrication of complete thick freestanding GaN wafers by the LLO technique. In the fabrication 1 inch of freestanding GaN wafer by the LLO technique, a GaN thickness of 200 μm suffices to keep the freestanding GaN wafer crack free. However, to fabricate a 1.5 inch freestanding GaN wafer, the thickness of the GaN thick-film on sapphire must be increased to 250 μm to maintain the wafer complete after LLO. To obtain 2 inch freestanding GaN wafers, the GaN layer on sapphire should be over 300 μm-thick.

4.4 References

1. M. K. Kelly, O. Ambacher, B. Dahlheimer, G. Groos, R. Dimitrov, H. Angerer, and M. Stutzmann, Appl. Phys. Lett. **69**, 1749 (1996).

2. W. S. Wong, T. Sands, and N. W. Cheung, Appl. Phys. Lett. **72**, 599 (1998).

3. C. R. Miskys, M. K. Kelly, O. Ambacher, and M. Stutzmann, Phys. Stat. Sol. (c) **0**, 1627 (2003).

4. M. Leszczynski, T. Suski, H. Teisseyre, P. Perlin, I. Grzegory, J. Jun, S. Porowski, and T. D. Moustakas, J. Appl. Phys. **76**, 4909 (1994).

5. O. Ambacher, M.S. Brandt, R. Dimitrov, T. Metzger, M. Stutzmann, R.A. Fischer, A. Miehr, A. Bergmaier, and G. Dollinger, J. Vac. Sci. Technol. B **14**, 3532 (1996).

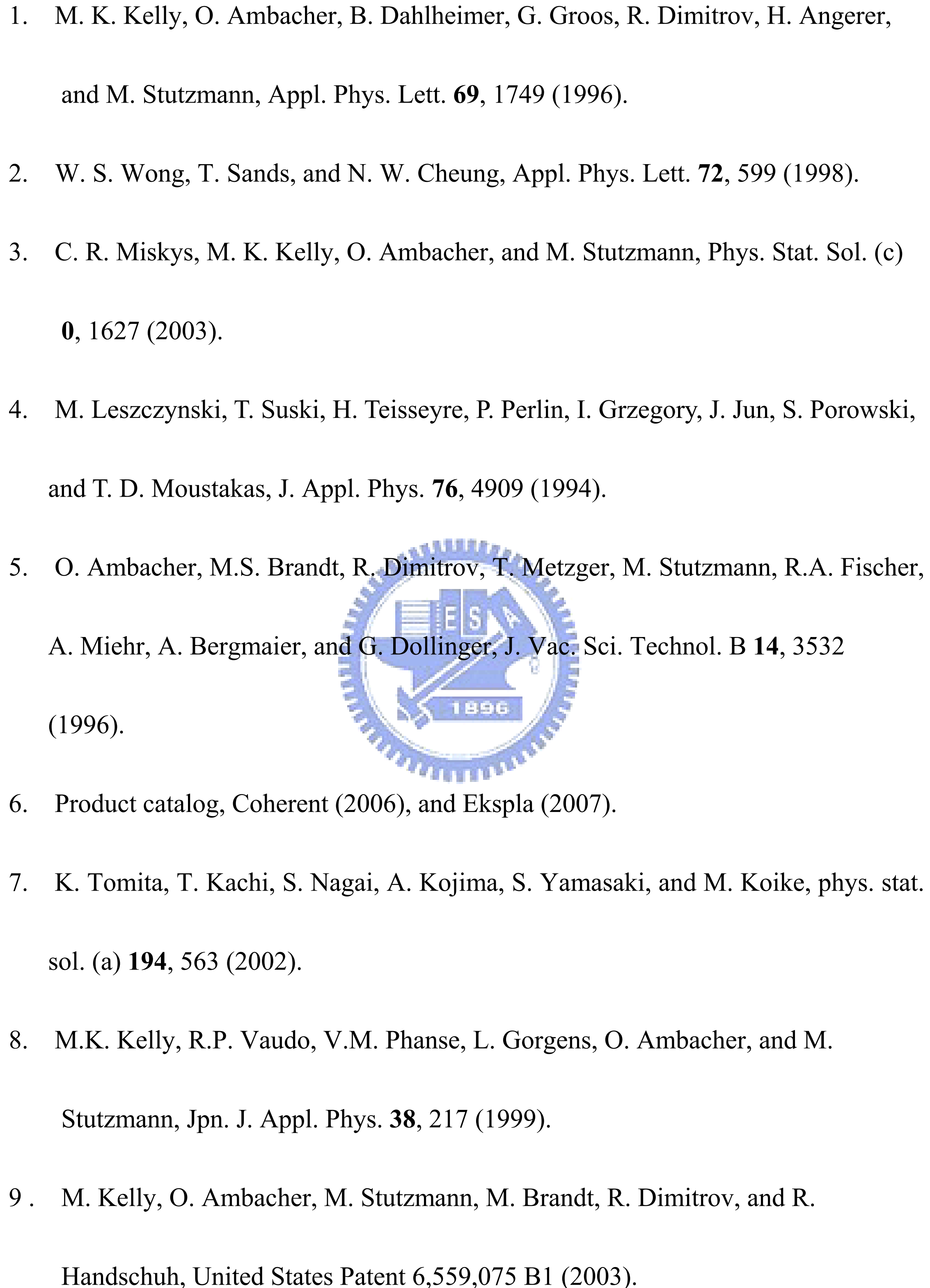

6. Product catalog, Coherent (2006), and Ekspla (2007).

7. K. Tomita, T. Kachi, S. Nagai, A. Kojima, S. Yamasaki, and M. Koike, phys. stat. sol. (a) **194**, 563 (2002).

8. M.K. Kelly, R.P. Vaudo, V.M. Phanse, L. Gorgens, O. Ambacher, and M. Stutzmann, Jpn. J. Appl. Phys. **38**, 217 (1999).

9. M. Kelly, O. Ambacher, M. Stutzmann, M. Brandt, R. Dimitrov, and R. Handschuh, United States Patent 6,559,075 B1 (2003).

10. W.S. Wong, T. Sands, N.W. Cheung, M. Kneissl, D.P. Bour, P. Mei, L.T. Romano, and N.M. Johnson, Appl. Phys. Lett. **75**, 1360 (1999).

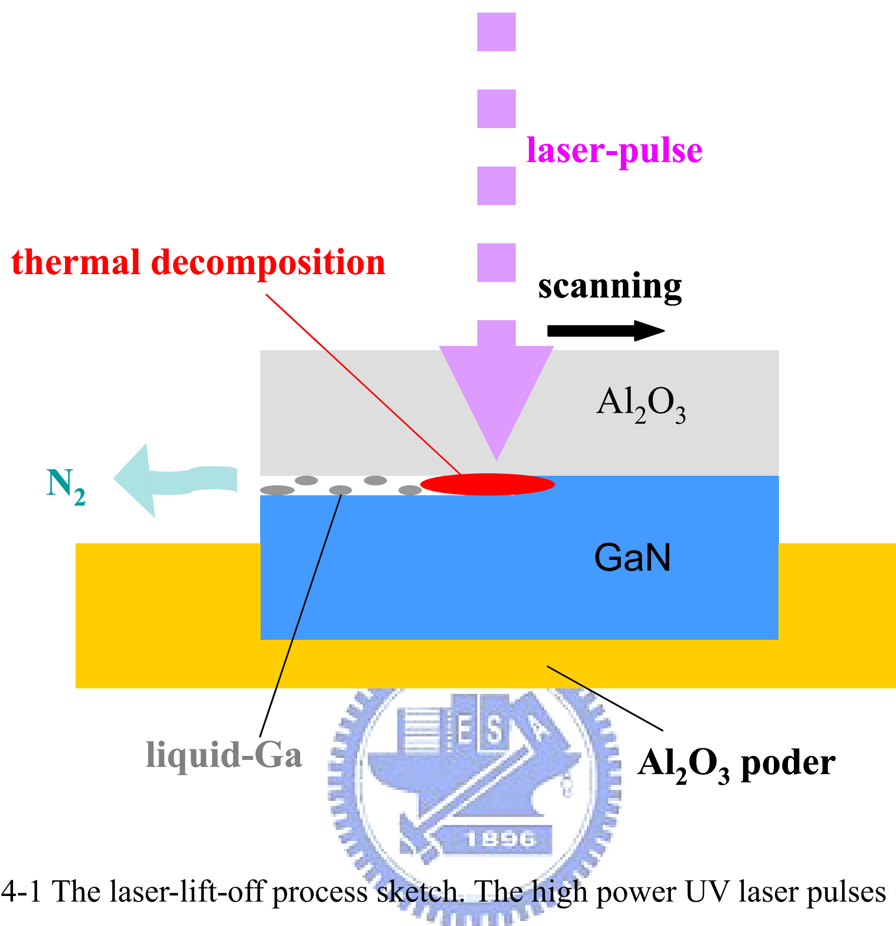

Fig. 4-1 The laser-lift-off process sketch. The high power UV laser pulses enter the GaN/sapphire interface via the sapphire substrate. A rough 100 nm GaN layer was thermal decomposed into Ga droplets and nitrogen gas. A hot plate was used for homogeneous heating for preventing the bowing of GaN/sapphire.

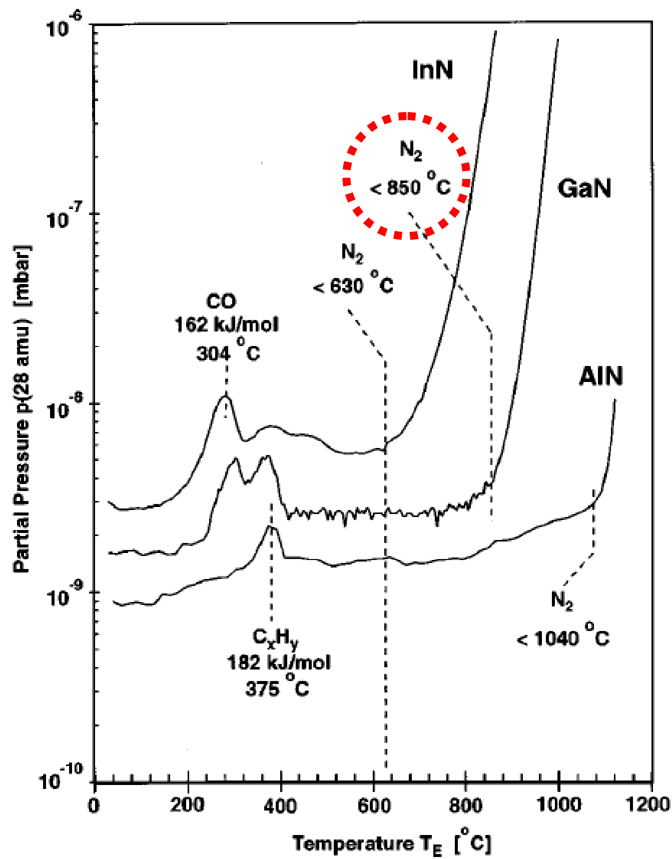

Fig. 4-2 The thermally induced decomposition of nitride semiconductors using a heating rate of 0.3 K/s.[5]

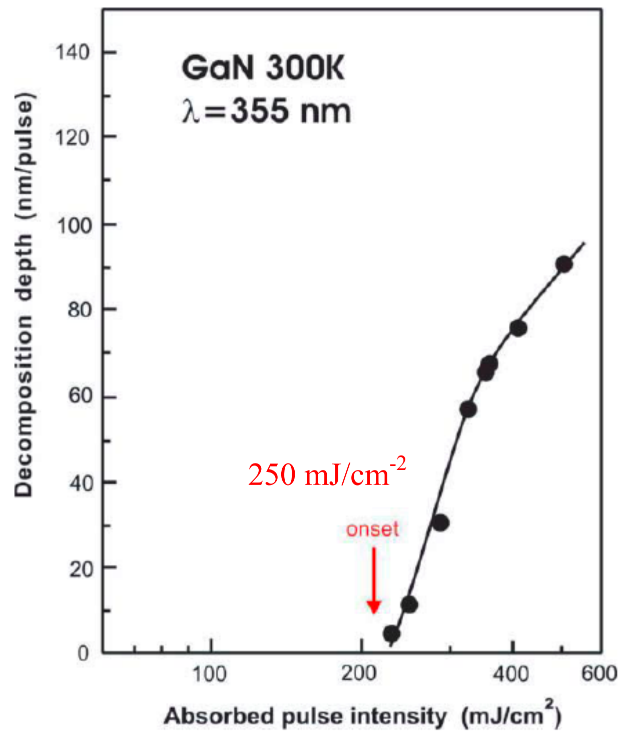

Fig. 4-3 The relation of decomposition depth caused by a single pulse and absorbed pulse intensity of the Nd:YAG laser.[3]

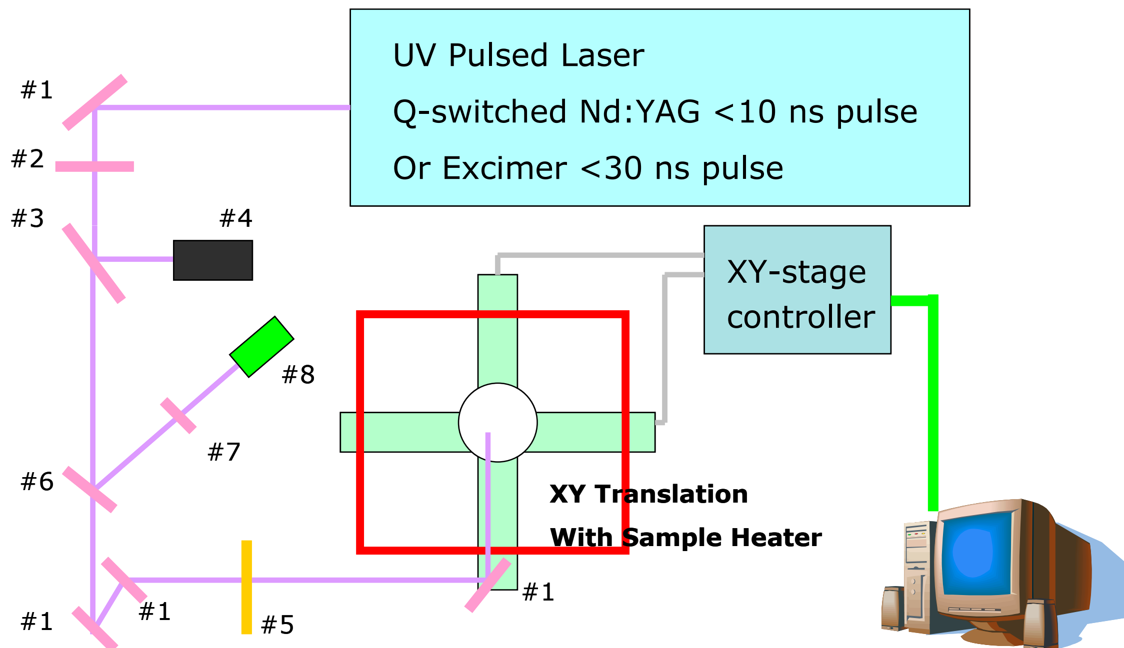

Fig. 4-4 The sketch of the laser lift-off system. Including:

1、Reflective mirror

2、Half-wave retarding plate

3、Polarizing beam splitter

4、Beam dump

5、Laser shutter

6、Beam sampler

7、Beam expansion

8、Power meter

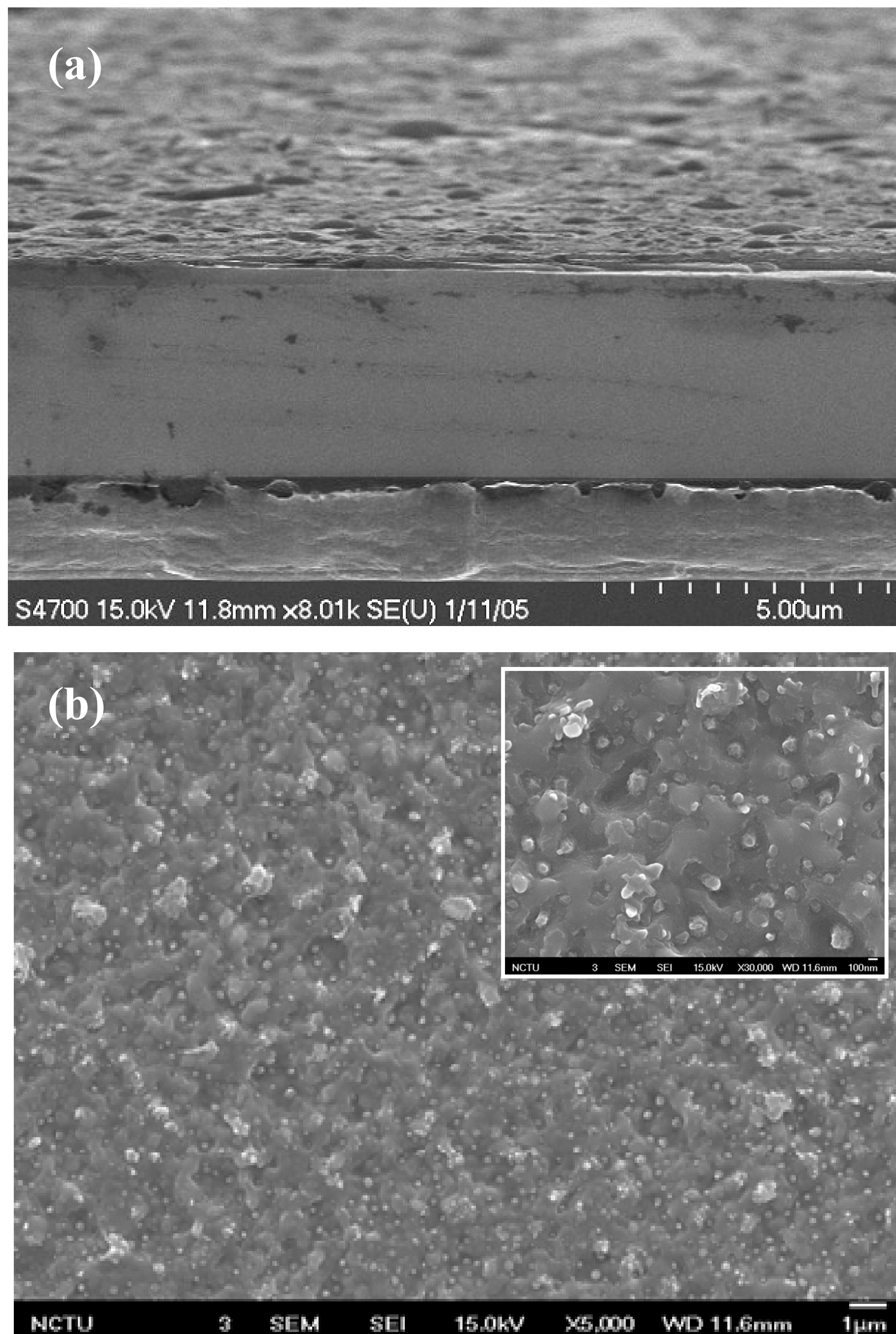

Fig. 4-5 The SEM images of the backside of GaN films after LLO process. (a) 4 μm-thick GaN layer bonding on GaAs substrate and the sapphire was separated by Nd:YAG laser. (b) The backside of thick GaN film after LLO process, the insert is the magnification.

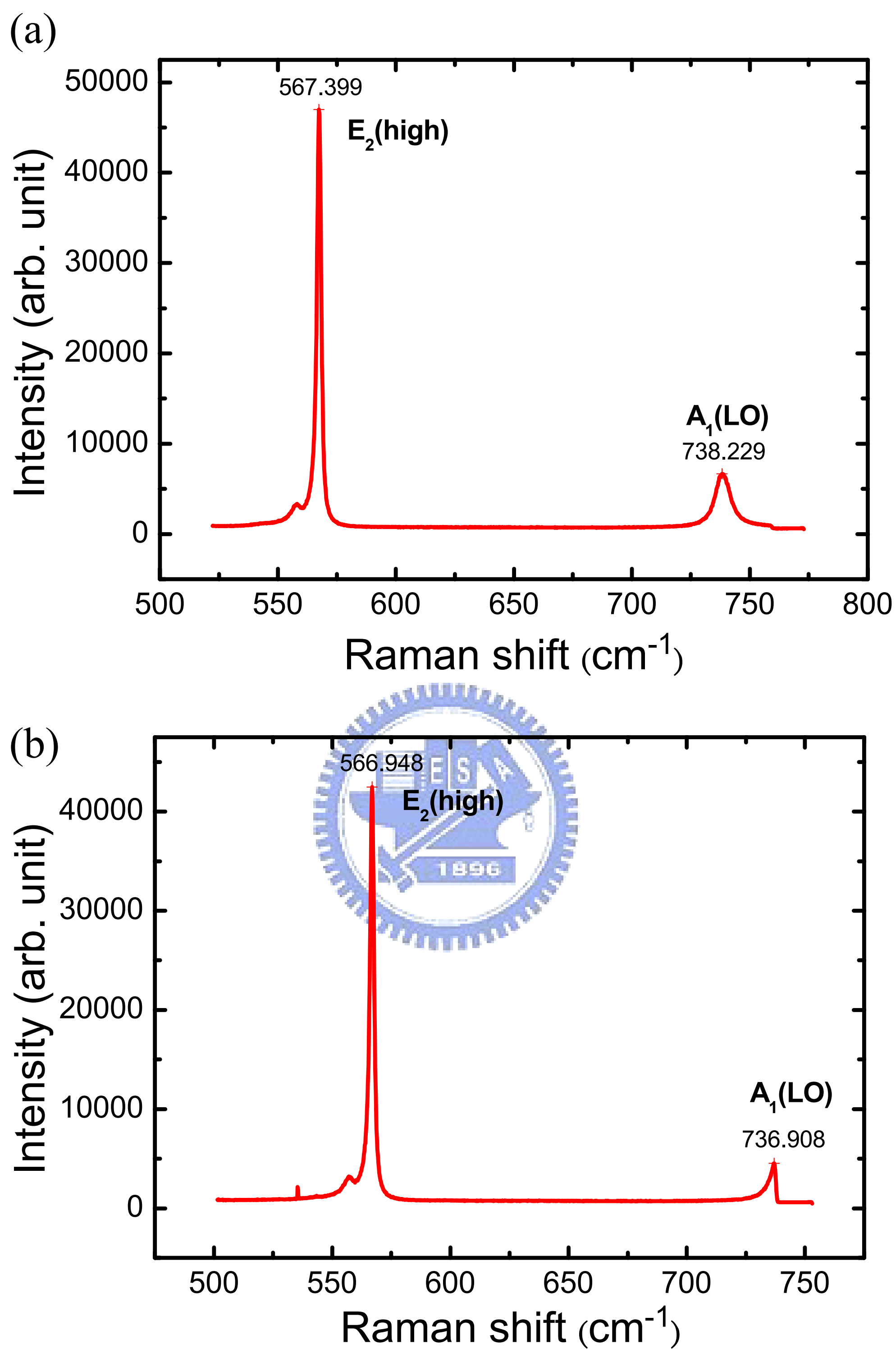

Fig. 4-6 The plane view Raman spectra of GaN thick-film before (a) and after (b) LLO process.

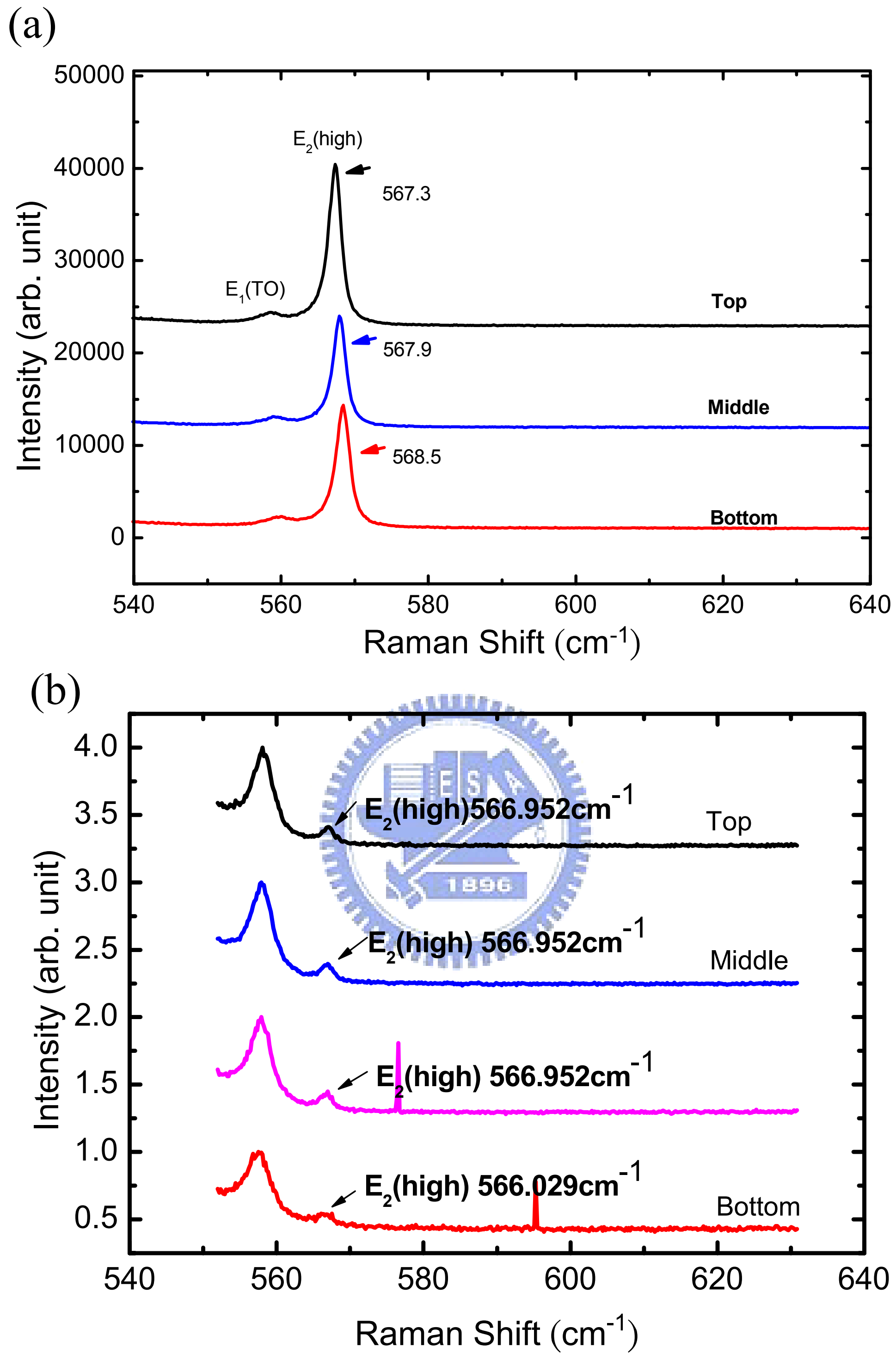

Fig. 4-7 The cross sectional Raman spectra of GaN thick-film before (a) and after (b) LLO process.

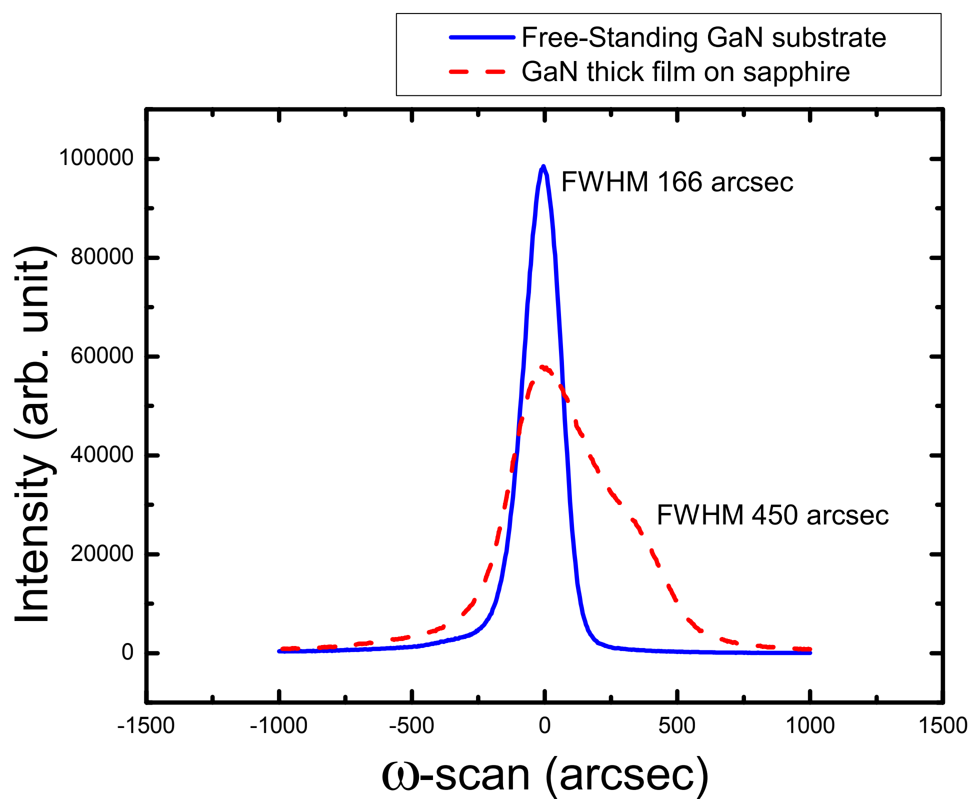

Fig. 4-8 The XRD rocking curve of GaN thick-film before and after LLO process.

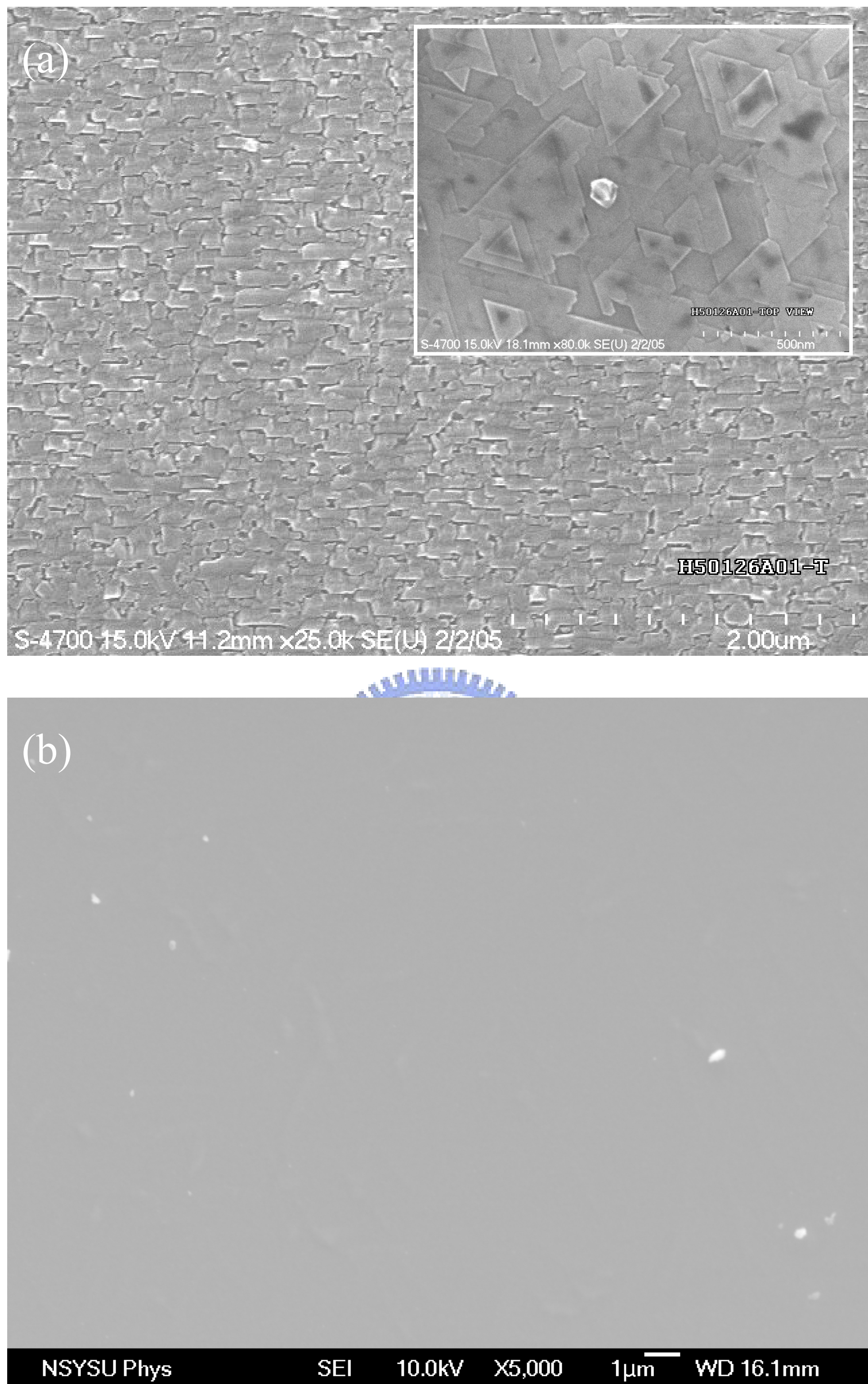

Fig. 4-9 The SEM images of GaN thick-film after LLO process in (a) air ambient (b) nitrogen ambient.

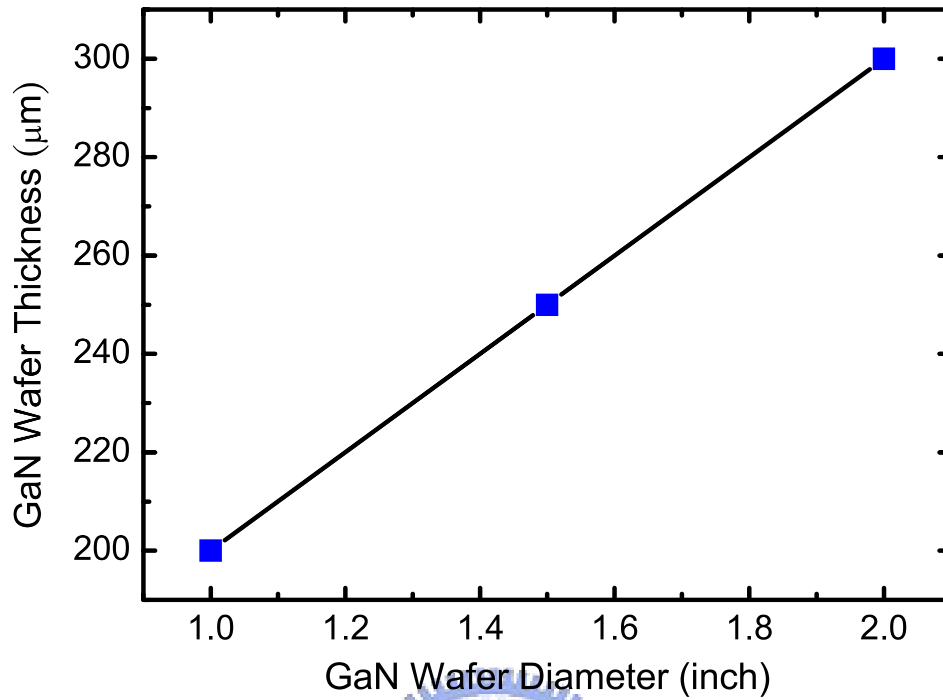

Fig. 4-10 The experimentally determined epitaxial layer thickness as a function of diameter for fabrication complete GaN wafers.

Tab. 4-1 The Comparsion of Nd:YAG and excimer KrF lasers

Laser	**Beam profile**	**Pulse duration**	**Wave length**	**Critical power density of laser pulse for separation GaN/sapphire (mJ/cm^2, per pulse)**	**Cost**
Nd:YAG	circle	3-6ns	~355nm	$> 200 mJ/cm^2$	low
Excimer KrF	rectangle	20-25ns	~248nm	$> 600 mJ/cm^2$	high

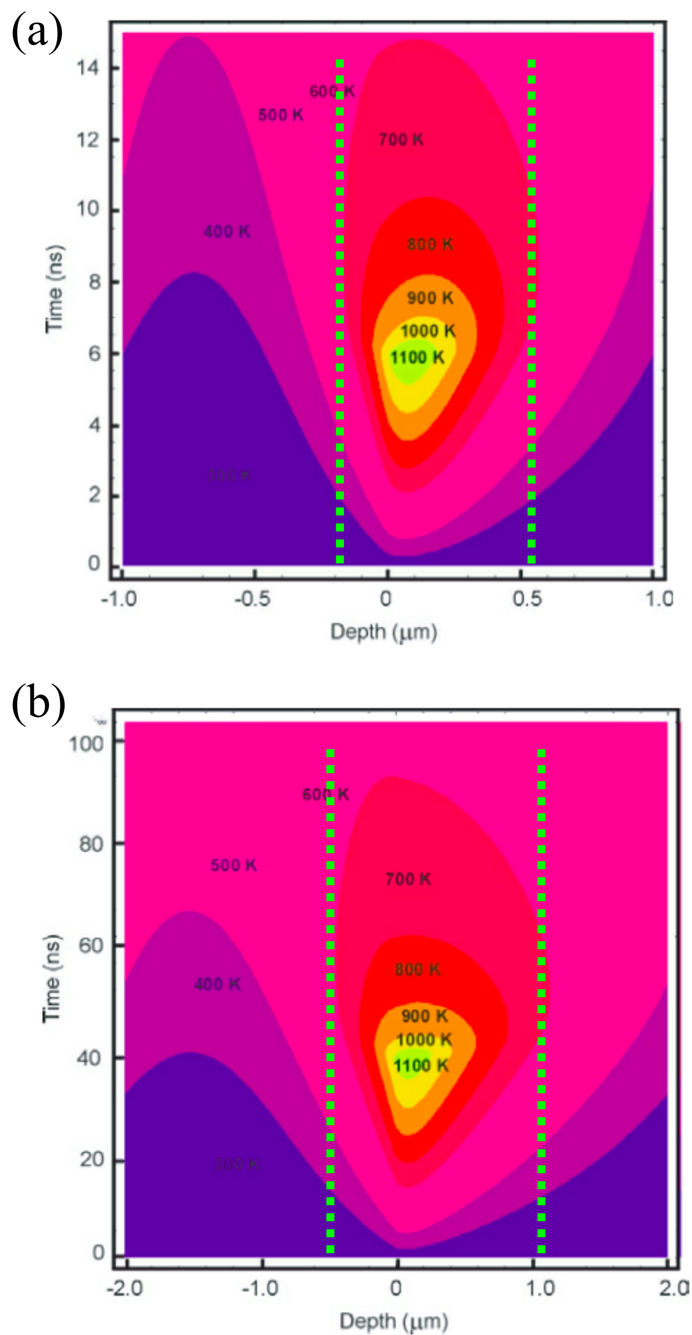

Fig. 4-11 The temporal and spatial variation of the temperature at GaN/sapphire interface (depth 0) during and after the laser pulses of (a) Nd:YAG 355 nm and (b) excimer KrF 248 nm laser pulse.[3] The depth of KrF laser at 700 K is twice over the Nd:YAG laser.

(a)

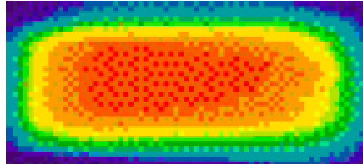

(b)

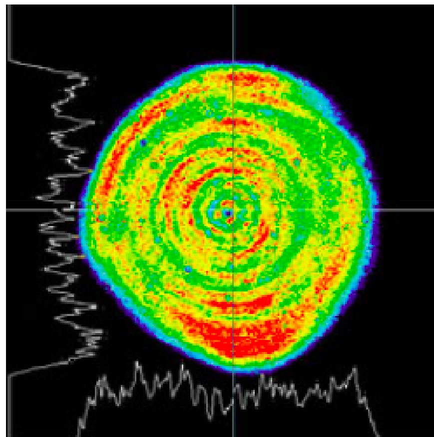

1896

Fig. 4-12 The beam profile of (a) excimer 248 nm KrF and (b) 355 nm Nd:YAG lasers.[6]

Chapter 5. Extended Micro-tunnels in GaN Prepared by Wet Chemical Etch

5.1 Introduction

It is demonstrated in GaN that micro-tunnels extended beyond hundreds of microns can be easily achieved using wet chemical etch. To obtain this result, specially designed structures of GaN layers are first grown on sapphire substrates with metal-organic chemical vapor deposition and subsequently hydride vapor phase epitaxy techniques. The prepared samples are then chemically etched in molten KOH. With the designed structure of GaN layers, extended micro-tunnels (EMT) with triangular cross sections are formed. Two kinds of EMTs were found in this investigation. If the designed patterns were along the $<1\bar{1}00>$ direction of GaN, the crystallographic planes of the triangular bevels belong to the $\{11\bar{2}2\}$ family. The etch rate of the tunnel can be as high as 10 μm/min at proper etching conditions. If the designed patterns were along the $<11\bar{2}0>$ direction of GaN, the crystallographic planes of the triangular bevels belong to the $\{10\bar{1}\bar{1}\}$ family. The etch rate of the tunnel can be as high as 5 μm/min at proper etching conditions.

For tunnels along the $<1\bar{1}00>$ and $<11\bar{2}0>$ directions of GaN, the $\{11\bar{2}\bar{2}\}$ and $\{10\bar{1}\bar{1}\}$ facets are the etch stop planes with activation energies of 23 kcal/mol

determined by the wet chemical etching. The axial etching rate of the tunnels in the $<1\bar{1}00>$ direction is twice larger than that along the $<11\bar{2}0>$ direction. The highest etching rate of the tunnels in the axial direction is 1000 μm/h.

GaN and its alloys are widely employed on optoelectronic devices, such as light emitting diodes (LEDs) and laser diodes (LDs) because they have a wide direct band gap, high thermal stability, and unusual chemical stability. However, its excellent chemical stability also makes wet chemical etching difficult. Most methods of GaN etching involve dry etching processes such as reactive ion etching or inductively coupled plasma etching.[1-3] While dry etching has favorable characteristics, including a high etching rate and the ability to yield vertical sidewalls, it also has several disadvantages, including the damage caused by ion bombardment and the difficulty of obtaining smoothly etched sidewalls. Furthermore, tunnels structures buried in semiconductor can not be realized by dry etching or photoenhanced electrochemical (PEC) techniques. Numerous research groups demonstrated PEC etching techniques,[5-14, 35-37] but in most cases the etched surface of GaN was roughened.

In this letter, extended microtunnels (EMTs) in GaN were prepared by wet chemical etching with an average etching rate of more than 15 μm/min. The etch stop facets of GaN EMTs are the $\{11\bar{2}\bar{2}\}$ or $\{10\bar{1}\bar{1}\}$ crystal planes, depending on the

direction of the designed patterns of epitaxial lateral overgrowth (ELOG) directions. Several groups have tried to grow semipolar LEDs or LDs on the $\{11\bar{2}2\}$, $\{10\bar{1}1\}$ and $\{10\bar{1}\bar{1}\}$ GaN crystal facets, which could result in higher-power or lower-threshold devices due to reduced internal piezoelectric polarization field.[15-22] But the properties of these facets are still not clearly understood to this date. GaN EMTs are demonstrated in this report to further understand the etching properties of these facets. Besides, these microtunnels offer a channel for micro-fluid studies, especially in the applications of microelectromechanical system.[23]

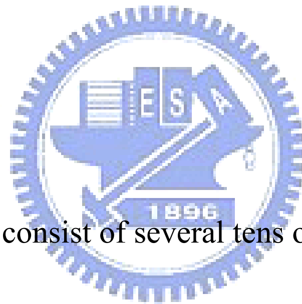

5.2 Experiment

All of the samples herein consist of several tens of microns of GaN in thickness grown by hydride vapor phase epitaxy (HVPE) on sapphire substrate. In the first growth process, 4 μm thickness GaN template was grown by metal-organic chemical vapor deposition technique on a (0001) c-plane sapphire substrate. The second growth process was the deposition of an SiO_2 layer in 300 nm thickness by plasma-enhanced chemical vapor deposition. Then, standard photolithography was performed to fabricate the stripes of a 5 μm-wide SiO_2 mask that are separated by 5 μm-wide windows in the $<1\bar{1}00>$ and $<11\bar{2}0>$ directions of GaN. Subsequently, the GaN layer with the patterned SiO_2 mask was used as an ELOG template for the regrowth of

a thick GaN film of several tens of microns by HVPE at 1050 ^{o}C. Ammonia gas was used as a nitrogen source and the GaCl generated by liquid Ga metal and HCl gas at 850 ^{o}C was used as the Ga source. After the GaN regrowth by the HVPE system, the samples were sliced into small pieces for wet chemical etching, which was conducted in molten KOH between 170 ^{o}C to 250 ^{o}C. Long-distance EMTs buried in GaN were obtained after wet chemical etching in the molten KOH.

5.3 Results and Discussion

Fig.5-1(a) illustrates the cross section of the completed structure of EMTs along the $<1\bar{1}00>$ direction of GaN. Fig. 5-1(b) is the cross sectional scanning electron microscopic (SEM) picture of the EMT in a sample after being etched for more than 120 minutes in molten KOH at 230 ^{o}C. It is clearly observed that extended micro-tunnels (EMT) right above the SiO_2 masking regions have been etched into the GaN layer. Optical microscope (OM) is used to measure the depth of the tunnels. Fig. 2 illustrates an OM image of the sample from its top. It is seen that the tunnels has extended beyond 300 μm, which corresponds to an average tunnel etch rate of more than 10 μm/min. It is also observed that, even with such an extended tunnel depth, adjacent tunnels remain separated, which indicates that the etch rates along the tunnel's axial direction and on the tunnel's cross section are very different. Therefore,

ES 1896

the etch process in the axial direction and in the cross sectional direction of the tunnels are different and should be discussed separately.

Figure 5-3 shows the cross sectional SEM micrographs of the EMTs with different etching conditions. Figures 5-3(a) is the as-grown sample before etch while Fig. 5-3(b) shows the result of the sample after being etched in molten KOH at 170 ^{o}C for 30 minutes. Energy dispersive x-ray (EDX) measurements has been applied onto the tunnel's cross section region and found no traces of Si or oxygen, which implies that SiO_2 mask has been removed by molten KOH. A possible reaction mechanism between SiO_2 and KOH have been proposed by Blohowiak *et al.* before as follows:[39]

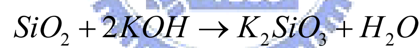

$$SiO_2 + 2KOH \rightarrow K_2SiO_3 + H_2O$$

Apparently, after SiO_2 is removed, molten KOH starts to etch the GaN right above the original SiO_2 masking region. Since this is the region where laterally overgrown GaN layers coalesce, the quality of GaN in this region may not be perfect and etching of GaN in this region may be easier. However, when the etchant reaches the $\{11\bar{2}2\}$ family planes, etch rate becomes very slow. This family of planes has a 58° of angle with respect to the (0001) plane, which is exactly the angle of the bevels as measured in Fig. 5-1(b) and Fig. 5-3(b), 5-3(d). It is believed that the etch process in the cross sectional direction can be divided into three steps, as illustrated in Fig. 5-3(d). The

first step is the removal of the SiO_2 mask. The second step is a relatively fast etch of the less-dense GaN on the top of the SiO_2 masking region to form a equilateral triangular cross section with $\{11\bar{2}2\}$ family of planes as the etch stop planes. The final step is the slow etch in the $<11\bar{2}2>$ direction.

Figure 5-4 shows the cross-sectional SEM image of EMTs along the $<11\bar{2}0>$ direction formed by wet chemical etching in molten KOH at different temperatures for 10 minutes. Figure 5-4(a) and 5-4(b) show the samples etched at 170°C and 190°C, respectively. At both of these two etchant temperatures, the etch rate of SiO_2 and GaN are quite slow. Thus, for 10 minute molten KOH etch, most of the SiO_2 still remain and the GaN is barely etched. Figure 5-4(c) shows the sample etched at 210°C. The triangular cross sections of tunnels were formed completely as shown in the figure. But the etch rate of SiO_2 and GaN is still restricted by the lower etchant temperature and short reacting time. Thus, EMTs have not formed long enough yet under this etching condition. Figure 5-4(d) shows the cross section of triangular prism-like EMTs formed by etching in molten KOH at 230 °C. The etching depth of microtunnels in this condition was 30 μm.

Figure 5-5 shows scanning electron microscopy (SEM) images of initial state of GaN EMTs formation in the molten KOH. First, the SiO_2 layer was removed by the molten KOH. After the SiO_2 was removed, the GaN right above the SiO_2 mask region

starts to be etched by the molten KOH. When the etchant reached the etch stop planes, the GaN EMTs formed. The etching mechanism of GaN EMTs by the molten KOH has been described in detail elsewhere.[24, 34]

Figure 5-6 shows the cross-sectional SEM images of ELOG stripes in two directions after wet chemical etching. As presented in Figs. 5-6(a) and (b), when the SiO_2 stripes were aligned in the $<1\bar{1}00>$ direction of GaN, the sidewall of GaN EMTs had a 58° of angle after the wet chemical etching, corresponding to the $\{11\bar{2}\bar{2}\}$ crystal facets of GaN. As shown in Figs. 5-6(c) and (d), when the SiO_2 stripes were aligned in the $<11\bar{2}0>$ direction, the sidewalls of the GaN EMTs were at 62° corresponding to the $\{10\bar{1}\bar{1}\}$ crystal facets.

The depths of the GaN tunnels for two SiO_2 stripes in two directions were measured individually under an optical microscope. The etching rates of the tunnels differed in the axial direction, as shown in Fig. 5-7. The etching rate of the tunnels in the $<1\bar{1}00>$ direction substantially exceeds that in the tunnels in the direction of $<11\bar{2}0>$. The average etching rate of the tunnels in the $<1\bar{1}00>$ direction was as high as 15 μm/min at 250 ^{o}C, and the average etching rate of the tunnels in the $<11\bar{2}0>$ direction was only 5 μm/min at 250 ^{o}C. The etching rate of the tunnels was highest in the $<1\bar{1}00>$ direction, reaching 1000 μm/h in the initial 30 min of etching at 250 ^{o}C. Factors that may influence the etching rate of GaN EMTs include

the width and thickness of the SiO_2 mask, the removal rate of SiO_2 mask, the etching rate of the nitrogen-face GaN, and the etching rates of the various special crystal facets of GaN. The first three factors are the same for tunnels in different directions, so the factor that is most probably responsible for the variation in axial etching rates is the variation among etching rates of the $\{10\bar{1}\bar{1}\}$ and $\{11\bar{2}\bar{2}\}$ planes of GaN. The $\{10\bar{1}\bar{1}\}$ family of planes of GaN is more stable and hardly etched by wet chemical etching than the $\{11\bar{2}\bar{2}\}$ family of planes mainly due to lower density of nitrogen atoms or surface energy.[25-30] The stability of $\{10\bar{1}\bar{1}\}$ family of planes makes cross-section size of GaN EMTs along the $\langle 11\bar{2}0 \rangle$ direction larger than that along the $\langle 1\bar{1}00 \rangle$ direction. The etchant exchange in tunnels with larger cross-section is easier than the small one. It makes the axial etching rate of tunnels along the $\langle 11\bar{2}0 \rangle$ direction lower than that in the $\langle 1\bar{1}00 \rangle$ direction.

Figure 5-8 plots the etching depths of GaN tunnels in two directions at various etching temperatures. The etching rate of GaN tunnels depended strongly on temperature. In this investigation, the etching temperature was between 170 ^{o}C and 250 ^{o}C. When the etching temperature was below 190 ^{o}C, the etching rate became very low in both directions of the tunnels. In Fig. 5-8(a), the tunnels of GaN were aligned in the $\langle 1\bar{1}00 \rangle$ direction. The etching rate declined as the etching time increased, as presented in Fig. 5-8 (a). In the first 30 min of the wet chemical etching

at 250 °C, the mean etching rate was higher than 15 μm/min. However, after 90 min of etching, the mean etching rate attenuated to 8 μm/min at the same temperature. Although the etching rate declined with the reaction time, it still exceeds that of dry or PEC etching. In Fig. 5-8 (b), the tunnels of GaN were aligned in the $\langle 11\bar{2}0 \rangle$ direction. The decline in the etching rate with the reaction time was not observed in these samples, and the etching rate of GaN tunnels was almost one half of that of tunnels in the $\langle 1\bar{1}00 \rangle$ direction at the same temperature, because the etching rate of the GaN tunnels along $\langle 11\bar{2}0 \rangle$ was much lower than that along $\langle 1\bar{1}00 \rangle$, and no clear attenuation was observed during 90 min of reaction.

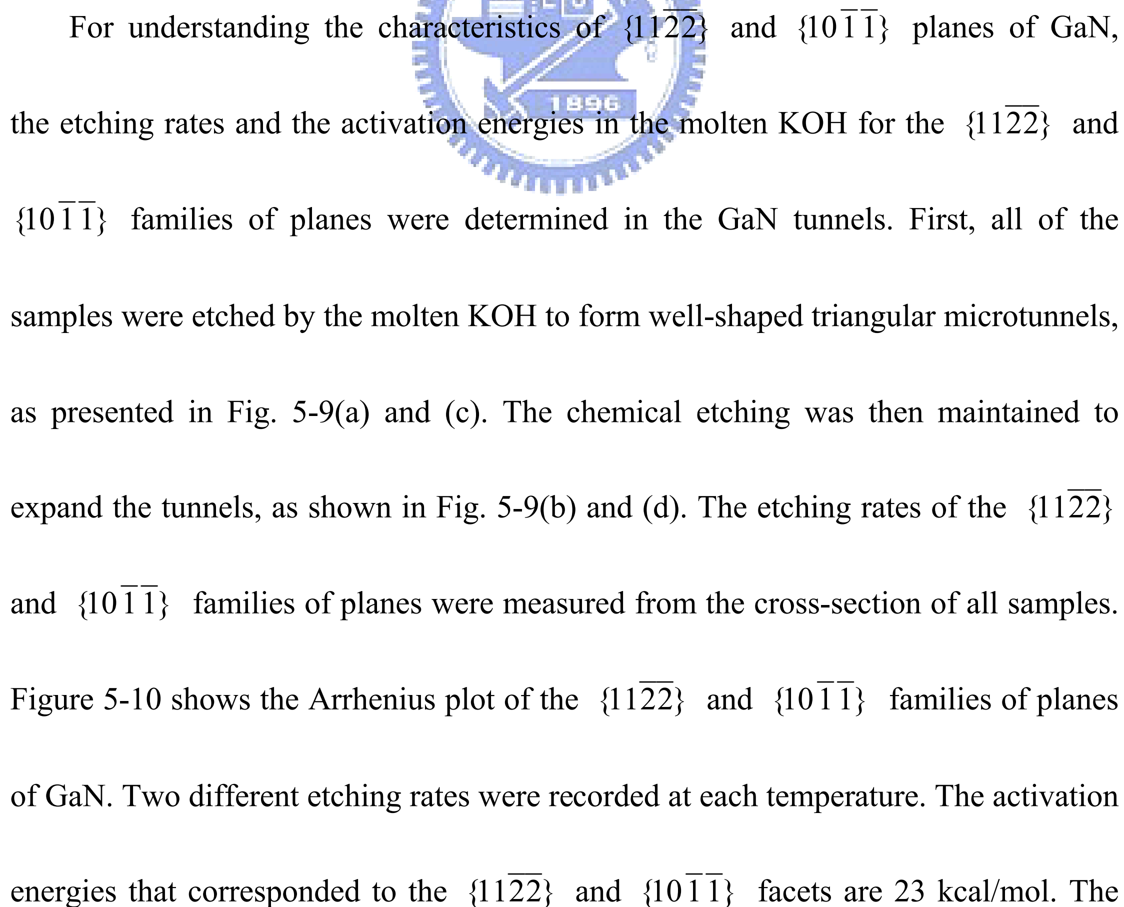

For understanding the characteristics of $\{11\bar{2}\bar{2}\}$ and $\{10\bar{1}\bar{1}\}$ planes of GaN, the etching rates and the activation energies in the molten KOH for the $\{11\bar{2}\bar{2}\}$ and $\{10\bar{1}\bar{1}\}$ families of planes were determined in the GaN tunnels. First, all of the samples were etched by the molten KOH to form well-shaped triangular microtunnels, as presented in Fig. 5-9(a) and (c). The chemical etching was then maintained to expand the tunnels, as shown in Fig. 5-9(b) and (d). The etching rates of the $\{11\bar{2}\bar{2}\}$ and $\{10\bar{1}\bar{1}\}$ families of planes were measured from the cross-section of all samples. Figure 5-10 shows the Arrhenius plot of the $\{11\bar{2}\bar{2}\}$ and $\{10\bar{1}\bar{1}\}$ families of planes of GaN. Two different etching rates were recorded at each temperature. The activation energies that corresponded to the $\{11\bar{2}\bar{2}\}$ and $\{10\bar{1}\bar{1}\}$ facets are 23 kcal/mol. The

activation energy of the $\{10\bar{1}\bar{1}\}$ and $\{11\bar{2}\bar{2}\}$ facets of GaN indicated that the etching was reaction-rate limited. If the etching rate had been diffusion-limited, the activation energy in the 1-6 kcal/mol range would be expected. The characteristics of reaction-rate limited implied a higher crystal quality.[31-33, 38] The activation energy obtained herein can be compared with that obtained by Stocker *et al*.[4, 32] They determined the activation energy of $\{10\bar{1}0\}$ and $\{10\bar{1}\bar{2}\}$ crystal facets of GaN. Their results are very close to those obtained herein.

5.4 Conclusion

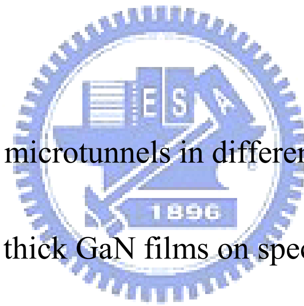

In conclusion, extended microtunnels in different directions with triangular cross-sections were formed in thick GaN films on specially designed ELOG structures. For tunnels in the $<1\bar{1}00>$ direction, the $\{11\bar{2}2\}$ family of planes were the etch stop planes, while for tunnels in the $<11\bar{2}0>$ direction, the $\{10\bar{1}\bar{1}\}$ family of planes were the more stable planes. The activation energies of wet chemical etching for the $\{11\bar{2}2\}$ family of planes and the $\{10\bar{1}\bar{1}\}$ planes were determined to be 23 kcal/mol. The $\{10\bar{1}\bar{1}\}$ family of planes were more stable and harder to be etched than the $\{11\bar{2}\bar{2}\}$ family of planes. Consequently, the depths of the tunnels in the $<1\bar{1}00>$ direction were more than twice deeper than that along the $<11\bar{2}0>$ direction. The highest etching rate of the tunnels along the axial direction is 1000

μm/h. These straight triangular microtunnels with well-formed side walls may serve as a vehicle for micro-fluid applications.

5.5 Reference

1. R. J. Shul, A. J. Howard, S. J. Pearton, C. R. Abernathy, and C. B. Vartuli, *J. Electrochem. Soc*. **143**, 3285 (1996).
2. J. M. Lee, K. M. Chang, I. H. Lee, and S. J. Park, *J. Electrochem. Soc*. **147**, 1859 (2000).
3. J. M. Lee, S. W. Kim, and S. J. Park, *J. Electrochem. Soc*. **148**, G254 (2001).
4. D. A. Stocker, E. F. Schubert, and J. M. Redwing, *Appl. Phys. Lett*. **73**, 2654 (1998).
5. C. Youtsey, L. T. Romano, R. J. Molnar, and I. Adesida, *Appl. Phys. Lett*. **74**, 3537 (1999).

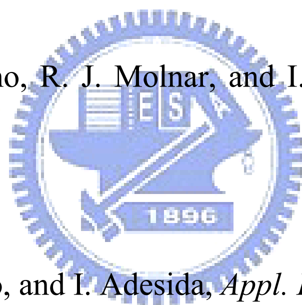

6. C. Youtsey, L. T. Romano, and I. Adesida, *Appl. Phys. Lett*. **73**, 797 (1998).
7. C. Youtsey and I. Adesida, *Appl. Phys. Lett*. **71**, 2151 (1997).
8. H. Peng and C. W. Chuang, *Appl. Phys. Lett*. **72**, 939 (1997).
9. P. Visconti, K. M. Jones, and M. A. Reshchikov, *Appl. Phys. Lett*. **77**, 3532 (2000).
10. M. Tiginyanu, V. Popa, and O. Volciuc, *Appl. Phys. Lett*. **86**, 174102 (2005).
11. H. Lu, Z. Wu, and l. Bhat, *J. Electrochem. Soc*. 144, L8 (1997).
12. D. A. Stocker and E. F. Schubert, *J. Electrochem. Soc*. 146, 2702 (1999).

13. I. M. Huygens, K. Strubbe, and W. P. Gomes, *J. Electrochem. Soc*. **147**, 1797 (2000).

14. H. Hartono, C. B. Soh, S. J. Chua, and E. A. Fitzgerald, *J. Electrochem. Soc*. **154**, H1004 (2007).

15. M. Funato, M. Ueda, Y. Kawakami, Y. Narukawa, T. Kosugi, M. Takahashi, and T. Mukai, *Jpn. J. Appl. Phys*. **45**, L659 (2006).

16. T. J. Baker, B. A. Haskell, F. Wu, J. S. Speck, and S. Nakamura, *Jpn. J. Appl. Phys*. **45**, L154 (2006).

17. H. Zhong, A. Tyagi, N. N. Fellows, F. Wu. R. B. Chung, M. Saito, K. Fujito, J. S. Speck, S. P. DenBaars, and S. Nakamura, *Appl. Phys. Lett*. **90**, 233504 (2007)

18. T. J. Baker, B. A. Haskell, F. Wu, P. T. Fini, J. S. Speck, and S. Nakamura, *Jpn. J. Appl. Phys*. **44**, L920 (2005)

19. K. Nishizuka, M. Funato, Y. Kawakami, Sg. Fujita, Y. Narukawa, and T. Mukai, *Appl. Phys. Lett*. **85**, 3122 (2004)

20. H. Masui, T. J. Baker, R. Sharma, P. M. Pattison, M. Iza, H. Zhong, S. Nakamura, and S. P. DenBaars, *Jpn. J. Appl. Phys*. **45**, L904 (2006)

21. A. Chakraborty, T. J. Baker, B. A. Haskell, F. Wu, J. S. Speck, S. P. Denbaars, S. Nakamura, and U. K. Mishra, *Jpn. J. Appl. Phys*. **44**, L945 (2005)

22. A. Tyagi, H. Zhong, R. B. Chung, D. F. Feezell, M. Saito, K. Fujito, J. S. Speck, S. P. DenBaars, and S. Nakamura, *Jpn. J. Appl. Phys*. **46**, L444 (2007)

23. V Cimalla, J Pezoldt, and O Ambacher, *J. Phys. D: Appl. Phys*. **40,** 6386 (2007)

24. H. H. Huang, H. Y. Zeng, C. L. Lee, S. C. Lee, and W. I. Lee, *Appl. Phys. Lett*. **89**, 202115 (2006).

25. J. E. Northrup and J. Neugebauer, *Phys. Rev. B* **60**, 8473 (1999).

26. Y. Gao, M. D. Craven, and J. S. Speck, *Appl. Phys. Lett*. **84**, 3322 (2004).

27. D. Zhuang and J. H. Edgar, Mater. *Sci. Eng. R*, **48**, 1 (2005)

28. D. Li, M. Sumiya, S. Fuke, D. Yang, and D. Que, *J. Appl. Phys*. **90**, 4219 (2001)

29. H. M. Ng, N.G. Weimann, A. Chowdhury, *J. Appl. Phys*. **94,** 650 (2003).

30. J. R. Mileham, S. J. Pearton, C. R. Abernathry, J. D. MacKenzie, R. J. Shul, and S. P. Kilcoyne, *Appl. Phys. Lett*. **67**, 1119 (1995).

31. S. S. Tan, M. Ye, and A. G. Milnes, *Solid State Electronics* **38**, 17 (1994).

32. D. A. Stocker, and I. D. Goepfert, E. F. Schubert, K. S. Boutros, and J. M. Redwing, *J. Electrochem. Soc*. **147**, 763 (2000).

33. C. B. Vartuli, S. J. Pearton, J. W. Lee, C. R. Abernathy, J. D. MacKenzie, J. C. Zolper, R. J. Shul, and F. Ren, *J. Electrochem. Soc*. **143**, 3681 (1996).

34. H. H. Huang, H. Y. Zeng, and W. I. Lee, *Physica Status Solidi (B)* **244**, 1872

(2007).

35. Z. H. Hwang, J. M. Hwang, H. L. Hwang, and W. H. Hung, *Appl. Phys. Lett*. **84**, 3759 (2004).

36. R. T. Green, W.S. Tan, P. A. Houston, T. Wang, and P. J. Parbrook, *J. Electron. Mater*. **36**, 397 (2007).

37. J. A. Bardwell, J. B. Webb, H. Tang, J. Fraser, and S. Moisa, *J. Appl. Phys*. **89,** 7 (2001).

38. S. Adachi and K. Oe, *J. Electrochem. Soc*. **131**, 126 (1984).

39. K. Y. Blohowiak, D. R. Treadwell, and B. L. Muller, Chem. Mat. **6**, 2177 (1994).

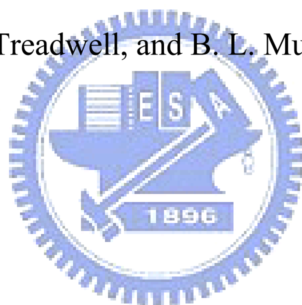

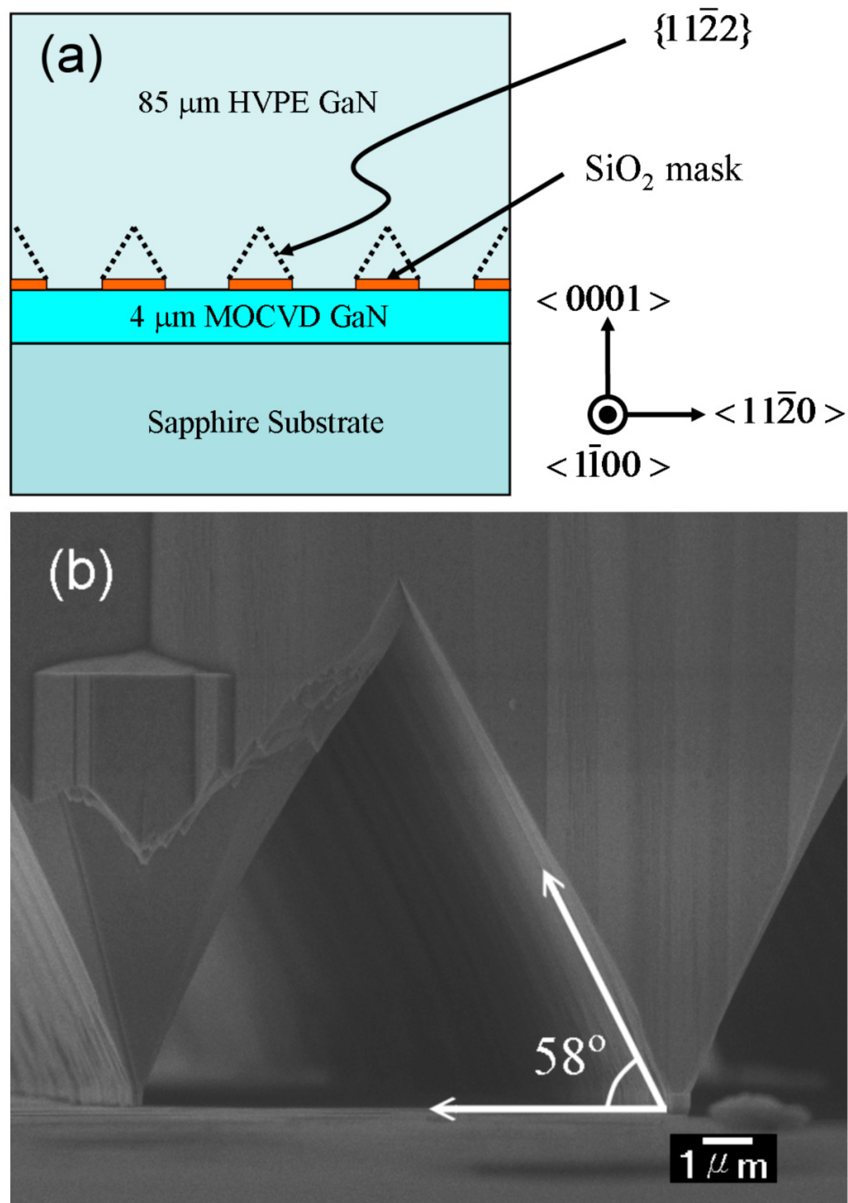

Fig. 5-1 (a) Cross sectional structure of the GaN sample prepared for chemical etch. The SiO_2 stripes are aligned to $<1\bar{1}00>$ direction. Also indicated in the figure are the $\{11\bar{2}2\}$ family planes. (b) Cross sectional SEM image of the GaN EMT after being etched for more than 120 minutes in molten KOH at 230 ^{o}C.

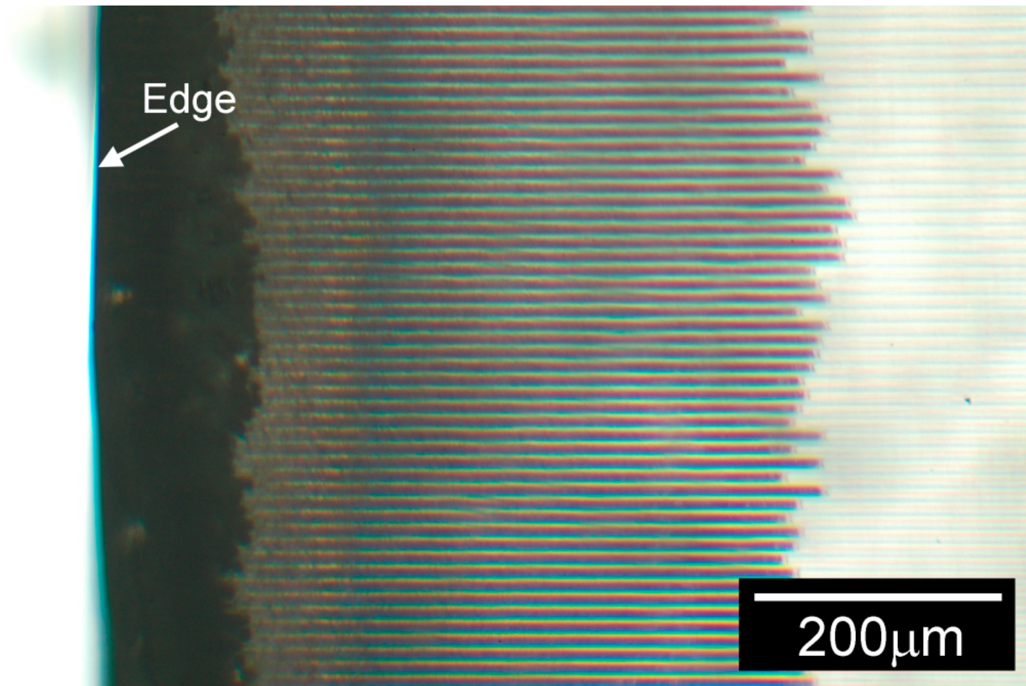

Fig. 5-2 Optical microscopic image of GaN EMTs after 30 minutes' etch in molten KOH at 250 ^{o}C.

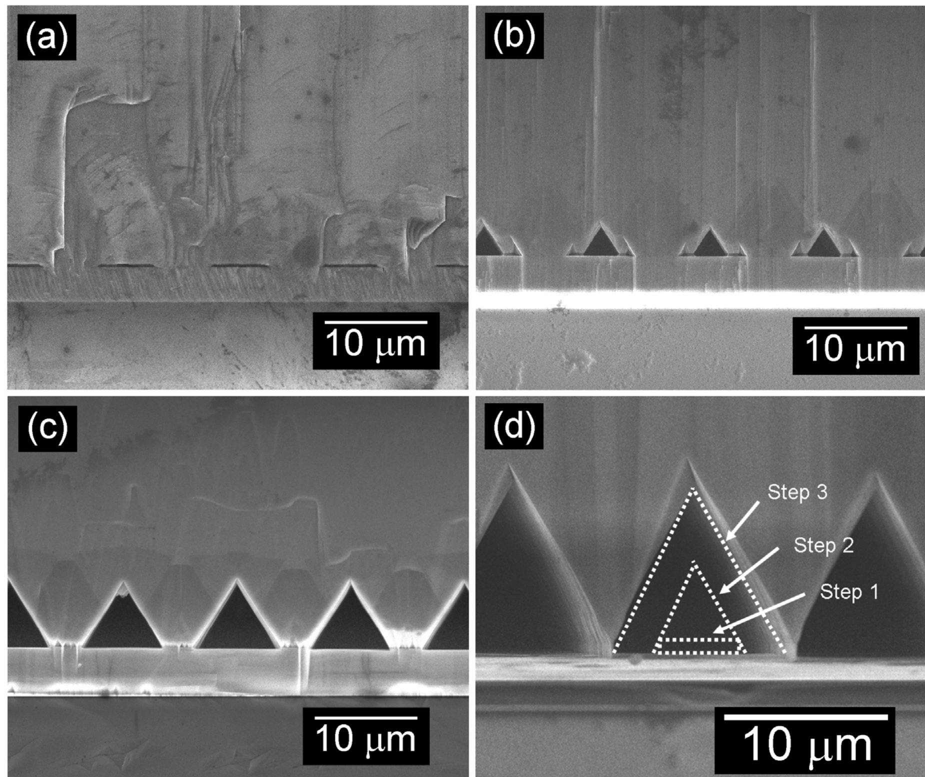

Fig. 5-3 Cross sectional SEM image of: (a) an as-grown GaN sample before KOH tech, (b) of GaN EMTs after 30 minutes' KOH etch at 170 ^{o}C, (c) of GaN EMTs after 30 minutes' KOH etch at 230 ^{o}C, and (d) of GaN EMTs after 120 minutes etch at 230 ^{o}C, along with an illustration of the suggested etching process in the cross section regions.

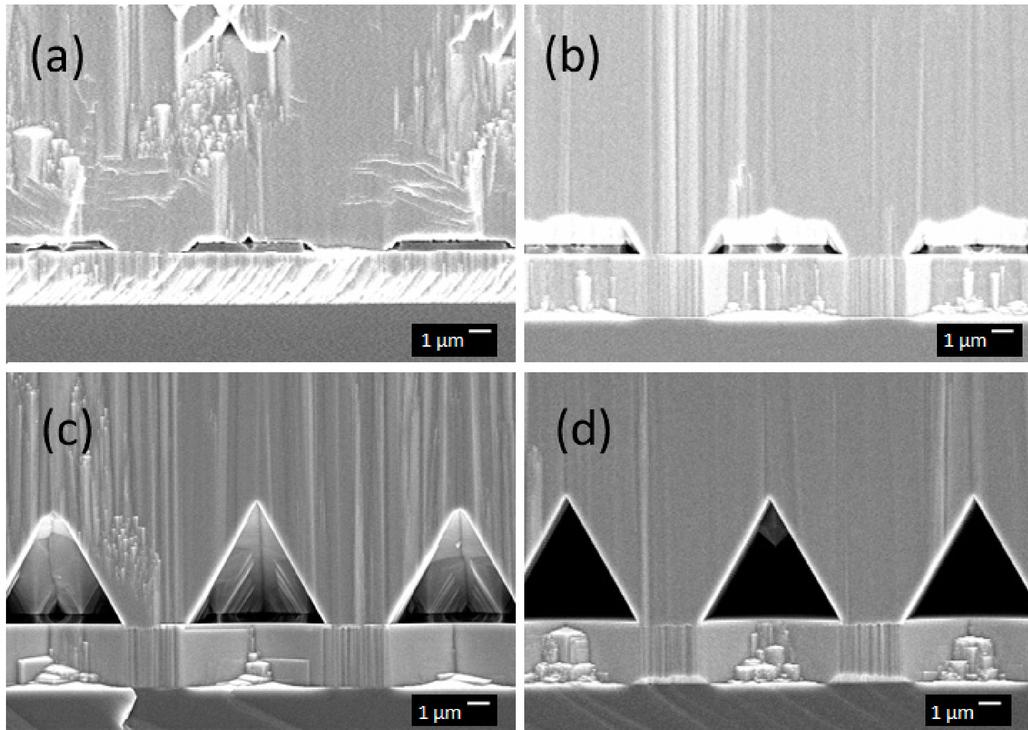

Fig. 5-4 Cross-sectional SEM images of EMTs along the $<11\bar{2}0>$ direction produced by etching in molten KOH at (a) 170°C, (b) 190°C, (c) 210°C, and (d) 230 °C for 10 minutes.

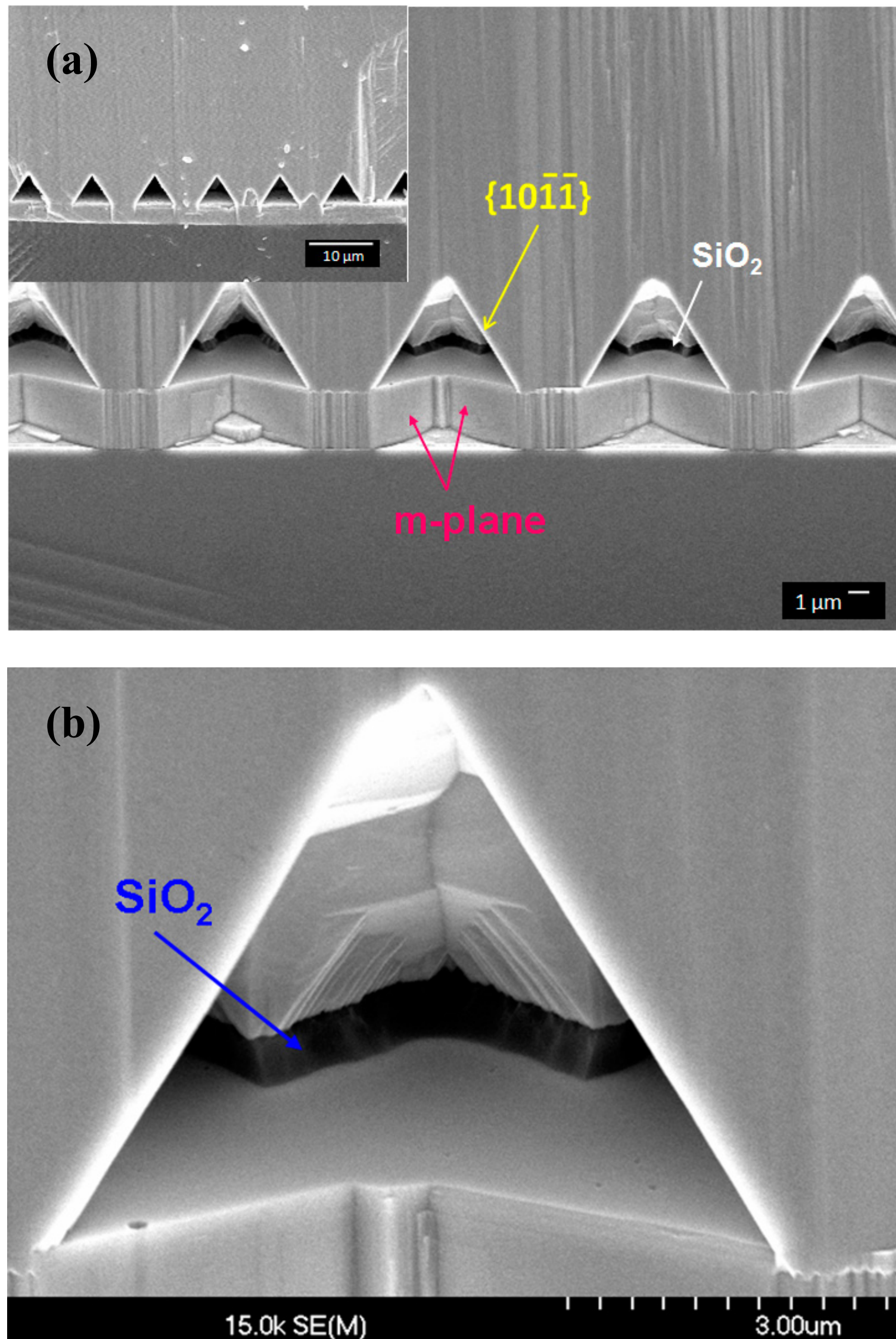

Fig. 5-5 (a) The bird-view cross-sectional SEM images of EMTs along the $<11\bar{2}0>$ direction and the insert along the $<1\bar{1}00>$ directions produced by wet chemical etching in molten KOH at 210 °C for 10 minutes. (b) The magnitude of (a).

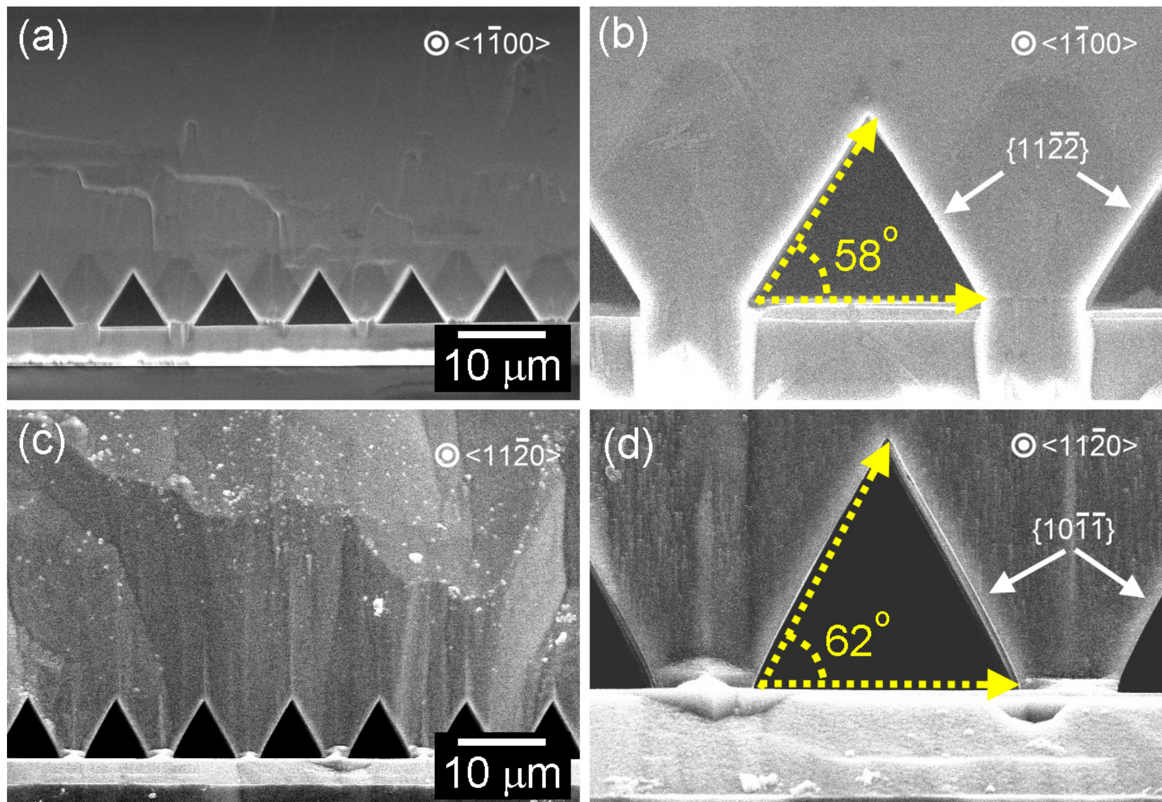

Fig. 5-6 SEM images of cross section of GaN after the wet chemical etching. (a) Tunnels aligned along the $<1\bar{1}00>$ direction. (b) Magnified image of one tunnel in the $<1\bar{1}00>$ direction with an inclined angle of 58°. (c) Tunnels aligned in the $<11\bar{2}0>$ direction. (d) Magnified image of one tunnel in the $<1\bar{1}00>$ direction with an inclined angle of 62°.

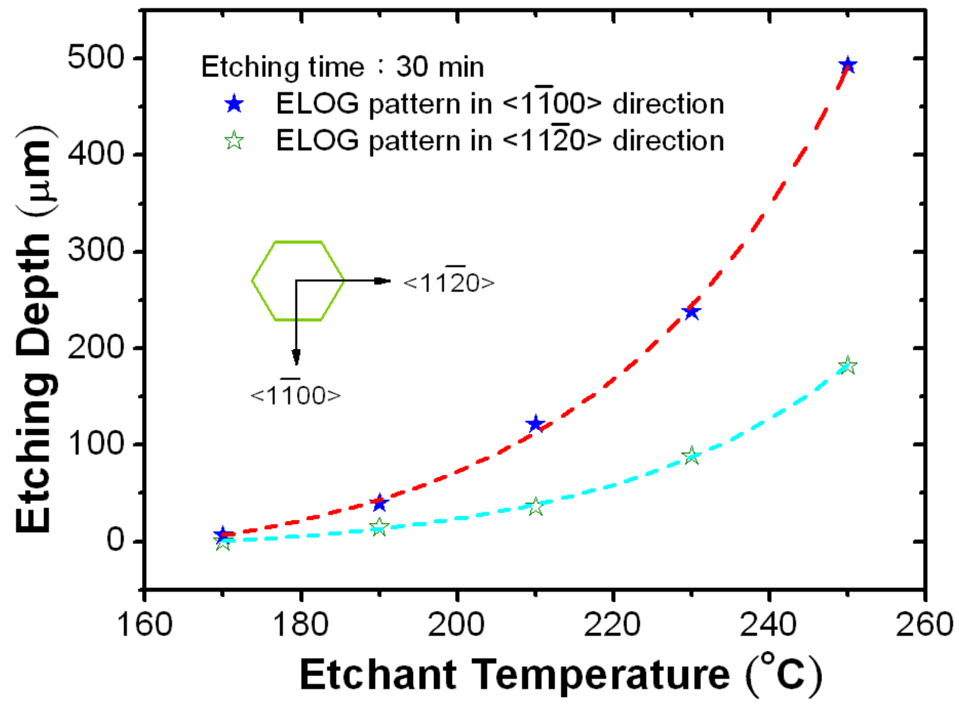

Fig. 5-7 Plot of the depth of GaN tunnels in different directions as a function of etchant temperature at a fixed etching time of 30 min in the molten KOH.

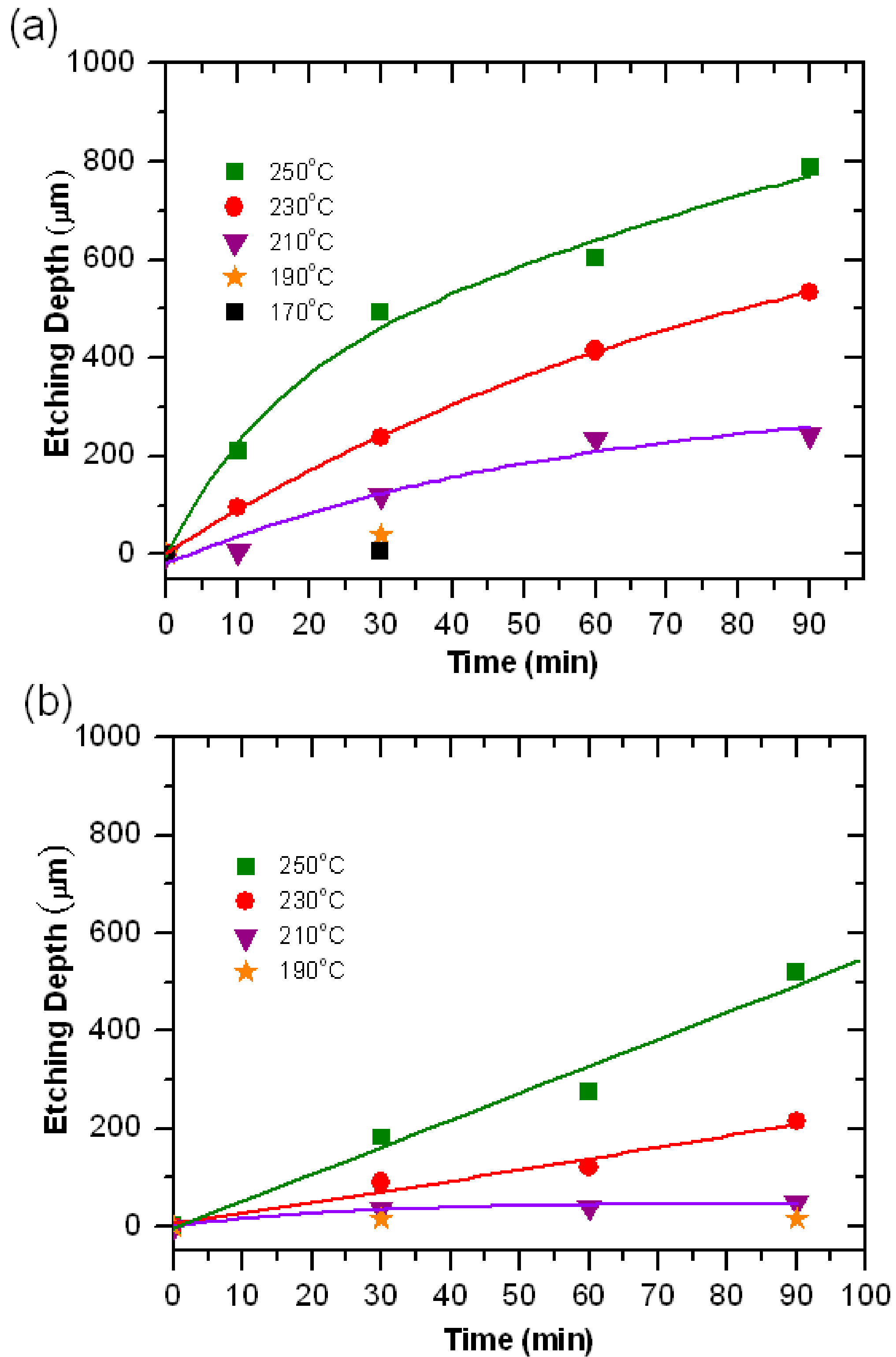

Fig. 5-8 Time-dependence of the etching depth of GaN tunnels at various temperatures. (a) ELOG pattern in $<1\bar{1}00>$ direction. (b) ELOG pattern in $<11\bar{2}0>$ direction.

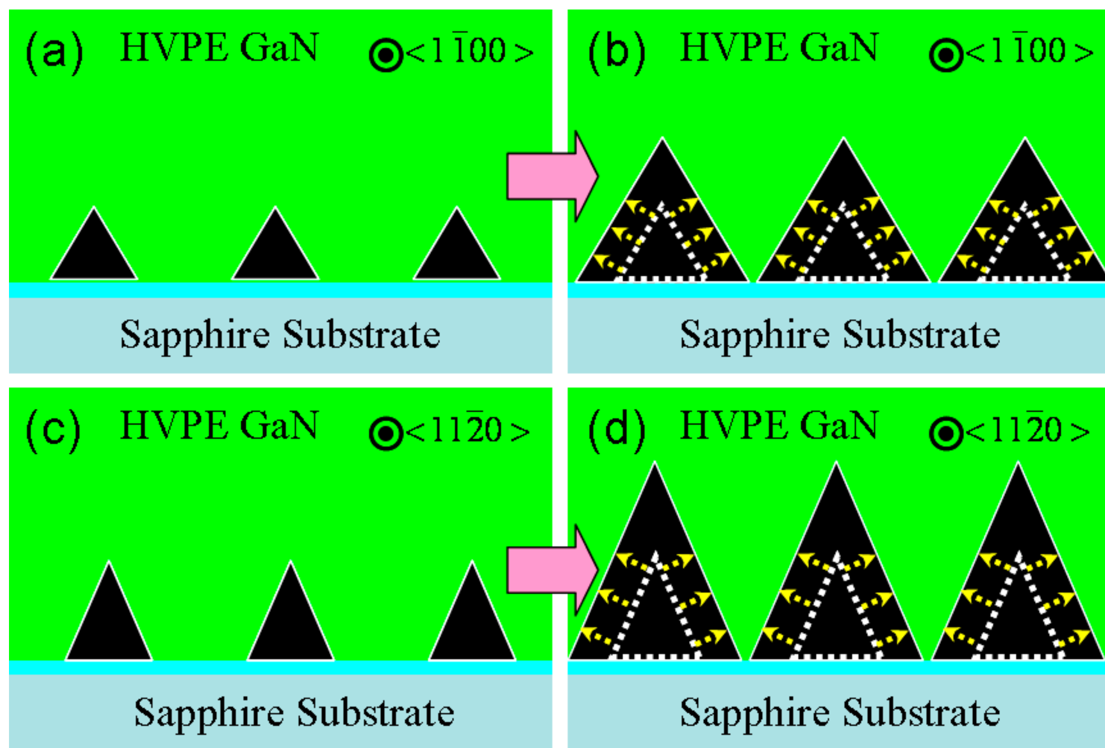

Fig. 5-9 Cross sectional structure of (a) GaN EMTs, beginning to form well-shaped triangular tunnels. (b) GaN EMTs, forming larger triangular tunnels upon facet etching.

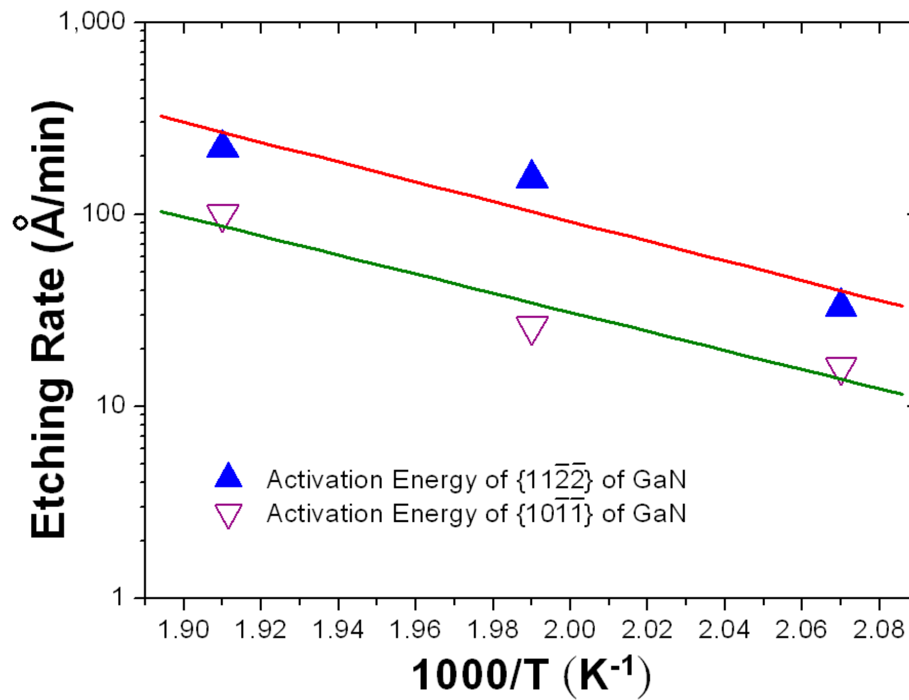

Fig. 5-10 Arrhenius plot of etching rates of two crystal facets of GaN. Solid and hollow dot symbols represent the etching rates on the $\{11\bar{2}2\}$ and $\{10\bar{1}\bar{1}\}$ crystal facets, respectively.

Tab. 5-1 Dangling bonds and surface energy of GaN facets

Crystal Facet	**DB (nm^{-2})**	**Activation energy (kcal/mol)**	**Crystal-lography**	**solution**	**Atomic density**	**Surface energy (meV/A^2)**	
(0001)	11.4					123~ 125	APL 74, 2319
(1010)	12.2		m			110 118	Ga terminated stoichiometric APL 74, 2319 PRB, 60, 8473(1999)
(1120)	14.0	21	a	KOH		123	APL 74, 2319 PRB, 60, 8473(1999)
(1012)	14.6	21	r	KOH			
(1011)	16.2	23		KOH		125	APL 74, 2319 PRB, 60, 8473(1999)
(1122)	18	23		KOH			Ga-face JJAP 45, L154 N-face JJAP 45, L659
(1013)							N-face JJAP 45, L154

Chapter 6 Conclusion

In the last decade, the saving of energy and the reduction of carbon output have attracted much attention because of both the effect on global warming and the inflation of the cost of energy. GaN and its related materials are important in saving energy, such as when they are used in solid state lighting. However, lattice-matched substrates are lacking and so most of nitride base devices are currently hetero-epitaxially grown on lattice-mismatched substrates. Large mismatches between lattice constants of substrates and epitaxial films cause high defect densities. Furthermore, differences between the thermal expansion coefficients of substrates and epitaxial films cause large warpage or bowing of the epi-layers.

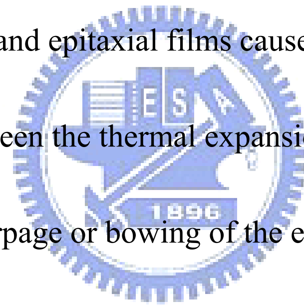

In this dissertation, freestanding GaN wafers were developed to fabricate GaN substrate to solve the aforementioned problems. Several structures and techniques were employed to relive thermal stress and eliminate crack. They are fllows.

1、 A high-void air-bridged structure GaN thick-film was developed and discussed. The growth mechanism of the high-void air-bridged structure differs from that of the conventional pendeo structure because of the formation of high voids by the sidewall passivation of the GaN seed. CL, HRXRD, EPD, and Raman spectra show that the HVAB growth process

substantially improves GaN quality. The relaxation of the residual stress of the HVAB structure exceeds that in the conventional pendeo structure, which factor is important in the growth of a GaN thick-film by HVPE.

2、 To eliminate the disadvantages of a striped air-bridged structure and to relax the thermal stress, the strain-reduced structure called a dot air-bridged structure was developed for GaN thick-film growth by HVPE. The compressive stress could be reduced to as low as 0.04 GPa to prevent cracking in the epitaxial process of GaN growth. This technique yielded a large-area GaN thick-film which can be used to fabricate a freestanding GaN wafer.

E S A 1896

3、 A very simplified technique without complex process for preventing cracking of a GaN thick-film grown by HVPE, called the temperature ramping technique, is developed. High-quality 1.5 and 2 inch large-area freestanding GaN layers with a thickness of more than 300 μm were thus obtained after the lift-off process. The FWHM of HRXRD of GaN (002) was around 156.7 arcsec and the dislocation density was about 1×10^{7} cm^{-2}. No additional designed-patterned structure in these samples was required to reduce the dislocation density and thermal stress.

4、 The laser lift-off technique for bulk GaN was developed. Homogeneous

heating to over 950 ^{o}C using a hot plate in N_2 ambient was performed in the LLO process to lift-off the large area crack-free GaN wafer. The power density of a 355 nm Nd:YAG laser was controlled between 200 to 250 mJ/cm^2 for bulk GaN/sapphire separation. The diameter of the spot of the laser pulse was approximately 1 mm and the trace of the scanning laser probe spiraled toward the center of the wafer. In this dissertation, a 360 μm-thick free standing GaN wafer with a 2 inch diameter was successfully lifted-off using the LLO technique.

5、 In work on the chemical properties of GaN, extended microtunnels in various directions with triangular cross-sections were formed in thick GaN films on especially designed ELOG structures. For tunnels in the $<1\bar{1}00>$ direction, the $\{11\bar{2}2\}$ family of planes were the etch stop planes, while the tunnels in the $<11\bar{2}0>$ direction, the $\{10\bar{1}\bar{1}\}$ family of planes were the more stable planes. The activation energies of wet chemical etching for the $\{11\bar{2}2\}$ family of planes and the $\{10\bar{1}\bar{1}\}$ planes were determined to be 23 kcal/mol. The $\{10\bar{1}\bar{1}\}$ family of planes were more stable and harder to be etched than the $\{11\overline{22}\}$ family of planes. Consequently, the depths of the tunnels in the $<1\bar{1}00>$ direction were more than twice as deep as those in the $<11\bar{2}0>$ direction. The highest

etching rate of the tunnels in the axial direction is 1000 μm/h. These straight triangular microtunnels with well-formed side-walls may be useful in micro-fluid applications.

In summary, a large-area (2 inch) freestanding crack-free GaN wafer was successfully developed using various techniques described above. Future work will develop the regrowth and surface treatment technique for the fabrication of GaN substrate.

Appendix A

The below table contains the investigations about GaN and AlN by HVPE of international research groups:
(1997-2008)

Research Groups	Type of HVPE Reactor	Foreign Substrate	Investigation	a. Is freestanding substrate? b. What kind of material? c.What is the size of substrate?
Department of Chemical Engineering, Wisconsin Univ. USA [1-3]	Vertical & Horizontal	Sapphire	1. Lateral epitaxial overgrowth of GaN using diethyl gallium chloride in metal organic vapor phase epitaxy 2. The impact of initial growth and substrate nitridation on thick GaN growth on sapphire by HVPE 3. Influences of mask width, fill factor, HCl addition and C doping on wing tilts in the epitaxial laterally overgrown GaN films by HVPE	a. No b. GaN
ATMI, Inc. USA (Combined by Cree) [4-6]	Vertical	Sapphire	1. Growth and characterization of low defect GaN by HVPE 2. Fabrication of GaN wafers for electronic and optoelectronic devices 3. Large Free-Standing GaN Substrates by HVPE and Laser-Induced liftoff	a. Yes b. GaN c. 2 inch
Aixtron AG, Germany [7-8]	Vertical & Horizontal	Sapphire	1. In-plane epitaxial relationships between a-plane sapphire substrates and GaN layers grown by different techniques 2. Influence of growth parameters on crack density in	a. No b. GaN

			thick epitaxially lateral overgrown GaN layers by HVPE	
Department of Material Engineering, Sungkyunkwan Univ. South Korea [9-10]	Horizontal & Vertical	Sapphire & AlN/Si	1. Low temperature buffer growth to improve HVPE of GaN 2. Pre-treatment of low temperature GaN buffer layer deposited on AlN/Si substrate by HVPE	a. No b. GaN
Quantum-Functional Semiconductor Research Center, Dongguk Univ. South Korea [11-12]	Vertical & Horizontal	Sapphire	1. Comparison of HVPE GaN films and substrates grown on sapphire and on MOCVD GaN epi-layer 2. Preparation of large area free-standing GaN substrates by HVPE using mechanical polishing liftoff method	a. Yes b. GaN c. 30*30 mm^2
I. Physics Institute, Justus-Liebig Univ. Germany [13-14]	Vertical	Sapphire	1. Modulated growth of thick GaN with hydride vapor phase epitaxy 2. Dislocation reduction in GaN grown by HVPE via growth interruption modulation	a. No b. GaN
MIT, USA [15-17]	Vertical	Sapphire	1. Electronic and structural properties of GaN grown by HVPE 2. Hall-effect analysis of GaN films grown by HVPE 3. Microcathodoluminescence of impurity doping at gallium nitride/sapphire interfaces	a. No b. GaN
Compound Semiconductors, Samsung Advanced Instituted of Technology Korea [18-23]	Horizontal	Sapphire	1. Optical properties of GaN grown by HVPE 2. Free-standing GaN Substrates by HVPE 3. Electrical, structural, and optical characterization of freestanding GaN template grown by HVPE 4. Structural and optical properties of thick freestanding GaN templates	a. Yes b. GaN c. 2 inch

			5. Ga vacancies as dominant intrinsic acceptors in GaN grown by HVPE 6. Characteristics of free-standing HVPE-grown GaN with very low defect concentration	
High Pressure Research Center PAS Poland [24-25], [49-56]	Vertical & Horizontal	Sapphire	1. Directional crystallization of GaN on high-pressure solution grown substrates by growth from solution and HVPE 2. Thick GaN layers grown by HVPE: hetero- versus homo-epitaxy	a. No b. GaN
UMR CNRS, Univ. France [26], **[57-58]**	Horizontal	GaAs **Sapphire**	Temperature influence on the growth of gallium nitride by HVPE in a mixed H_2/N_2 carrier gas	a. **Yes** b. GaN
TDI, Inc. USA [27-28] (Combined by Oxford)	Horizontal	SiC	1. Dislocation structure of GaN bulk crystals grown on SiC 2. High quality GaN layers grown by HVPE — a high resolution X-ray diffractometry and synchrotron X-ray topography study	a. Yes b. GaN c. 1.5 inch
Lumilog Inc. France [29-31]	Horizontal	Sapphire	1. High quality ELO-GaN layers on GaN/Al_2O_3 patterned substrates by HVPE 2. Luminescence and reflectivity studies of undoped, n- and p-doped GaN on (0001) sapphire 3. Spatially resolved photoluminescence of laterally overgrown GaN	a. Yes b. GaN
Materials Department, College of Engineering, UCSB USA [32-34], [59-62]	Horizontal	Sapphire	1. Two-step growth of high-quality GaN by HVPE 2. Structural and morphological characteristics of planar (11-20) a-plane gallium nitride grown by HVPE 3. Defect reduction in (11-20) a-plane gallium nitride	a. No b. GaN c. AlN

			overgrowth by HVPE 4. Ammonothermal growth of bulk GaN	
Department of Electronics, Nagoya Univ. Japan [35]	Horizontal	Sapphire	HVPE growth of a high quality GaN film using a ZnO buffer layer	a. No b. GaN
Tsukuba Research Laboratory, Sumitomo Chemical Co., Ltd., Japan [36-39], [68]	Horizontal	Sapphire/ GaAs	1. Optical and Crystalline Properties of ELOG-GaN Using Tungsten Mask by HVPE 2. Crystal Orientation Fluctuation of ELOG GaN with W Mask and SiO_2 Mask Observed by Transmission Electron Diffraction and X-Ray Rocking curves 3. Carrier-gas dependence of ELO GaN grown by HVPE 4. Preparation of Large Freestanding GaN Substrates by HVPE Using GaAs as a Starting Substrate	a. Yes b. GaN c. 2 inch
Advanced Research Center, Hitachi Cable, Ltd., Japan [40], [64-66]		Sapphire	Preparation of Freestanding GaN Wafers by HVPE with Void-Assisted Separation	a. Yes b. GaN c. 3 inch
Cree Research EED [41-42]		SiC	1. GaN Layers Grown by HVPE on P-type 6H-SiC Substrates 2. Growth and characterization of plasma assisted molecular beam epitaxial grown AlGaN/GaN heterostructures	a. Yes b. GaN c. 2 inch

1896

			on free standing hydride vapor phase epitaxy GaN substrates	
TDI Inc. USA [43-45], [63]	Horizontal	SiC Sapphire	1. AlN substrates: fabrication via vapor phase growth and characterization 2. Properties of AlN Layers Grown on SiC Substrates in Wide Temperature Range by HVPE 3. Thick AlN layers grown by HVPE	a. Yes b. AlN c. 2 inch
Sumitomo Co. Ltd., Japan [46], [67]	Horizontal	Sapphire SiC	1. Growth of Thick AlN Layer by Hydride Vapor Phase Epitaxy 2. AlN grown by sublimation method	a. No b. AlN
Tokyo University of Agriculture and Technology Japan [47-48], [69-70]	Horizontal	Sapphire	1. Growth of thick AlN layers by hydride vapor-phase epitaxy 2. Hydride vapor phase epitaxy of AlN: thermodynamic analysis of aluminum source and its application to growth	a. No b. AlN
Meijo University Japan [71-75]		Sapphire 6H-SiC	1. Growth of AlN layers by metalorganic vapor phase epitaxy 2. Growth of non-polar AlN films 3. AlN on 6H-SiC substrate	a. No b. AlN
Tohoku University Japan [76-79]			Growth of GaN layers by ammonothermal method	a. Yes b. GaN
Department of Physics and Measurement Technology, Linköping Univ. Sweden	Vertical	Sapphire	Growth of thick GaN layers by hydride vapor-phase epitaxy	a. Yes b. GaN c. 2 inch

[80-83]				
Institute of Semiconductors, Chinese Academy of Sciences China [84-87]	Vertical	Sapphire	Growth of thick GaN layers by hydride vapor-phase epitaxy	a. Yes b. GaN
Key Laboratory of Materials Physics, Institute of Solid State Physics, Chinese Academy of Sciences China [88-90]	Vertical	Sapphire	1. Growth of thick GaN layers by hydride vapor-phase epitaxy 2. Different polarity buffer layers grown by MBE	a. No b. GaN
Department of Physics, Chemistry and Biology, Link¨oping Univ. Sweden	Vertical	Sapphire	Growth of thick GaN layers by hydride vapor-phase epitaxy	a. Yes b. GaN

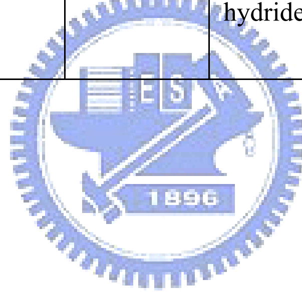

Reference

1. L. Zhang et al. “Lateral epitaxial overgrowth of GaN using diethyl gallium chloride in metal organic vapor phase epitaxy” Journal of Crystal Growth 235 pp115–123 (2002)
2. S. Gu et al. “The impact of initial growth and substrate nitridation on thick GaN growth on sapphire by HVPE” Journal of Crystal Growth 231 pp342–351 (2001)
3. Wang et al. “Influences of mask width, fill factor, HCl addition and C doping on wing tilts in the epitaxial laterally overgrown GaN films by HVPE” Appl. Phys. Lett., Vol. 80, No. 25, 24 June 2002
4. X. Xu et al. “Growth and characterization of low defect GaN by hydride vapor phase epitaxy” Journal of Crystal Growth 246 (2002) 223–229
5. X. Xu et al. “Fabrication of GaN wafers for electronic and optoelectronic devices” Optical Materials 23 (2003) 1–5
6. Michal K. KELLY et al. ”Large Free-Standing GaN Substrates by Hydride Vapor Phase Epitaxy and Laser-Lnduced Liftoff” ， Japan Journal of Applied Physics Vol.38 pp. L217~L219 (1999)
7. T. Paskova et al. “In-plane epitaxial relationships between a-plane sapphire substrates and GaN layers grown by different techniques” Journal of Crystal Growth 257 (2003) 1–6
8. C. Wang et al. “Influence of growth parameters on crack density in thick epitaxially lateral overgrown GaN layers by hydride vapor phase epitaxy” Journal of Crystal Growth 230 (2001) 377–380
9. J.-w. Lee et al. “Low temperature buffer growth to improve hydride vapor phase epitaxy of GaN” Materials Science and Engineering B59 (1999) 12–15

10. H. Jin Kim et al. “Pre-treatment of low temperature GaN buffer layer deposited on AlN/Si substrate by hydride vapor phase epitaxy” Surface and Coatings Technology 131 (2000) pp465-469
11. H.M. Kim et al. “Comparison of HVPE GaN films and substrates grown on sapphire and on MOCVD GaN epi-layer” Materials Letters 46 (2000) pp286–290
12. H.M. Kim et al. “Preparation of large area free-standing GaN substrates by HVPE using mechanical polishing liftoff method” Materials Letters 47 (2001) pp276–280
13. W. Zhang et al. “Modulated growth of thick GaN with hydride vapor phase epitaxy” Journal of Crystal Growth 234 (2002) pp616–622
14. Zhang et al. “Dislocation reduction in GaN grown by hydride vapor phase epitaxy via growth interruption modulation” Appl. Phys. Lett., Vol. 78, No. 6, 5 February 2001
15. W. Gotz et al. “Electronic and structural properties of GaN grown by hydride vapor phase epitaxy” Appl. Phys. Lett. 69 (2), 8 July 1996
16. Gotz et al. “Hall-effect analysis of GaN films grown by hydride vapor phase epitaxy” Appl. Phys. Lett., Vol. 72, No. 10, 9 March 1998
17. Goss et al. “Microcathodoluminescence of impurity doping at gallium nitride/sapphire interfaces” Appl. Phys. Lett., Vol. 78, No. 23, 4 June 2001
18. Oh et al. “Optical properties of GaN grown by hydride vapor-phase epitaxy” Appl. Phys. Lett., Vol. 78, No. 3, 15 January 2001
19. Sung S. PARK et al.“Free-standing GaN Substrates by Hydride Vapor Phase Epitaxy” ， Japan Journal of Applied Physics Vol.39 pp. L1141~L1142 (2000)
20. F. Yun et al. “Electrical, structural, and optical characterization of freestanding

GaN template grown by hydride vapor phase epitaxy” Solid-State Electronics 44 pp2225-2232 (2000)

21. J.A. Freitas Jr. et al. “Structural and optical properties of thick freestanding GaN templates” Journal of Crystal Growth 231 pp322–328 (2001)
22. Oila et al. “Ga vacancies as dominant intrinsic acceptors in GaN grown by hydride vapor phase epitaxy” Appl. Phys. Lett., Vol. 82, No. 20, 19 May 2003
23. Jasinski et al. “Characterization of free-standing hydride vapor phase epitaxy GaN” Appl. Phys. Lett., Vol. 78, No. 16,pp2297~2299(2001)
24. M. Bockowski et al. “Directional crystallization of GaN on high-pressure solution grown substrates by growth from solution and HVPE” Journal of Crystal Growth 246 (2002) 194–206
25. P.R. Hageman et al. “Thick GaN layers grown by hydride vapor-phase epitaxy/hetero- versus homo-epitaxy” Journal of Crystal Growth 255 (2003) 241–249
26. A. Trassoudaine et al. “Temperature influence on the growth of gallium nitride by HVPE in a mixed H2/N2 carrier gas” Journal of Crystal Growth 260 (2004) 7–12
27. I. Nikitina et al. “Dislocation structure of GaN bulk crystals grown on SiC substrates by HVPE” Materials Science and Engineering B 61–62 (1999) 325–329
28. J. Chaudhuri et al. “High quality GaN layers grown by hydride vapor phase epitaxy — a high resolution X-ray diffractometry and synchrotron X-ray topography study” Materials Science and Engineering B 78 (2000) 22–27
29. G. Nataf et al. “High quality ELO-GaN layers on GaN.Al_2O_3 patterned substrates by halide vapour phase epitaxy” Materials Science and Engineering B 59 (1999) 112–116

30. M. Leroux et al. “Luminescence and reflectivity studies of undoped, n- and p-doped GaN on (0001) sapphire” Materials Science and Engineering B 50 (1997) 97–104
31. P. Gibart et al. ” Spatially resolved photoluminescence of laterally overgrown GaN” Journal of Crystal Growth 201/202 (1999) pp365-370
32. Tavernier et al. ” Two-step growth of high-quality GaN by hydride vapor-phase epitaxy” Appl. Phys. Lett., Vol. 77, No. 12, 18 September 2000
33. Haskell et al. ” Structural and morphological characteristics of planar (11-20) a-plane gallium nitride grown by hydride vapor phase epitaxy” Appl. Phys. Lett., Vol. 83, No. 8, 25 August 2003
34. Haskell et al. “Defect reduction in (11-20) a-plane gallium nitride via lateral epitaxial overgrowth by hydride vapor-phase epitaxy” Appl. Phys. Lett., Vol. 83, No. 4, 28 July 2003
35. Detchprohm et al. “Hydride vapor phase epitaxial growth of a high quality GaN film using a ZnO buffer layer” Appl. Phys. Lett., Vol. 61, No. 22, 30 November 1992
36. H. Sone et al. “Optical and Crystalline Properties of Epitaxial-Lateral-Overgrown-GaN Using Tungsten Mask by Hydride Vapor Phase Epitaxy” Jpn. J. Appl. Phys., Vol.38, pp.L356~L359 (1999)
37. Yoshiaki Honda et al.”Crystal Orientation Fluctuation of Epitaxial-Lateral-Overgrown GaN with W Mask Observed by Transmission Electron Diffraction and X-Ray Rocking curves” ， Japan Journal of Applied Physics Vol.38 pp. L1299~L1302 (1999)
38. H. Miyake et al. “Carrier-gas dependence of ELO GaN grown by hydride VPE” Journal of Crystal Growth 237–239 (2002) 1055–1059
39. K. Motoki et al. “Preparation of Large Freestanding GaN Substartes by

Hydride Vapor Phase Epitaxy Using GaAs as a Starting Substrate" Jpn. J. Appl. Phys. Vol. 40 pp. L140–L143 (2001)

40. Y. OSHIMA et al. "Preparation of Freestanding GaN Wafers by Hydride Vapor Phase Epitaxy with Void-Assisted Separation" Jpn. J. Appl. Phys. Vol. 42 (2003) Pt. 2, No. 1A/B
41. D. F. Storm, et al "Growth and characterization of plasma-assisted molecular beam epitaxial-grown AlGaN/GaN heterostructures on free-standing hydride vapor phase epitaxy GaN substrates", J. Vac. Sci. Technol. B 23.3., May/Jun 2005
42. A.E. Nikolaev, et al. "GaN Layers Grown by HVPE on P-type 6H-SiC Substrates", N. S. R. Vol 1, Art 45
43. Yu. Melnik, et al. "AlN substrates: fabrication via vapor phase growth and characterization", phys. stat. sol. (a) 200, No. 1, 22–25 (2003)
44. O. Yu. Ledyaev, et al. "Properties of AlN Layers Grown on SiC Substrates in Wide Temperature Range by HVPE", phys. stat. sol. (c) 0, No. 1, 474–478 (2002)
45. O. Kovalenkov, et al. "Thick AlN layers grown by HVPE", Journal of Crystal Growth 281 (2005) 87–92
46. Yu-Huai Liu, et al. "Growth of Thick AlN Layer by Hydride Vapor Phase Epitaxy", Japanese Journal of Applied Physics Vol. 44, No. 17, 2005, pp. L 505–L 507
47. Yoshinao Kumagai, et al. "Growth of thick AlN layers by hydride vapor-phase epitaxy", Journal of Crystal Growth 281 (2005) 62–67
48. Y. Kumagai, et al. "Hydride vapor phase epitaxy of AlN: thermodynamic analysis of aluminum source and its application to growth", phys. stat. sol. (c) 0, No. 7, 2498–2501 (2003)

49. M. Bockowski et al. “Gallium nitride growth on sapphire/GaNtemplates at high pressure and high temperatures” Journal of Crystal Growth 274 (2005) 55–64
50. B. Łucznik et al. “Deposition of thickGaN layers by HVPE on the pressure grown GaN substrates” Journal of Crystal Growth 281 (2005) 38–46
51. M. Bockowski et al. “Growth of GaN on patterned GaN/sapphire substrates by high pressure solution method” Journal of Crystal Growth 281 (2005) 11–16
52. I. Grzegory et al. “Growth of bulk GaN by HVPE on pressure grown seeds” Proc. of SPIE Vol. 6121 612107
53. I. Grzegory et al. “Crystallization of low dislocation density GaN by high-pressure solution and HVPE methods” Journal of Crystal Growth 300 (2007) 17–25
54. M. Bockowski et al. “Platelets and needles: Two habits of pressure-grown GaN crystals” Journal of Crystal Growth 305 (2007) 414–420
55. M. Bockowski et al. “GaN crystallization by the high-pressure solution growth method on HVPE bulk seed” J. Crystal Growth (2008), doi:10.1016/j.jcrysgro.2008.06.030
56. G. Kamler et al. “High rate photoelectrochemical etching of GaN and the use of patterned substrates for HVPE regrowth” Journal of Crystal Growth 310 (2008) 3478– 3481
57. Yamina Andre et al. “Low dislocation density high-quality thick hydride vapour phase epitaxy (HVPE) GaN layers” Journal of Crystal Growth 306 (2007) 86–93
58. J. Tourret et al. “Low-cost high-quality GaN by one-step growth” Journal of Crystal Growth 310 (2008) 924–929

59. Derrick S. Kamber et al. "Direct heteroepitaxial growth of thick AlN layers on sapphire substrates by hydride vapor phase epitaxy" Journal of Crystal Growth 297 (2006) 321–325
60. Tadao Hashimoto et al. "Seeded growth of GaN by the basic ammonothermal method" Journal of Crystal Growth 305 (2007) 311–316
61. Tadao Hashimoto et al. "Status and perspectives of the ammonothermal growth of GaN substrates" Journal of Crystal Growth 310 (2008) 876–880
62. Tadao Hashimoto et al. "Ammonothermal growth of bulk GaN" J. Crystal Growth (2008), doi:10.1016/j.jcrysgro.2008.06.005
63. V. Soukhoveev et al. "Recent results on AlN growth by HVPE and fabrication of free standing AlN wafers" phys. stat. sol. (c) 3, No. 6, 1653–1657 (2006)
64. Yuichi Oshima et al. "Thermal and optical properties of bulk GaN crystals fabricated through hydride vapor phase epitaxy with void-assisted separation" JOURNAL OF APPLIED PHYSICS 98, 103509 2005
65. Yuichi Oshima et al. "Thermal and Electrical Properties of High-Quality Freestanding GaN Wafers with High Carrier Concentration" Japanese Journal of Applied Physics Vol. 45, No. 10A, 2006, pp. 7685–7687
66. Takehiro Yoshida et al. "Fabrication of 3-in GaN substrates by hydride vapor phase epitaxy using void-assisted separation method" Journal of Crystal Growth 310 (2008) 5–7
67. Michimasa Miyanaga et al. "Evaluation of AlN single-crystal grown by sublimation method" Journal of Crystal Growth 300 (2007) 45–49
68. Kensaku Motoki et al. "Dislocation reduction in GaN crystal by advanced-DEEP" Journal of Crystal Growth 305 (2007) 377–383
69. Y. Kumagai et al. "Thermodynamics on hydride vapor phase epitaxy of AlN

using AlCl3 and NH3" phys. stat. sol. (b) 243, No. 7, 1431–1435 (2006)

70. Ken-ichi Eriguchi et al. "High-temperature growth of thick AlN layers on sapphire (0 0 01) substrates by solid source halide vapor-phase epitaxy" J. Crystal Growth (2008), doi:10.1016/j.jcrysgro.2008.06.033

71. Masataka Imura et al. "Epitaxial lateral overgrowth of AlN on trench-patterned AlN layers" Journal of Crystal Growth 298 (2007) 257–260

72. N. Okada et al. "Growth of high-quality and crack free AlN layers on sapphire substrate by multi-growth mode modification" Journal of Crystal Growth 298 (2007) 349–353

73. T. Nagai et al. "Microstructure in nonpolar m-plane GaN and AlGaN films" Journal of Crystal Growth 298 (2007) 288–292

74. N. Okada et al. "Epitaxial lateral overgrowth of a-AlN layer on patterned a-AlN template by HT-MOVPE" Journal of Crystal Growth 300 (2007) 141–144

75. Masataka Imura et al. "Impact of high-temperature growth by metal-organic vapor phase epitaxy on microstructure of AlN on 6H-SiC substrates" Journal of Crystal Growth 310 (2008) 2308–2313

76. Tsuguo Fukuda et al. "Prospects for the ammonothermal growth of large GaN crystal" Journal of Crystal Growth 305 (2007) 304–310

77. Katsushi Fujii et al. "Near band-edge 3.357 eV emission of Ga-face (0001) GaN grown by ammonothermal method" phys. stat. sol. (a) 204, No. 12, 4266–4271 (2007)

78. Dirk Ehrentraut et al. "Ammonothermal synthesis of thick gallium nitride film employing acidic mineralizers" J Mater Sci (2008) 43:2270–2275

79. Dirk Ehrentraut et al. "Reviewing recent developments in the acid ammonothermal crystal growth of gallium nitride" J. Crystal Growth (2008),

doi:10.1016/j.jcrysgro.2008.06.017

80. A. Kasic et al. "Highly homogeneous bulk-like 2" GaN grown by HVPE on MOCVD–GaN template" Journal of Crystal Growth 275 (2005) e387–e393

81. Daniela Gogova et al. "High-Quality 2" Bulk-Like Free-Standing GaN Grown by HydrideVapour Phase Epitaxy on a Si-doped Metal Organic Vapour Phase Epitaxial GaN Template with an Ultra Low Dislocation Density" Japanese Journal of Applied Physics Vol. 44, No. 3, 2005, pp. 1181–1185

82. B. Monemar et al. "Growth of thick GaN layers with hydride vapour phase epitaxy" Journal of Crystal Growth 281 (2005) 17–31

83. A. Kasic et al. "Characterization of crack-free relaxed GaN grown on 2 sapphire" Journal of Applied Physics 98, 073525 2005

84. P. Ma et al. "HVPE-GaN Growth on Sapphire Substrate" Chinese Journal of Semiconductors Vol.28 No.6 (2007)

85. T.B. Wei et al. "Columnar Structures and Stress Relaxation in Thick GaN Films Grown on Sapphire by HVPE" Chin. Phys. Lett. Vol.24, No.3 (2007) 822

86. T.B. Wei et al. "Characterization of free-standing GaN substrate grown through hydride vapor phase epitaxy with a TiN interlayer" Applied Surface Science 253 (2007) 7423–7428

87. T.B. Wei et al. "Hillocks and hexagonal pits in a thick film grown by HVPE" Microelectron. J (2008), doi:10.1016/j.mejo.2008.02.024

88. Xie Xin-Jian et al. "Growth of Strain Free GaN Layers on (0001) Oriented Sapphire by Using Quasi-Porous GaN Template" Chin. Phys. Lett. Vol.23, No.6 (2006) 1619

89. KAI QIU et al. "Growth of GaN on Buffer Layers with Different Polarities

by Hydride Vapor-Phase Epitaxy” Journal of Electronic Materials, Vol. 36, No. 4, 2007

90. Qiu Kai et al. “Properties of GaN on different polarity buffer layers by hydride vapour phase epitaxy” Chin. Phys. Vol 16 No 7, July 2007

91. C. Hemmingsson et al. “Hydride vapour phase epitaxy growth and characterization of thick GaN using a vertical HVPE reactor” Journal of Crystal Growth 300 (2007) 32–36

92. C. Hemmingsson et al. “Modeling, optimization, and growth of GaN in a vertical halide vapor-phase epitaxy bulk reactor” Journal of Crystal Growth 310 (2008) 906–910

Publication List

Journal:

1. **Hsin-Hsiung Huang**, Hung-Yu Zeng, Chi-Ling Lee, Shih-Chang Lee, and Wei-I Lee "Extended microtunnels in GaN prepared by wet chemical etch", *Appl. Phys. Lett.* **89**, 202115 (2006).

2. **Hsin-Hsiung Huang**, Hung-Yu Zeng, and Wei-I Lee, " Preparation of Extended Micro-tunnels in GaN by Wet Chemical Etching", *Phys. Status Solidi (b)* **244**, 1872 (2007).

3. Chih-Ming Lai, Wen Yu Liu, Jenq-Dar Tsay, Po Chun Liu, Yih-Der Guo, **Hsin-Hsiung Huang**, Yu Hsiang Chang, and Jul Chin Yeh, "Self-separated freestanding GaN grown on patterned substrate by Hydride Vapor Phase Epitaxy ", *Phys. Status Solidi (c)* 4, 2231 (2006).

4. Pei-Lun Wu, **Hsin-Hsiung Huang**, Hung-Yu Zeng, Po-Chun Liu, Chih-Ming Lai, Jeng-Dar Tsay, and Wei-I Lee,**"**Comparison between Extended Microtunnels along Different Crystal Orientations in GaN**",** *Phys. Status Solidi (c)* **5**, 1671 (2008).

5. **Hsin-Hsiung Huang,** Pei-Lun Wu, Hung-Yu Zeng, Po-Chun Liu,Tung-Wei Chi, Jenq-Dar Tsay, and Wei-I Lee, "Triangular Extended Microtunnels in GaN Prepared by Selective Crystallographic Wet Chemical Etching", *J. Electrochm. Soc.,* **155,** H504 (2008).

6. **Hsin-Hsiung Huang**, Kuei-Ming Chen, Li-Wei Tu, Ting-Li Chu, Pei-Lun Wu, Hung-Wei Yu, Chen-Hao Chiang, and Wei-I Lee, "A Novel Technique to Grow Crack-Free GaN Thick-Film by Hydride Vapor Phase Epitaxy", accepted by JJAP.
7. **Hsin-Hsiung Huang**, Chu-Li Chao, Tung-Wei Chi, Yu-Lin Chang, Po-Chun Liu, Li-Wei Tu, Jenq-Dar Tsay, Hao-Chung Kuo, Shun-Jen Cheng, and Wei-I Lee, "Strain reduced GaN thick film grown by hydride vapor phase epitaxy utilizing dot air-bridged structure", summitted to JCG.
8. Kuei-Ming Chen, **Hsin-Hsiung Huang**,Yi-Lin Kuo, Pei-Lun Wu, Ting-Li Chu, Hung-Wei Yu, Wei-I Lee, " The bowing reduction of Freestanding GaN by N-face re-growth with hydride vapor-phase epitaxy", summitted to JCG.

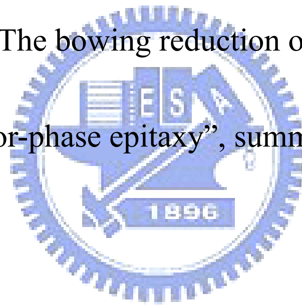

Conference Paper

1. **H.H. Huang**, F.K. Hsiao, Y.L. Kuo, W.I. Lee, “Large Area Free-Standing GaN Substrate Made By Hydride Vapor Phase Epitaxy”, Optics and Photonics 2005, Taiwan, Tainan (OPT).

2. **Hsin-Hsiung Huang**, Hung-Yu Zeng, Wei-I Lee, “ Selective Etching of GaN Extended Micro-tunnels by Wet Chemical Etching”, International electron devices and materials symposia 2006, Taiwan, Tainan (IEDMS).

3. **Hsin-Hsiung Huang**, Hung-Yu Zeng, Wei-I Lee, “ Extended Micro-tunnels in GaN Prepared by Wet Chemical Etching”, International Workshop on Nitride semiconductors 2006, Kyoto，Japan (IWN 2006).

4. **Hsin-Hsiung Huang**, Hung-Yu Zeng , Pei-Lun Wu , and Wei-I Lee, “ Long depth triangular micro-tunnels of GaN prepared by wet chemical etching”, Annual meeting of Physical Society R.O.C. 2007, Taiwan, Jungli.

5. Pei-Lun Wu, Hung-Yu Zeng, **Hsin-Hsiung Huang** , and Wei-I Lee, “ Investigation of Selective Wet chemical etching of Bulk GaN”, Annual meeting of Physical Society R.O.C. 2007, Taiwan, Jungli.

6. **Hsin-Hsiung Huang**, Pei-Lun Wu, Hung-Yu Zeng, Feng-Ke Hsiao, Po-Chun Liu, Tung-Wei Chi, Jenq-Dar Tsay, and Wei-I Lee,“Comparison Between Extended Microtunnels Along Different Crystal Orientations in GaN”, 7th International

Conference on Nitride Semiconductors 2007 (ICNS 7), USA, Las Vegas.

7. **Hsin-Hsiung Huang**, Po-Chun Liu, Tung-Wei Chi, Ming-Zheng Hsu, Yu-Lin Chang, Li-Wei Tu, Jenq-Dar Tsay, and Wei-I Lee, " Improvement of GaN Quality Prepared by Hydride Vapor Phase Epitaxy Using Air-Bridged Growth Technique", 7th International Conference on Nitride Semiconductors 2007 (ICNS 7), USA, Las Vegas.

8. **Hsin-Hsiung Huang**, Kuei-Ming Chen, Pei-Lun Wu, Hung-way Yu, Ting-Li Chu, Po-Chun Liu, Jenq-Dar Tsay, and Wei-I Lee," Freestanding GaN grown by Hydride Vapor Phase Epitaxiy", Annual meeting of Physical Society R.O.C. 2008, Taiwan, Hsinchu.

9. Ting-Li Chu, **Hsin-Hsiung Huang**, Po-Chun Liu, Tung-Wei Chi, Jenq-Dar Tsay, Kuei-Ming Chen, Pei-Lun Wu, and Wei-I Lee,"The study of chemical wet etching on a-plane GaN thin film", Annual meeting of Physical Society R.O.C. 2008, Taiwan, Hsinchu.

10. **Hsin-Hsiung Huang**, Chu-Li Chao, Tung-Wei Chi, Yu-Lin Chang, Po-Chun Liu, Li-Wei Tu, Jenq-Dar Tsay, Hao-Chung Kuo, Shun-Jen Cheng, and Wei-I Lee, "Strain reduced GaN thick film grown by hydride vapor phase epitaxy utilizing dot air-bridged structure", Second International Symposium on Growth of III-Nitrides 2008 (ISGN-2), Japan, Izy.

11. Kuei-Ming Chen, **Hsin-Hsiung Huang**, Feng-Ke Hsiao,Yi-Lin Kuo, Pei-Lun Wu, Ting-Li Chu, Hung-Wei Yu, and Wei-I Lee, " The bowing reduction of Freestanding GaN by N-face regrowth with hydride vapor-phase epitaxy", Second International Symposium on Growth of III-Nitrides 2008 (ISGN-2), Japan, Izy.

12. **Hsin-Hsiung Huang**, Chen-Hao Chiang, Kuei-Ming Chen, Ting-Li Chu, Pei-Lun Wu, Hung-Wei Yu, Wei-I Lee, and Li-Wei Tu," A Very Simple Technique to Grow Crack-Free Thick GaN Films by Hydride Vapor Phase Epitaxy", International Workshop on Nitride semiconductors 2008 (IWN 2008), Switzerland, Montreux.

13. Kuei-Ming Chen, **Hsin-Hsiung Huang**, Chen-Hao Chiang, Pei-Lun Wu, Ting-Li Chu, Hung-Wei Yu, and Wei-I Lee, Freestanding GaN by hydride vapor-phase epitaxy using template weakness with laser assistance technique", International Workshop on Nitride semiconductors 2008 (IWN 2008), Switzerland, Montreux.

14. C. H. Chiang, F. K. Hsiao, **H. H. Huang**, K. M. Chen, T. L. Chu, P. L. Wu, C. H. Cheng, K. L. Lin, Y. L. Hsiao, W. C. Huang, E.Y. Chang, J. F. Chen and W. I Lee," Nonpolar a-plane GaN grown on r-plane sapphire by metalorganic chemicalvapor deposition and hydride vapor phase epitaxy with sandwiched AlN buffer structure", International Workshop on Nitride semiconductors 2008 (IWN 2008), Switzerland, Montreux.

15. Chu Li Chao, Po Chun Liu, Tung Wei Chi, **Hsin-Hsiung Huang**, Jenq-Dar Tsay,

"Fabricating freestanding GaN thick films by Hydride Vapor-Phase Epitaxy with GaN nano rod assistance separation", International Workshop on Nitride semiconductors 2008 (IWN 2008), Switzerland, Montreux.

16. Tung-Wei Chi, Chu-Li Chao, **Hsin-Hsiung Huang**, Po-Chun Liu, Jenq-Dar Tsay, Tien-Chang Lu, Hao-Chung Kuo, and Shing-Chung Wang, "Free Standing GaN Thick Film Grown by Hydride Vapor Phase Epitaxy Using Dot Air-Bridged Structure", International Workshop on Nitride semiconductors 2008 (IWN 2008), Switzerland, Montreux.

Patents:

1. Wei-I Lee, **Hsin-Hsiung Huang**, and Hung-Yu Zeng, " Etching Method for Nitride Semiconductor", in requestion of ROC and USA patents, S96005_US1
2. Wei-I Lee, **Hsin-Hsiung Huang**, Kuei –Ming Chen, and Yen-Hsien, Yeh," A Novel Technique to Grow GaN Thick-Film by Hydride Vapor Phase Epitaxy", in requestion of ROC, PRC, and USA patents

Award:

H.H. Huang, F.K. Hsiao, Y.L. Kuo, W.I. Lee, "Large Area Free-Standing GaN Substrate Made By Hydride Vapor Phase Epitaxy", Optics and Photonics 2005, Taiwan, Tainan (OPT), student dissertation award.